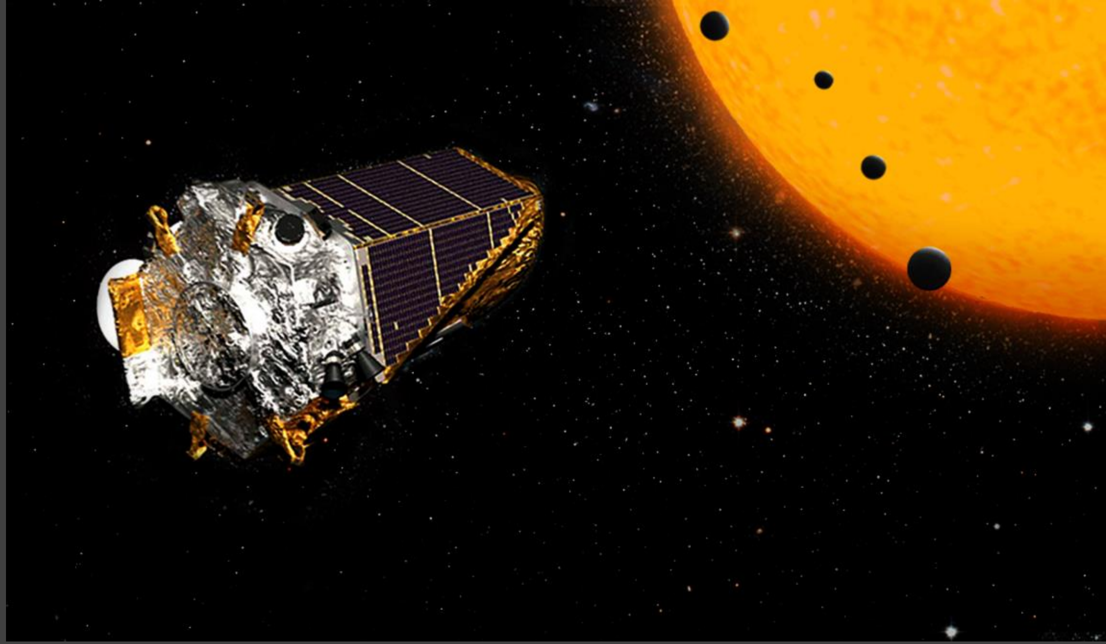

Planet detection methods

SERGEI POPOV

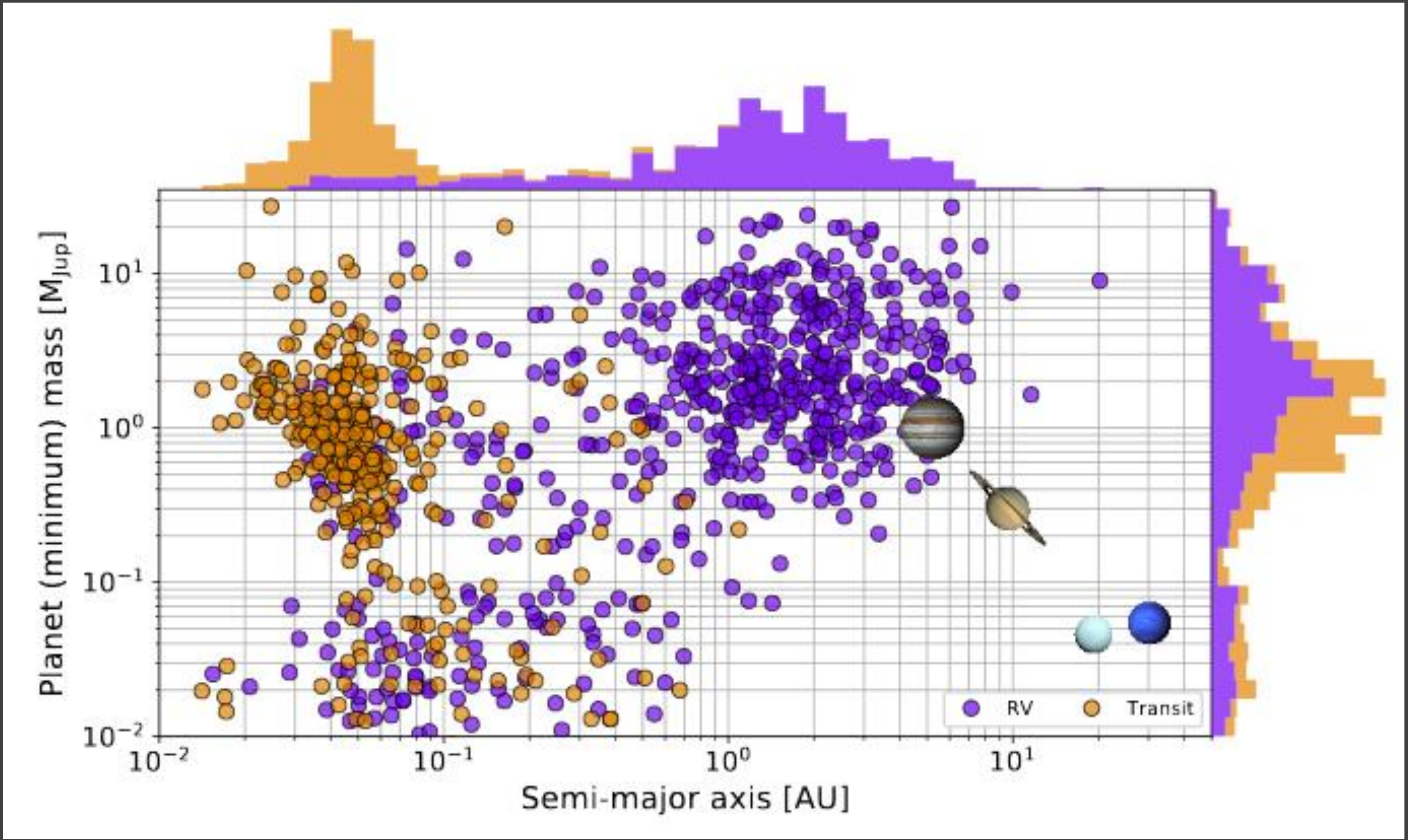
Planet (minimum) mass [M_{Jup}]
10^{1}
10^{0}
10^{-1}
10^{-2}
10^{-2}
10^{-1}
10^{0}
10^{1}
Semi-major axis [AU]
RV
Transit

1805.08391

Planets, brown dwarfs stars

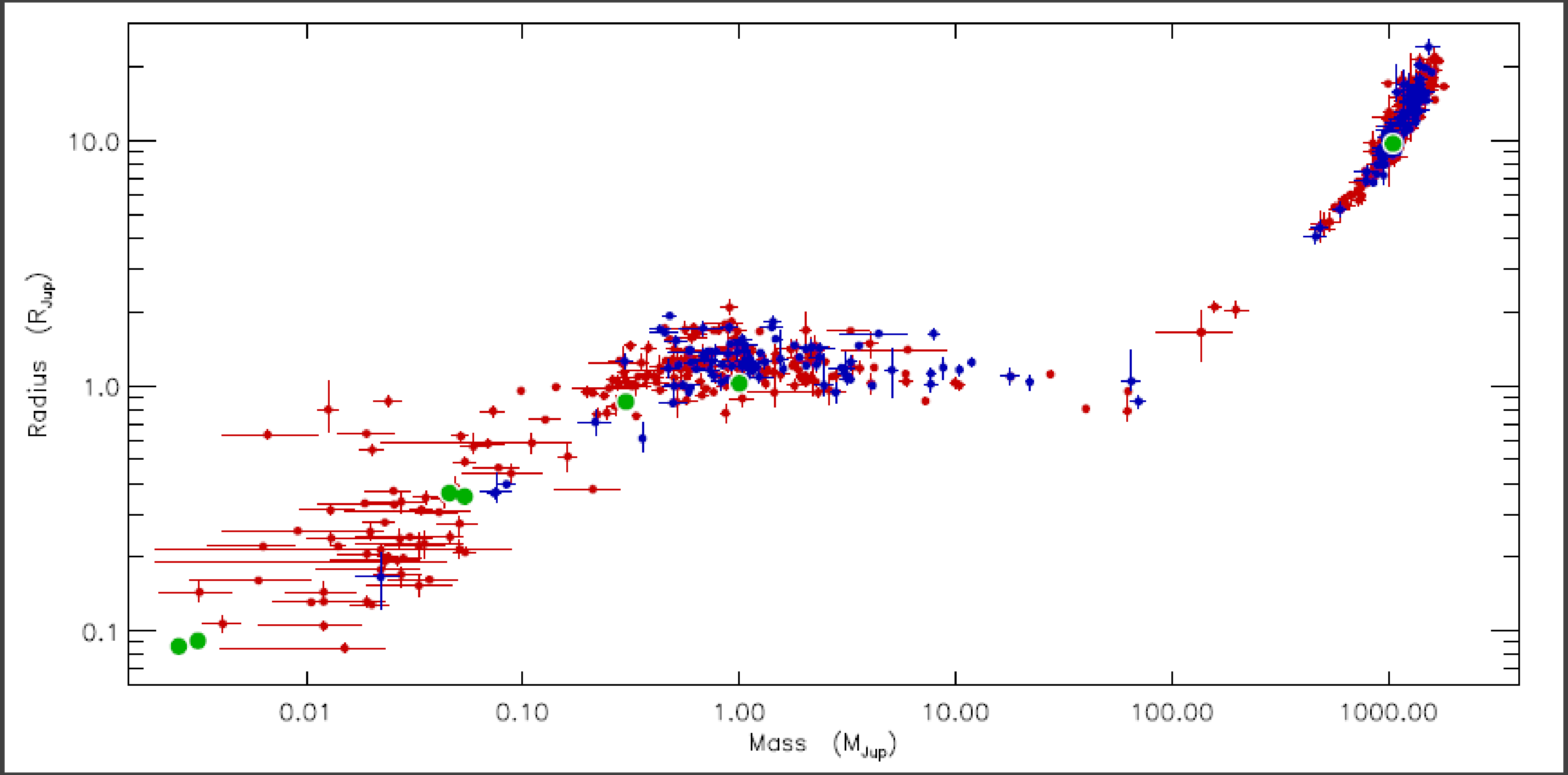

Brown dwarfs:
(12-13)<M<(75-80)
Jupiter masses

Exoplanet catalogues

Catalog	Mass criteria	Confidence criteria	Number of planets†
Exoplanet Encyclopaedia	$M_p - 1\sigma < 60 M_{\rm Jup}$	Submitted paper, conference talk	3741
NASA Exoplanet Archive	$M_p < 30 M_{\rm Jup}$	Accepted, refereed paper	3704
Open Exoplanet Catalog	None listed	Open-source	3504

†: as of February 27th, 2018.

http://exoplanets.org/

http://exoplanet.eu/catalog

http://exoplanetarchive.ipac.caltech.edu/index.html

http://www.openexoplanetcatalogue.com

1803.11158 1808.10236

See also http://www.astronet.ru/db/msg/1391325 (in Russian)

NASA Exoplanet Archive

All Exoplanets	4201
Confirmed Planets with Kepler Light Curves for Stellar Host	2362
Confirmed Planets Discovered by Kepler	2342
Kepler Project Candidates Yet To Be Confirmed	2418
Confirmed Planets with K2 Light Curves for Stellar Host	431
Confirmed Planets Discovered by K2	410
K2 Candidates Yet To Be Confirmed	889
Confirmed Planets Discovered by TESS [1]	67
TESS Project Candidates Integrated into Archive (2020-08-20 13:00:02) [2]	2174
Current date TESS Project Candidates at ExoFOP	2174
TESS Project Candidates Yet To Be Confirmed [3]	1317

Confirmed Exoplanet Statistics

Discovery Method	Number of Planets
Astrometry	1
Imaging	50
Radial Velocity	810
Transit	3191
Transit timing variations	21
Eclipse timing variations	16
Microlensing	96
Pulsar timing variations	7
Pulsation timing variations	2
Orbital brightness modulations	6
Disk Kinematics	1
Transiting Exoplanets	**3214**
All Exoplanets	**4201**

Exoplanet Mass and Radius

Confirmed Planets with mass	970
Confirmed Planets with m sin i	818
Confirmed Planets with radius	3214

Counts by Mass

M ≤ 3 M_Earth	38
3 < M ≤ 10 M_Earth	140
10 < M ≤ 30 M_Earth	97
30 < M ≤ 100 M_Earth	94
100 < M ≤ 300 M_Earth	222
300 M_Earth < M	379

Counts by Radius

R ≤ 1.25 R_Earth	408
1.25 < R ≤ 2 R_Earth	851
2 < R ≤ 6 R_Earth	1329
6 < R ≤ 15 R_Earth	460
15 R_Earth < R	166

https://exoplanetarchive.ipac.caltech.edu/docs/counts_detail.html, 28/08/2020

Radial velocities

Michel Mayor and Didier Queloz 1995

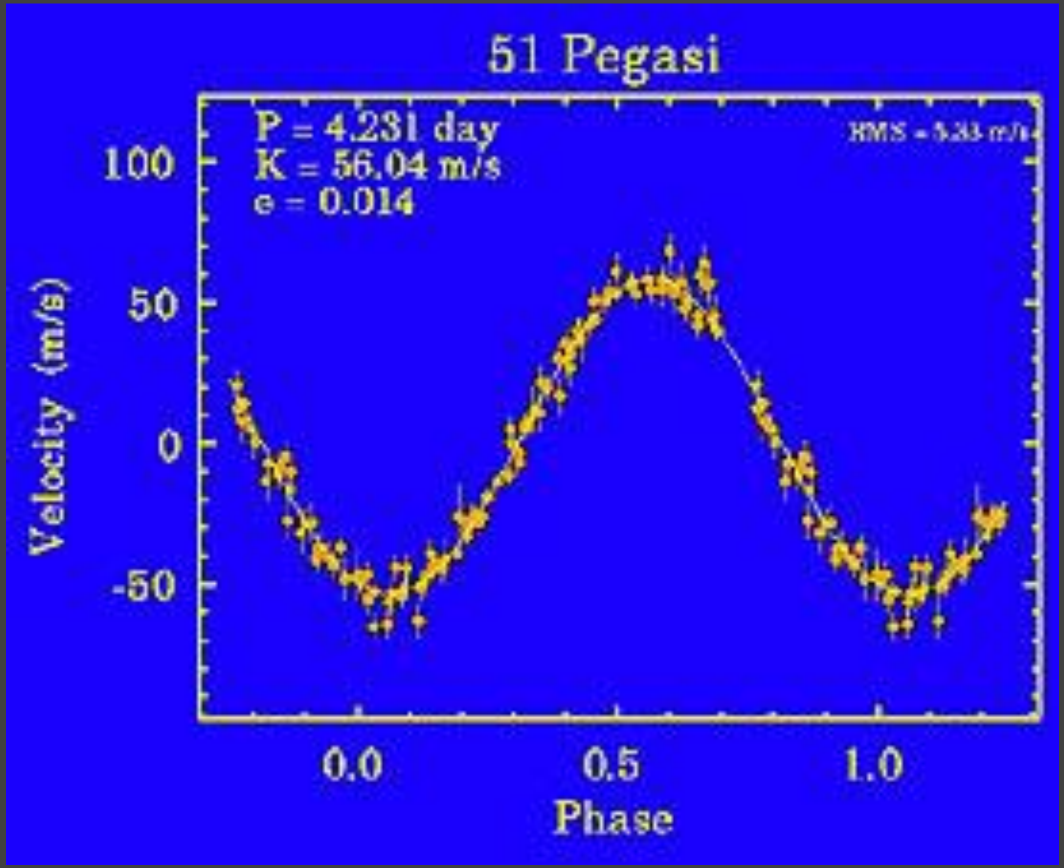

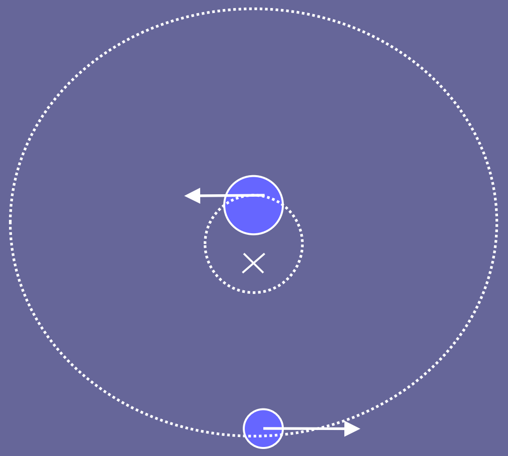

We see just the bright star.
We measure that its radial velocity periodically changes.

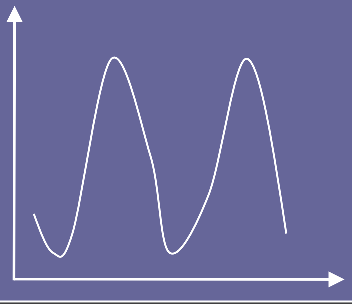

Measure:
- Period
- Mass

First light planets

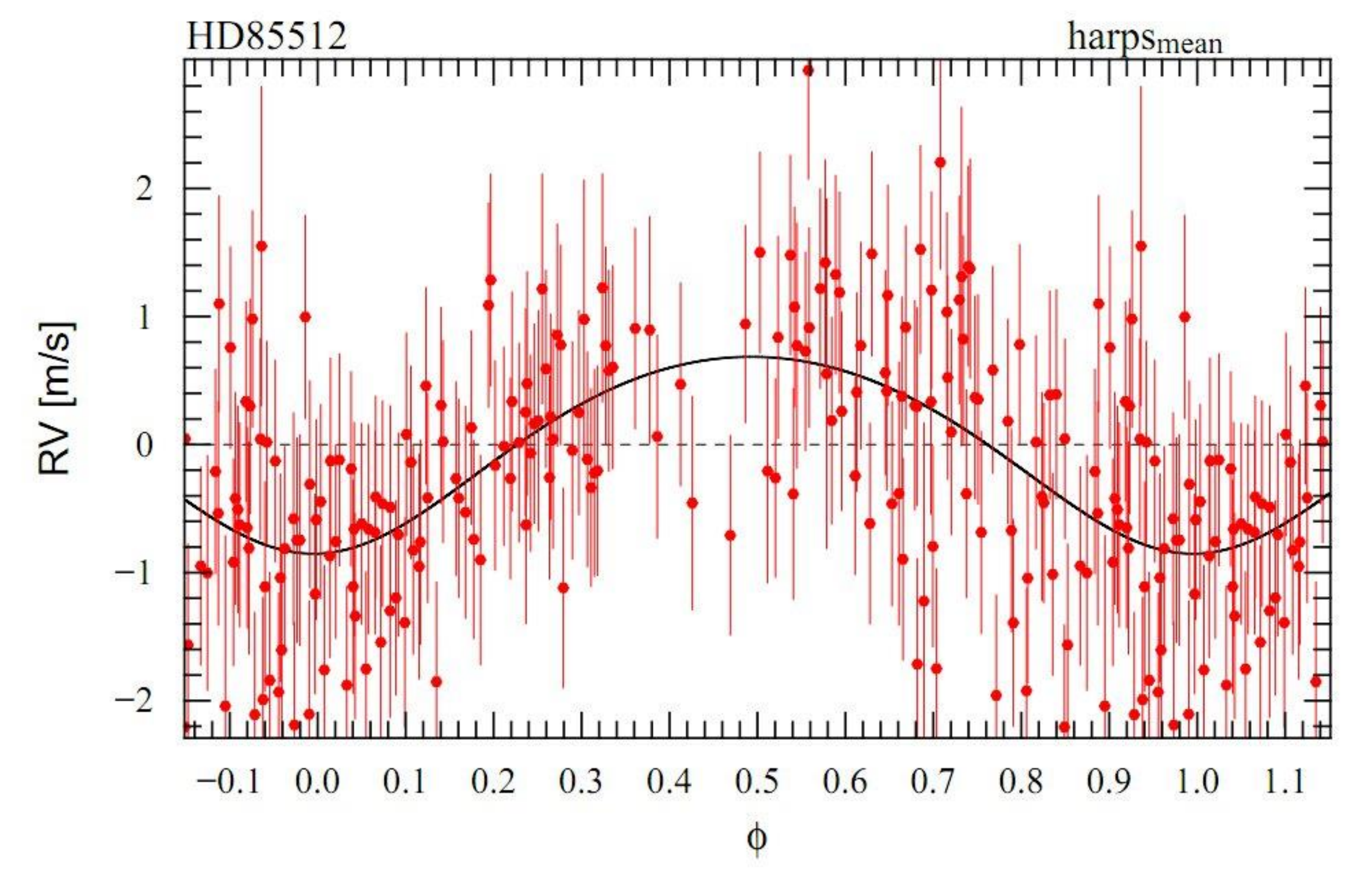

The problem is to measure
small velocity variations
for relatively long time.

Quality and stability of
the spectrograph is
more important than the telescope size.

This planet discovered by HARPS.
Situated just near the
zone of habilability.

Proxima Centauri b

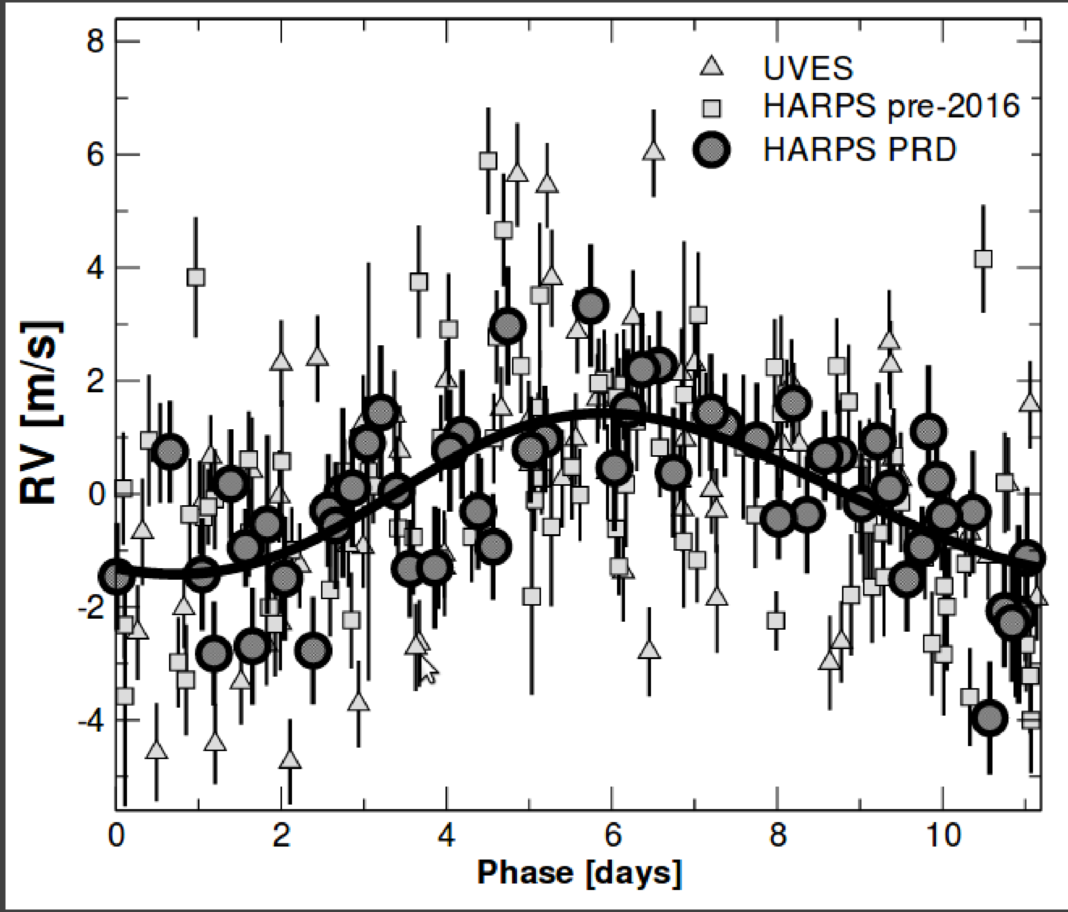

1.3 Earth masses
0.05 AU
11 days

Habitability zone

Radial velocities: data and measurements

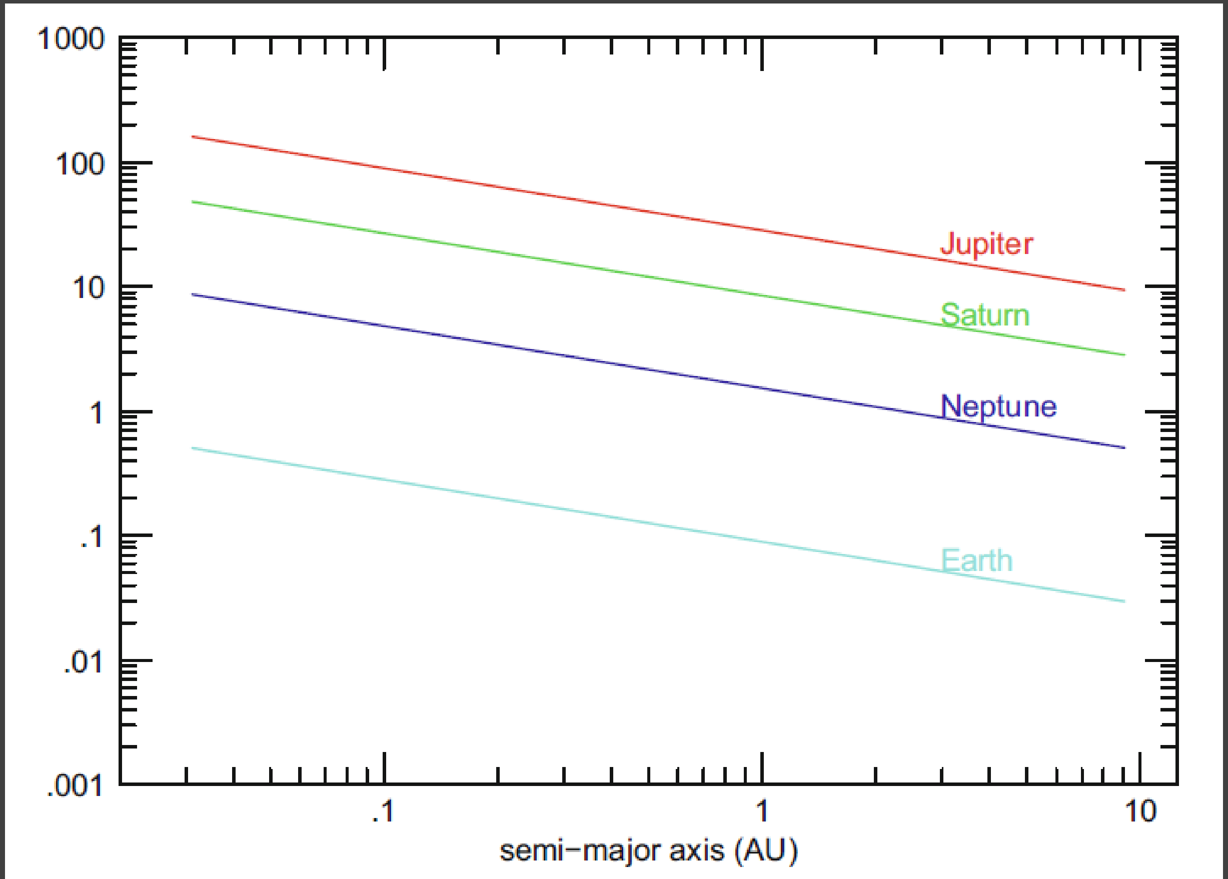

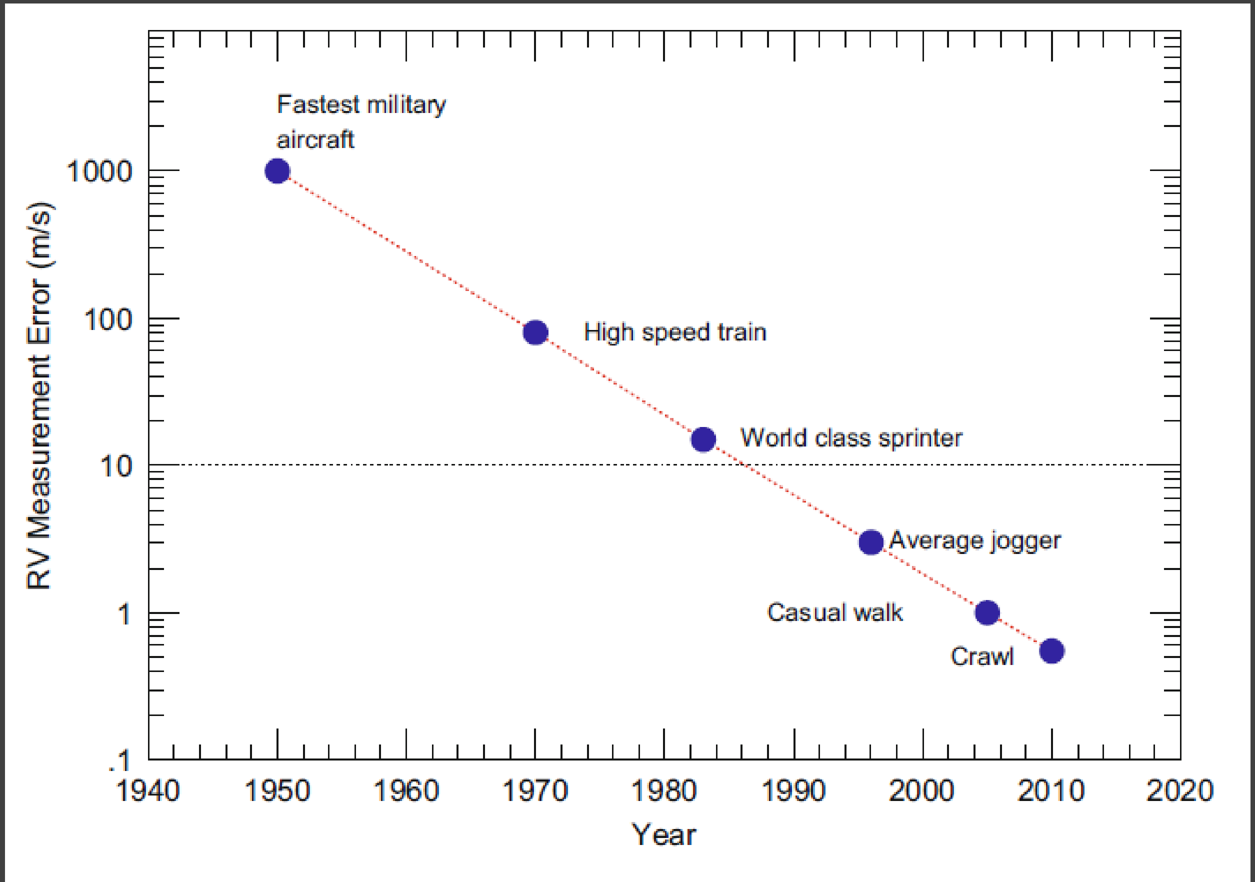

Artie Hatzes (in Bozza et al. 2016)

Role of a star

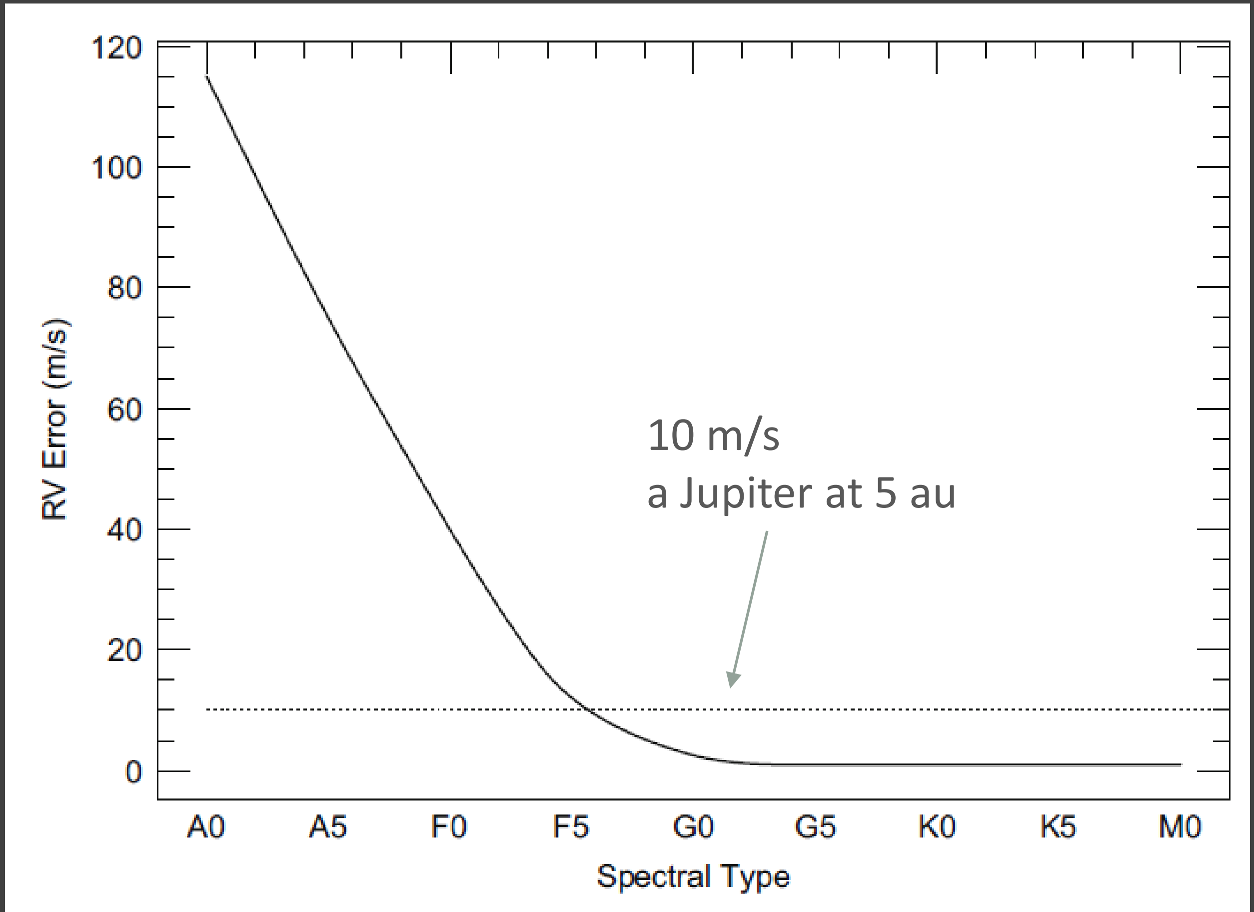

Difference is mainly due to

- Rapid rotation
- Smaller number of spectral lines

Without additional errors due to the instrument:

$$\sigma\,[\mathrm{m/s}] = C(\mathrm{S/N})^{-1} R^{-3/2} B^{-1/2} (v \sin i/2) f(\mathrm{SpT})$$

B- band width, R – resulution (λ /Δλ)

Artie Hatzes (in Bozza et al. 2016)

Necessity for simultaneous record of the stellar and calibration spectra

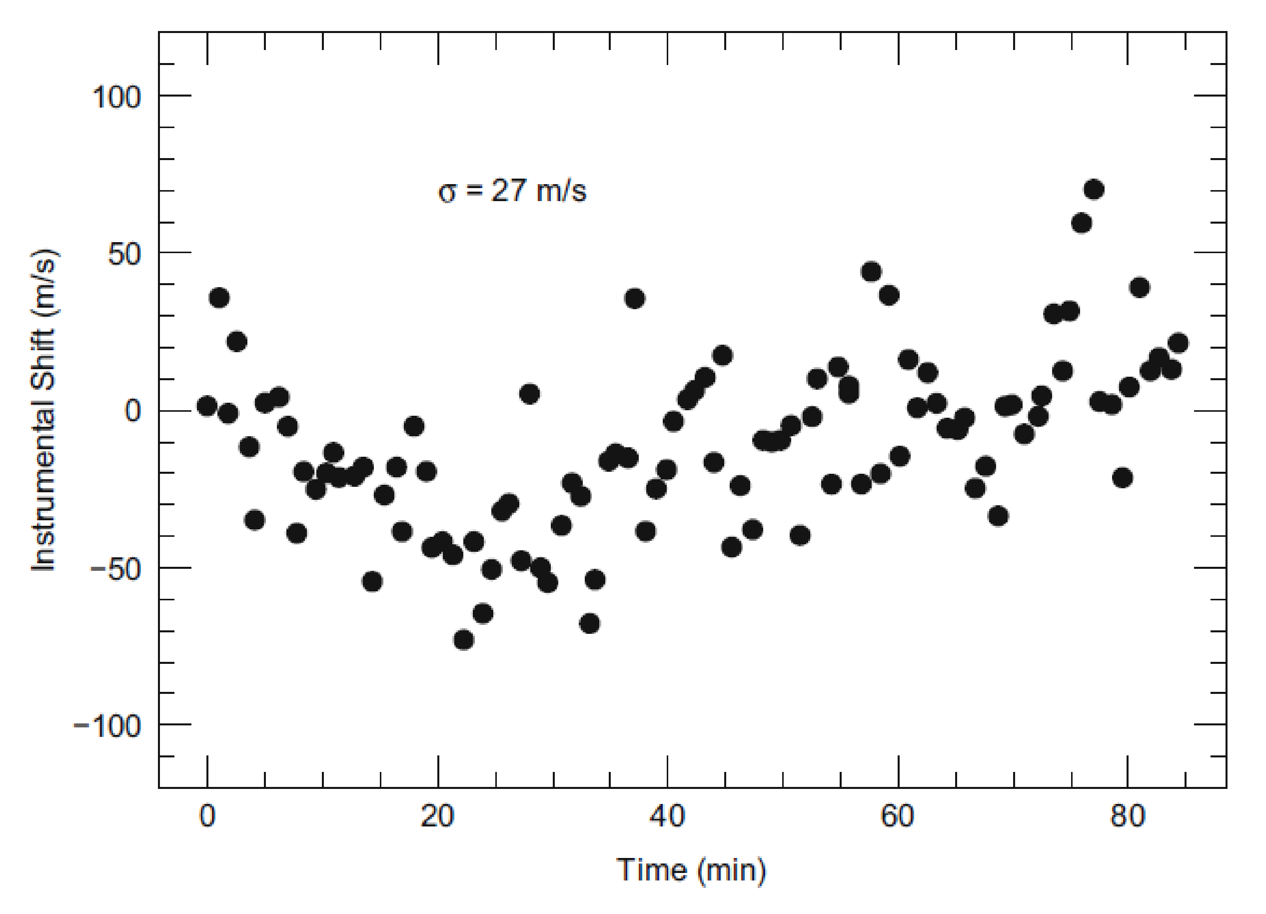

It is necessary to take the stellar and the laboratory spectra simultaneously, as the shift due to stellar velocity is very small and so the device cannot be stabilized to such level.
Any external mechanical influence can shift the detector so that the position of the line cannot be determined with precision high enough to detect the signal from the planet presence.

Artie Hatzes (in Bozza et al. 2016)

Molecular iodine cell

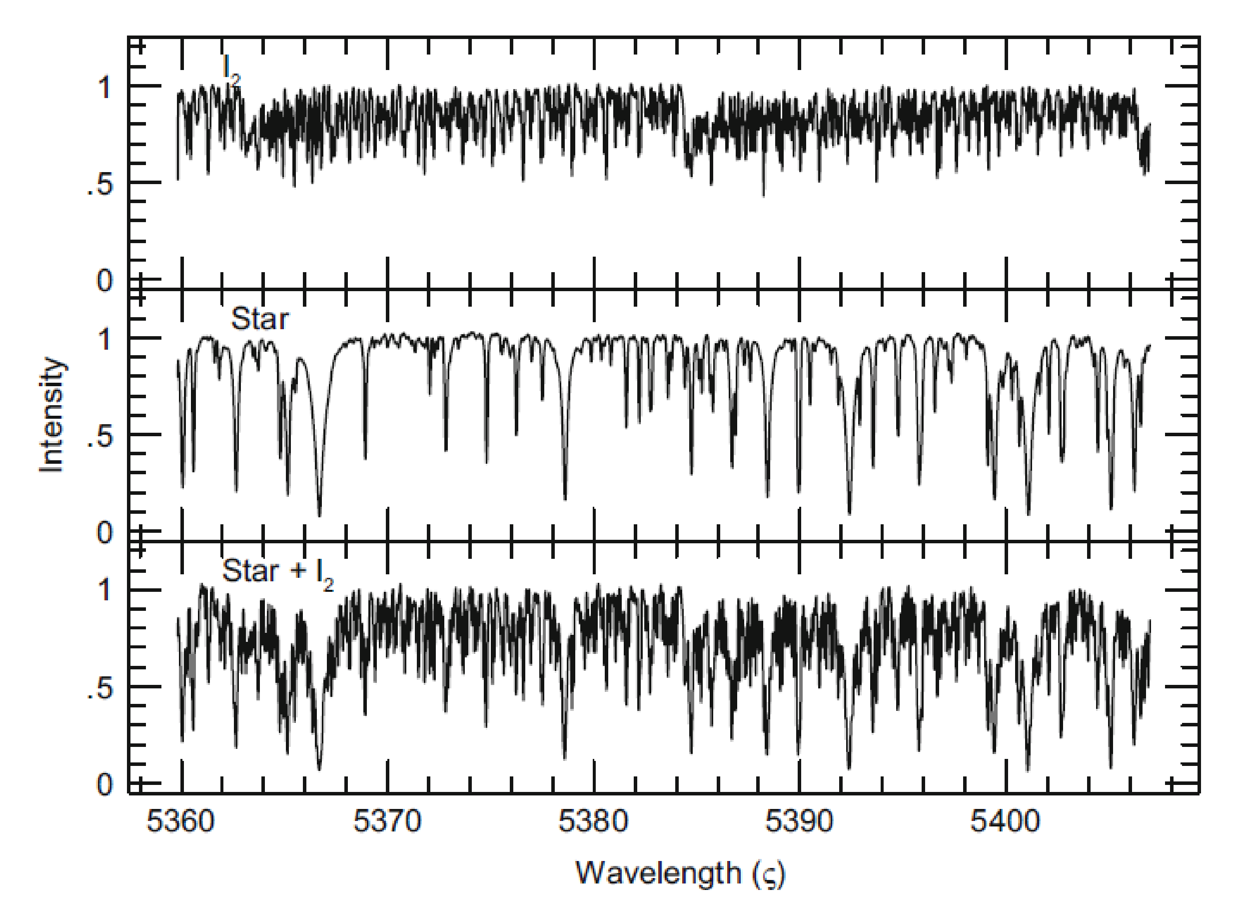

I_2 cell became the first effective tool to provide lines for RV measurements.

Velocity vs. phase for different orbits

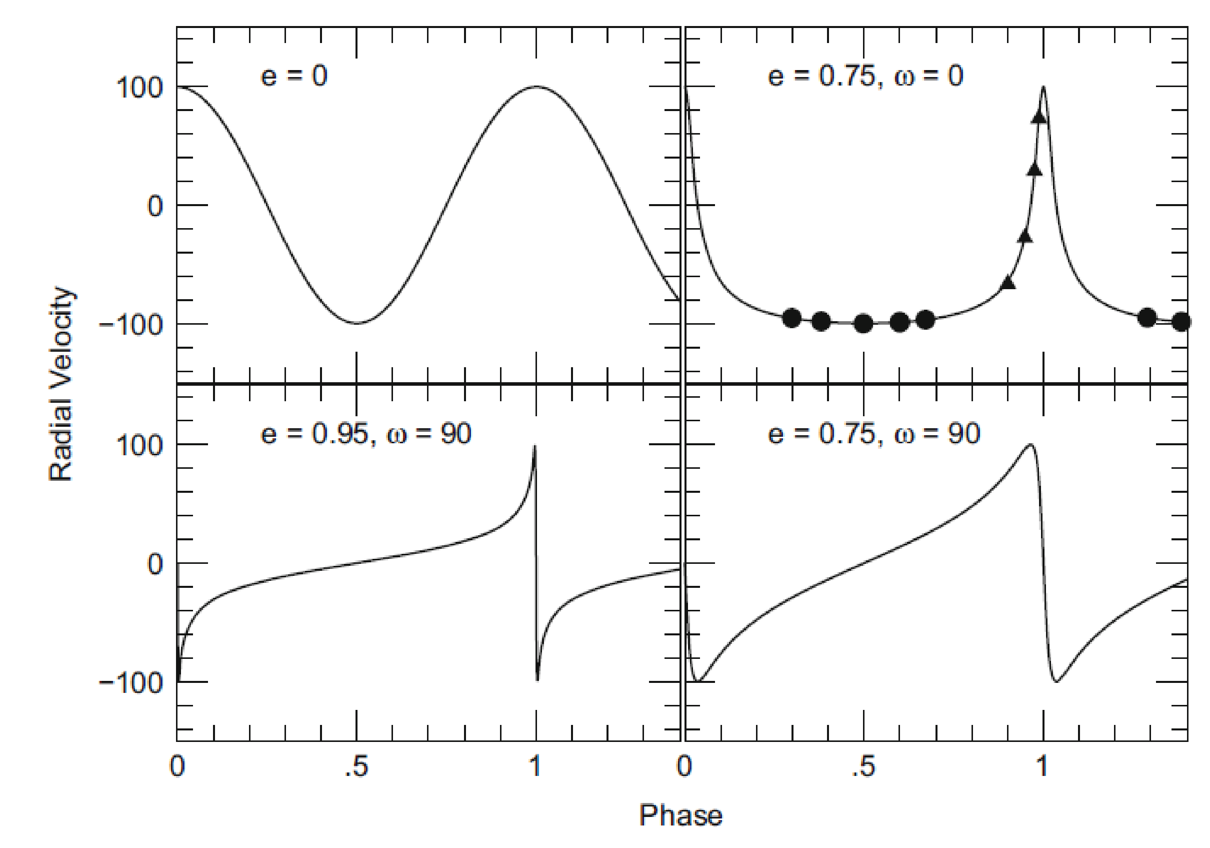

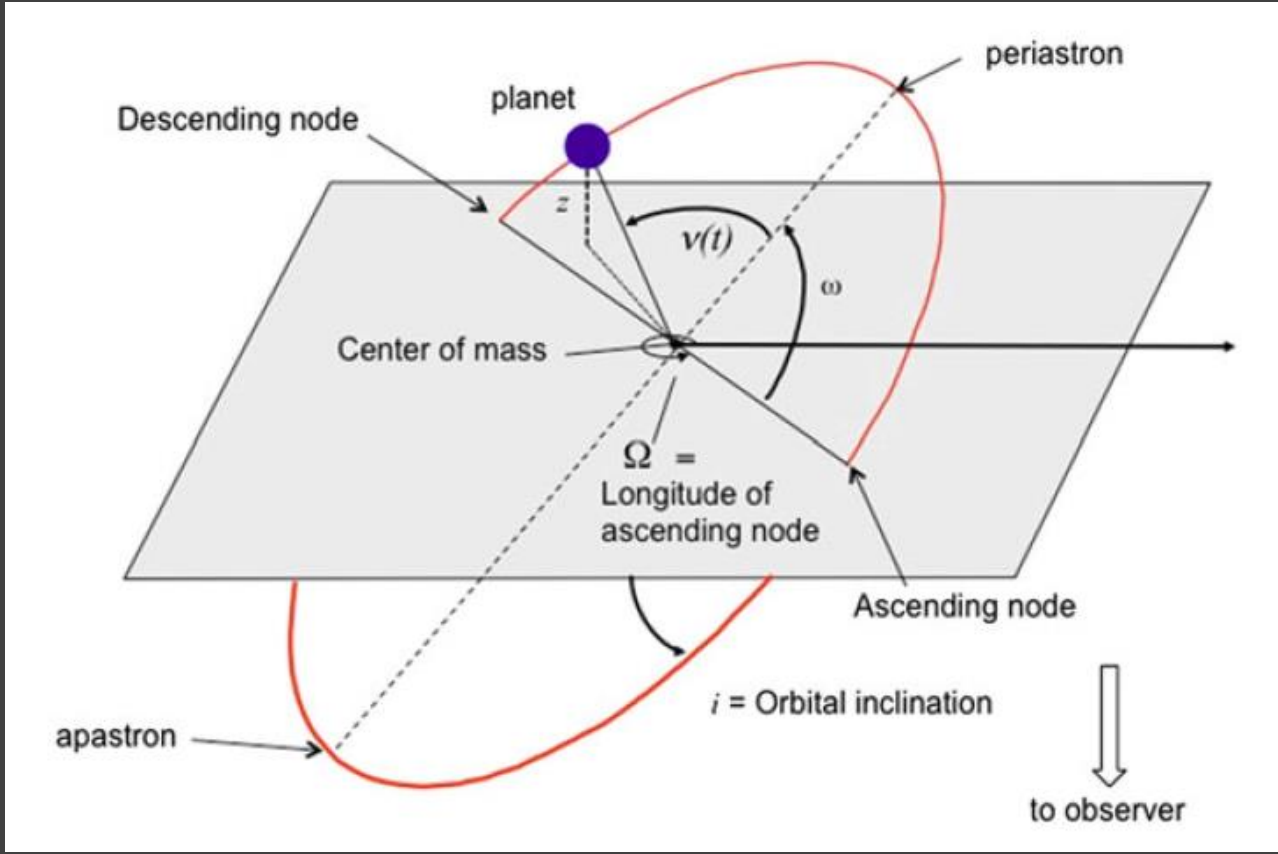

Artie Hatzes (in Bozza et al. 2016)

Planet mass

$$f(m) = \frac{M_2^3 \sin^3 i}{(M_1 + M_2)^2} = \frac{K_1^3 P (1 - e^2)^{3/2}}{2\pi G} \approx \frac{M_2^3 \sin^3 i}{M_1{}^2}$$

Thus, it is necessary to know the stellar mass (M_1)

$$\langle \sin\, i \rangle = \frac{\int_0^\pi p(i) \sin\, i\, di}{\int_0^\pi p(i)\, di} = \frac{\pi}{4} = 0.79$$

For the mass function
<$\sin^3$ i> is important:

$$\frac{\int_0^\pi p(i) \sin^3 i\, di}{\int_0^\pi p(i)\, di} = 0.5 \int_0^\pi \sin^4 i\, di = \frac{3\pi}{16} = 0.59$$

Stellar noise

Phenomenon	RV amplitude (m s^{-1})	Time scales
Solar-like oscillations	0.2–0.5	~5–15 min
Stellar activity (e.g., spots)	1–200	~2–50 days
Granulation/Convection pattern	~ few	~3–30 years

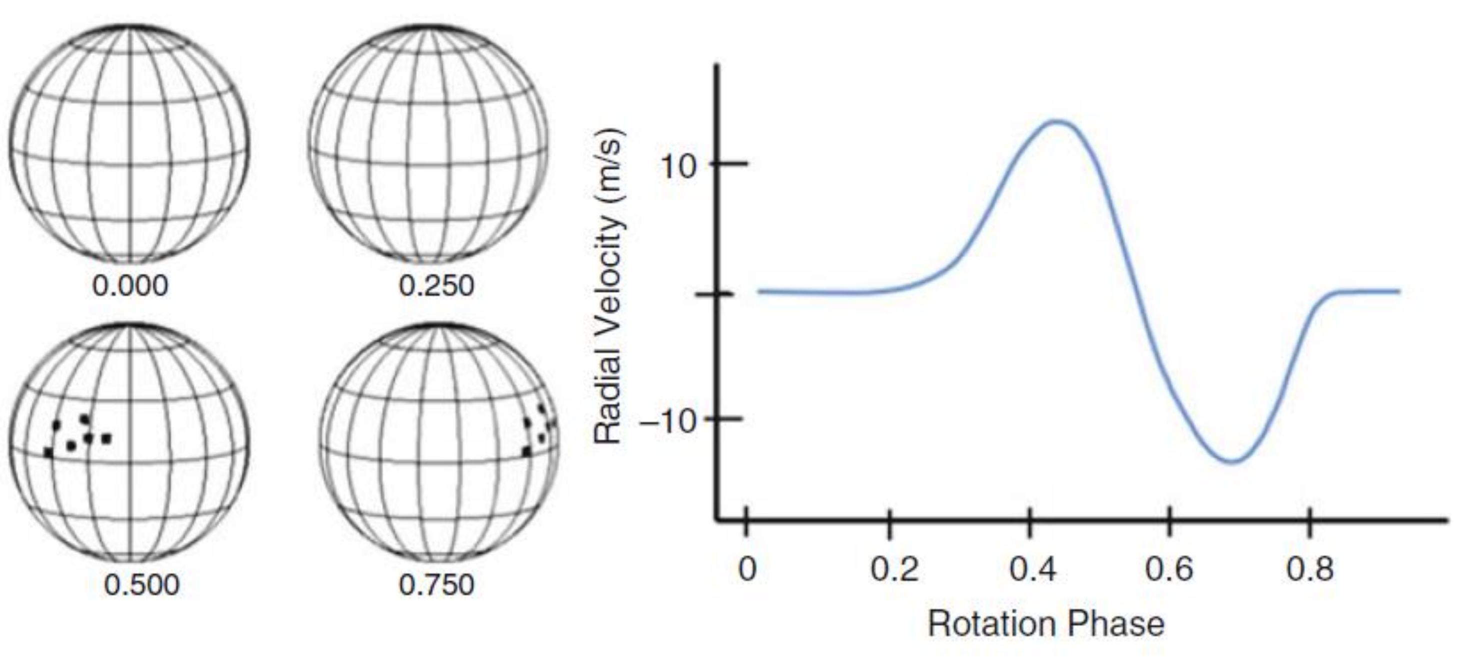

Proposals of special space mission

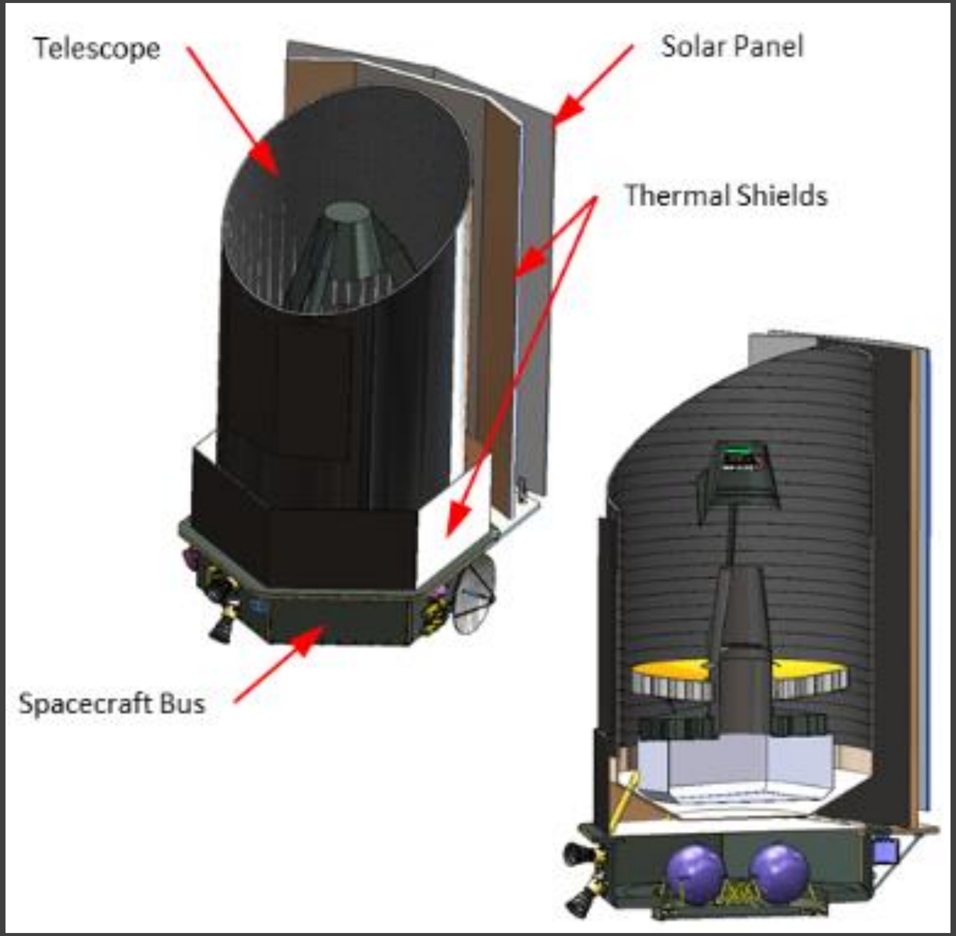

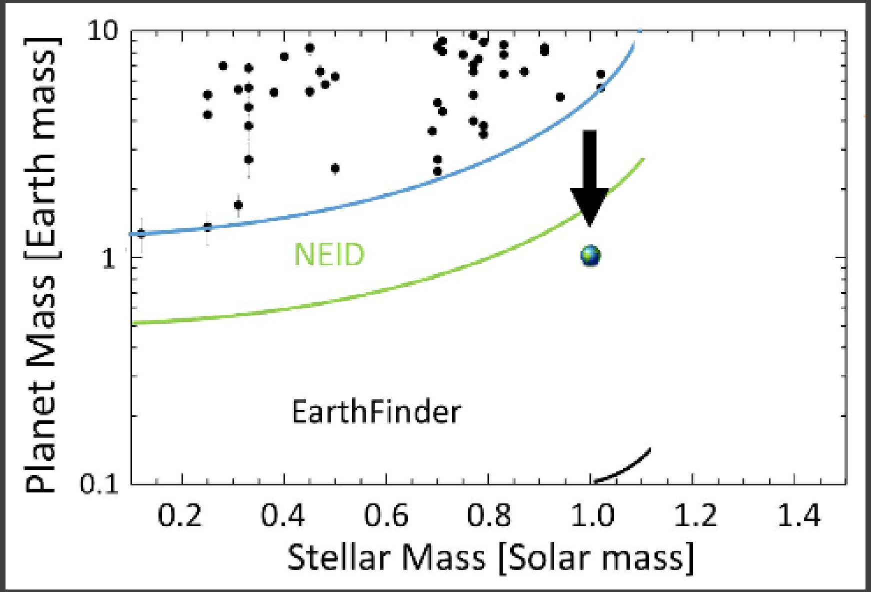

The nominal spacecraft design is based upon the Kepler spacecraft by Ball Aerospace, with a 1.4-m primary, with the starlight coupled into single-mode fibers illuminating three high-resolution, compact and diffraction-limited spectrometer "arms", one covering the near-UV (200-380nm), visible(380-900 nm) and near-infrared (NIR; 900-2500 nm) respectively with a spectral resolution of greater than 150,000 in the visible and near-infrared arms.

Planet transits

Proposed by
Otto Struve
in 1952

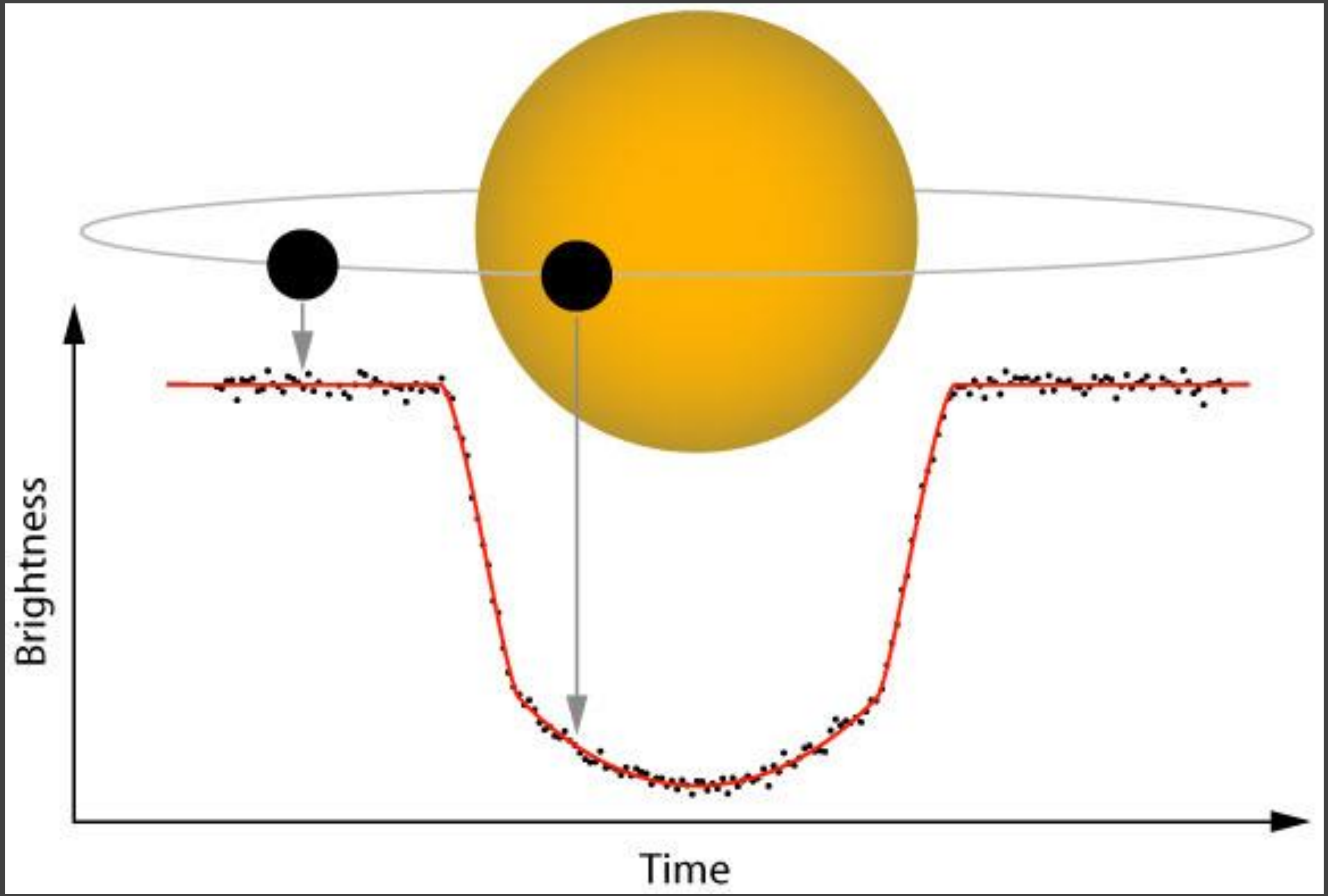

$$\frac{S_{star}-S_{planet}}{S_{star}}$$

Limb darkening
is important!!!

The first transit measurement. HD 209458

The first measurements of a transit was made from the ground for a planet discovered by RV, and so known orbital parameters.

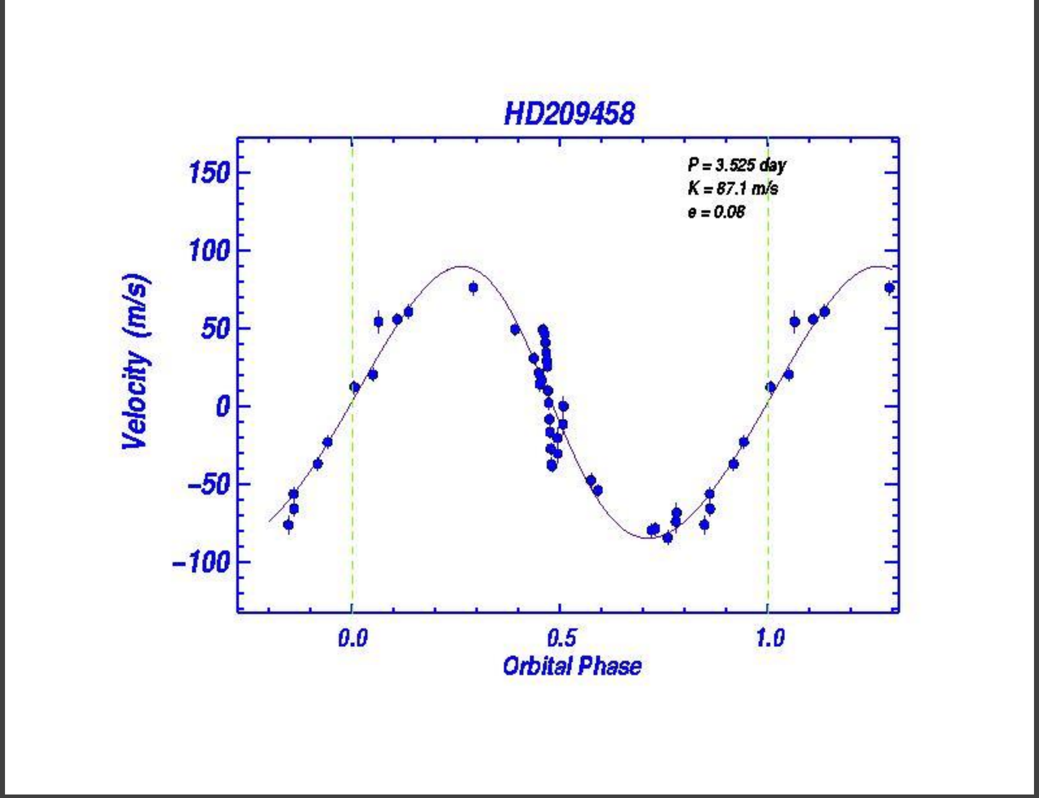

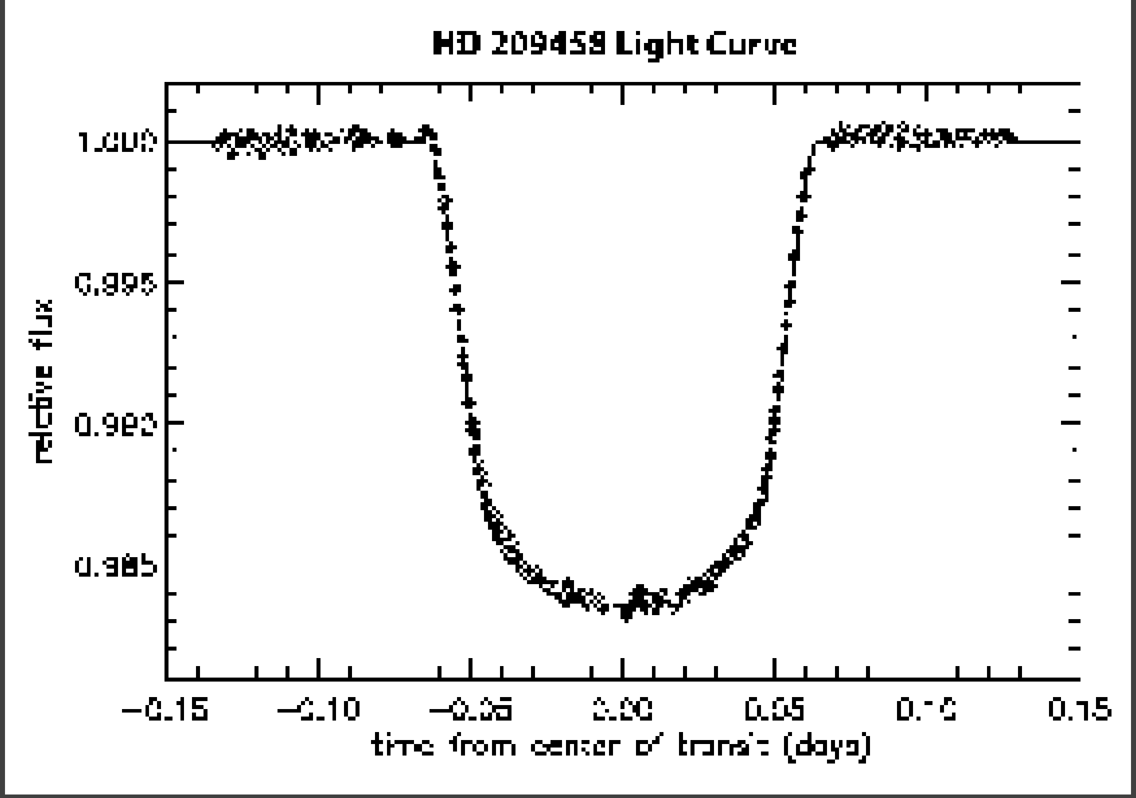

Kepler and CoRoT

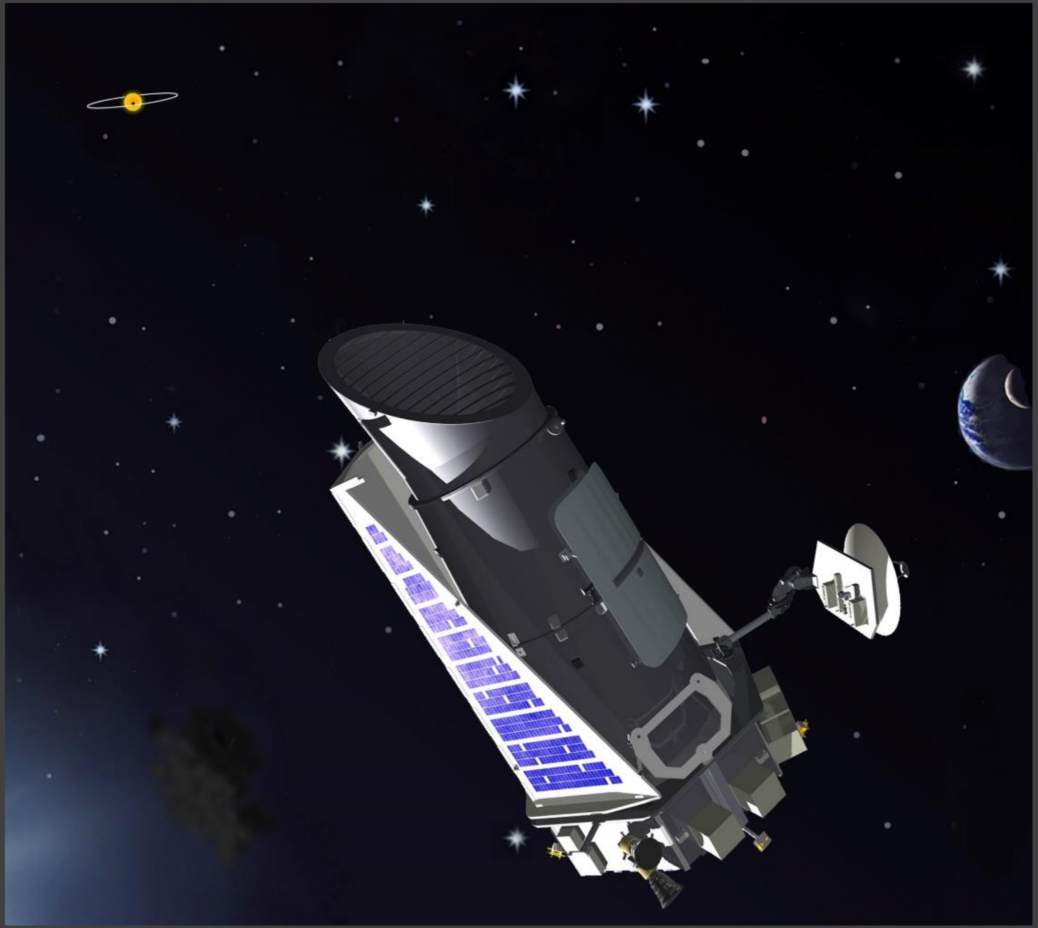

Rate of discovery

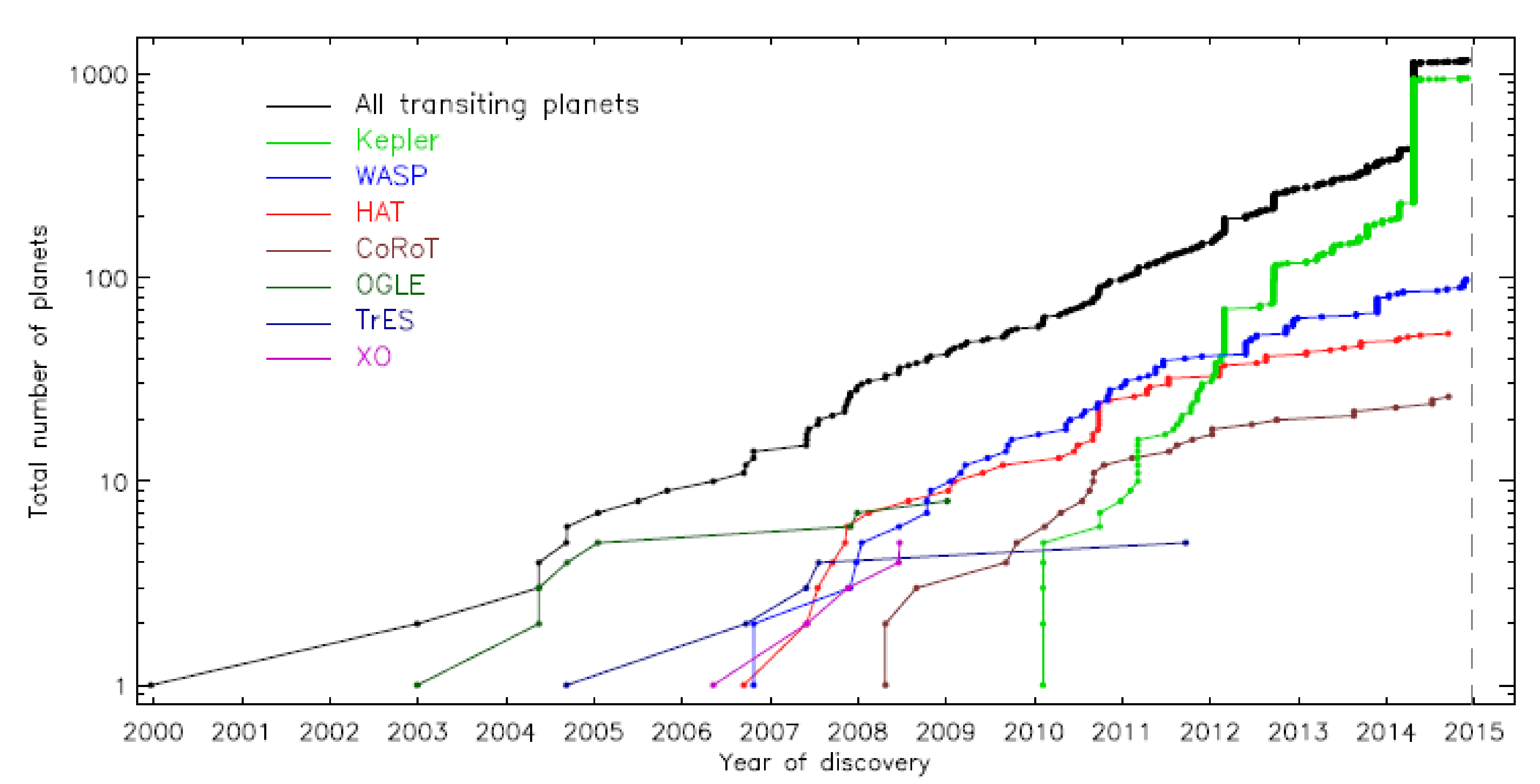

1411.5517

Transiting planets in the sky

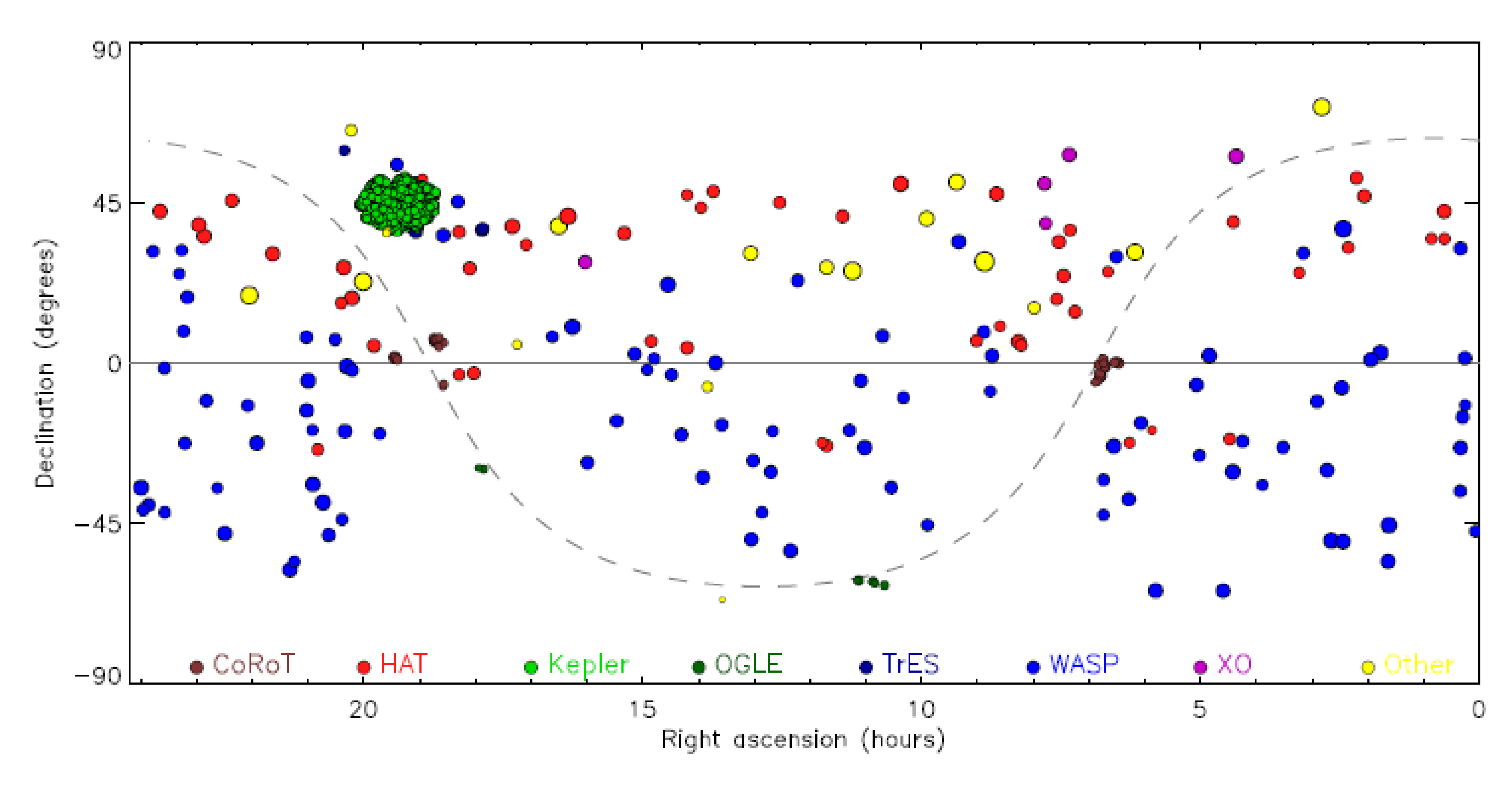

1411.5517

Very small planets

Kepler-37b
The first discovered exoplanet
with size smaller than Mercury

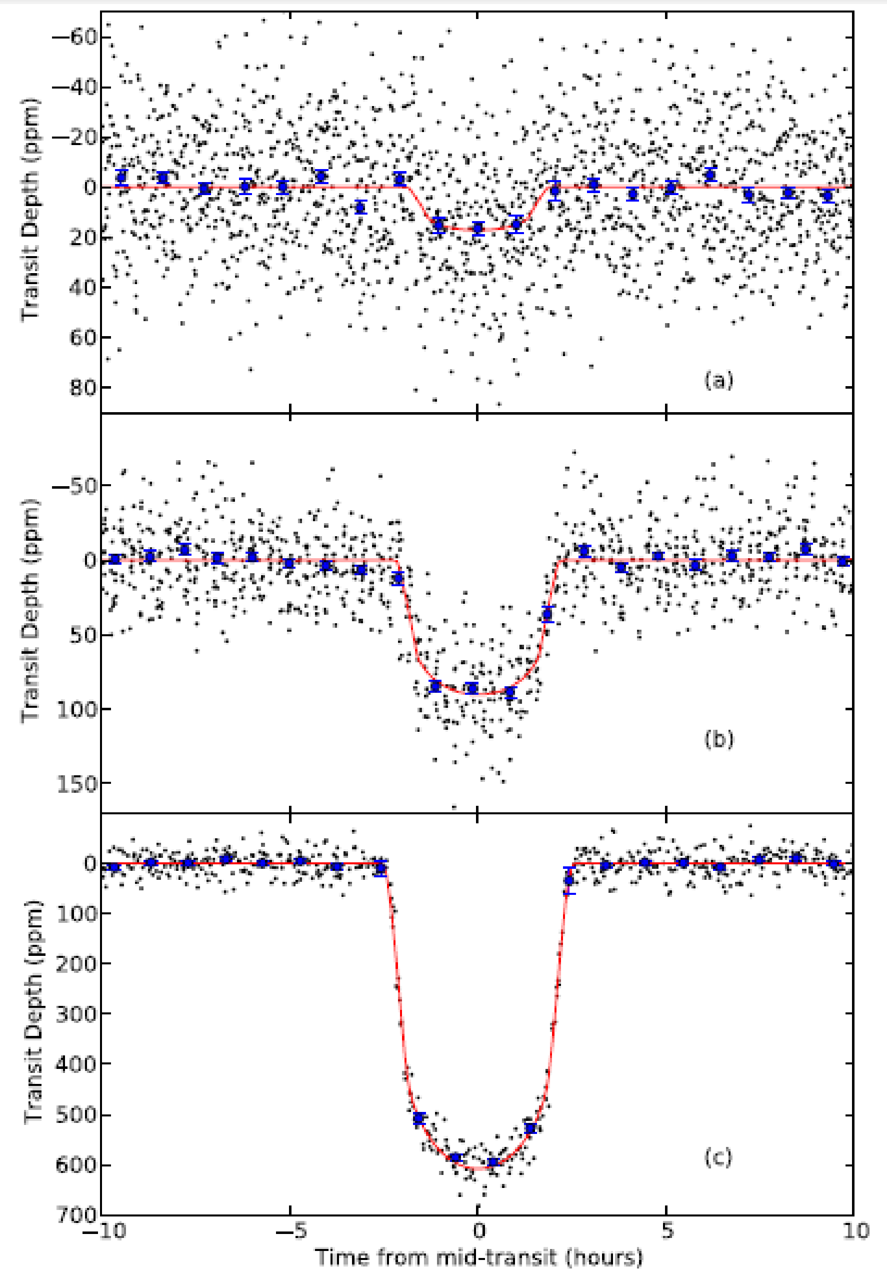

Transit probability

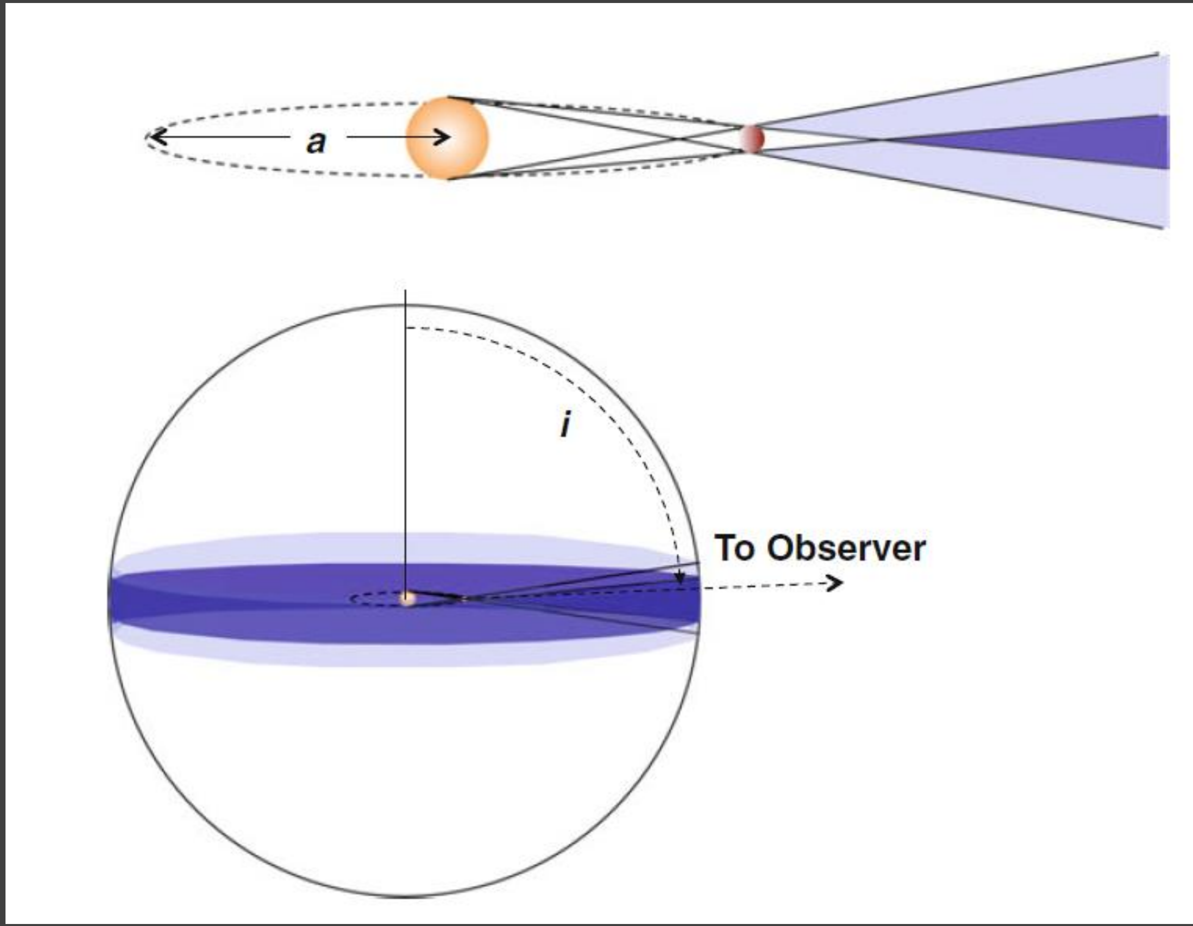

$$\Pr\left(\cos i < \frac{R_*}{a}\right) = \simeq 0.0046\left(\frac{R_*}{R_\odot}\right)\left(\frac{1\,\mathrm{au}}{a}\right).$$

Andrew Cameron (in Bozza et al. 2016)

Transit conditions

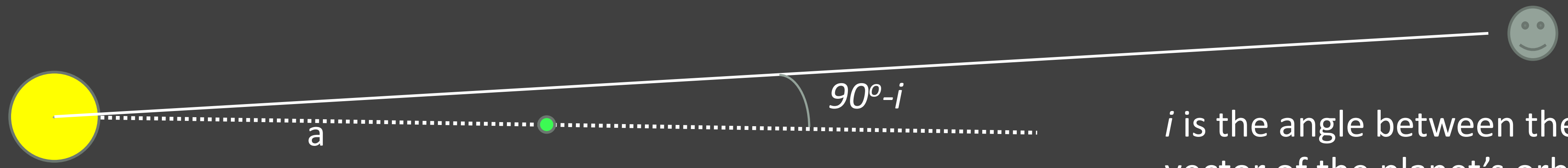

i is the angle between the angular-momentum vector of the planet's orbit andthe line of sight

$$b = \frac{a \cos i}{R_*}.$$

$$\frac{d\Omega}{4\pi} = \frac{2\pi \sin i \, di}{4\pi} = \frac{d(\cos i)}{2}.$$

$$\Pr\left(\cos i < \frac{R_* + R_\mathrm{p}}{a}\right) = \frac{1}{2}\int_{-(R_*+R_\mathrm{p})/a}^{(R_*+R_\mathrm{p})/a} = \frac{R_* + R_\mathrm{p}}{a}.$$

$$R_\mathrm{p} \ll R_*,$$

$$\Pr\left(\cos i < \frac{R_*}{a}\right) = \simeq 0.0046 \left(\frac{R_*}{R_\odot}\right)\left(\frac{1\,\mathrm{au}}{a}\right).$$

Selection in favour of close-in planets.

Andrew Cameron (in Bozza et al. 2016)

Transit depth

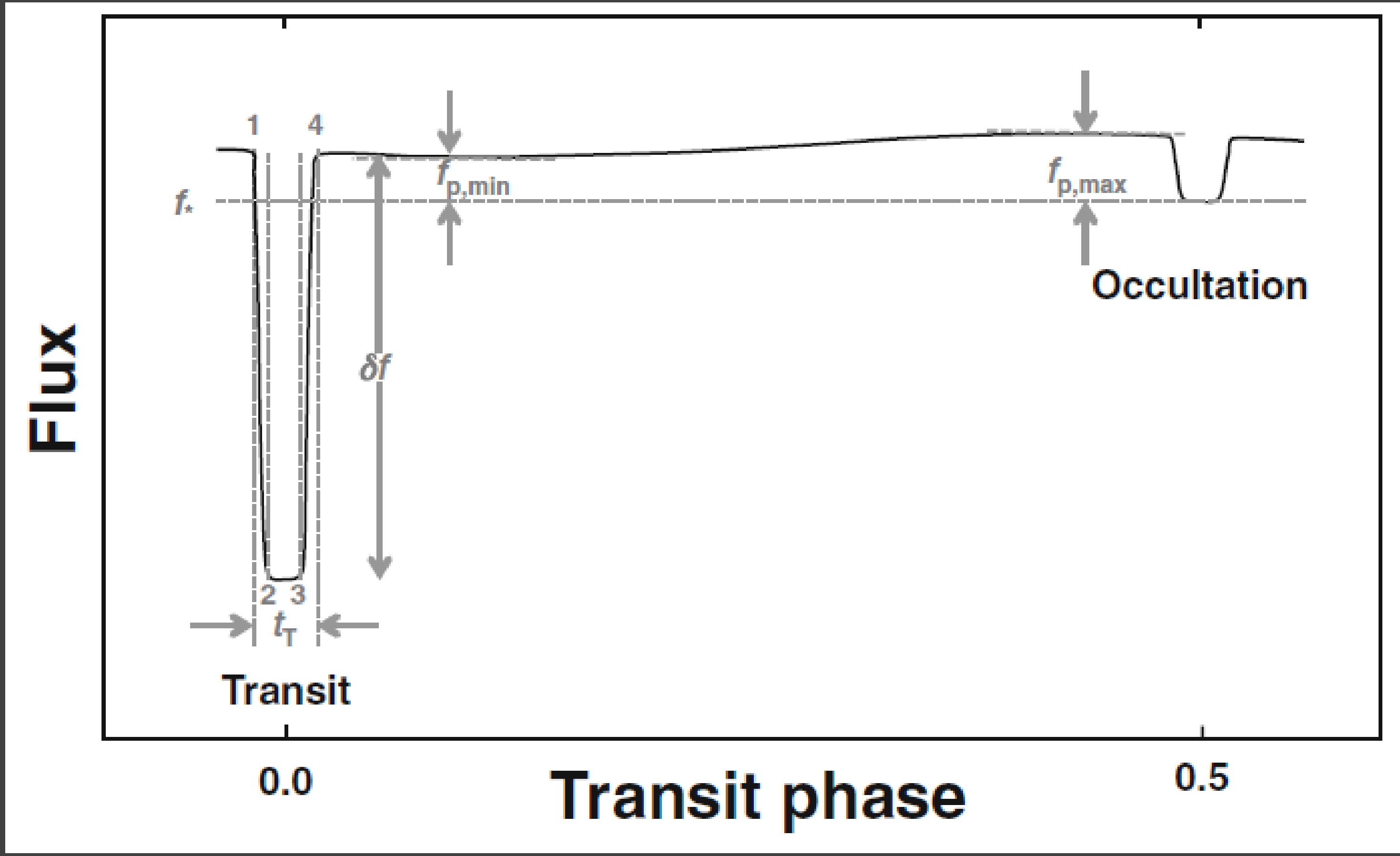

$$\frac{\Delta f}{f} \simeq \left(\frac{R_p}{R_*}\right)^2 = 0.0105\left(\frac{R_p}{R_{Jup}}\right)^2\left(\frac{R_*}{R_\odot}\right)^{-2}$$

Non-uniform brightness distribution (limb darkening) is important.

Limb darkening

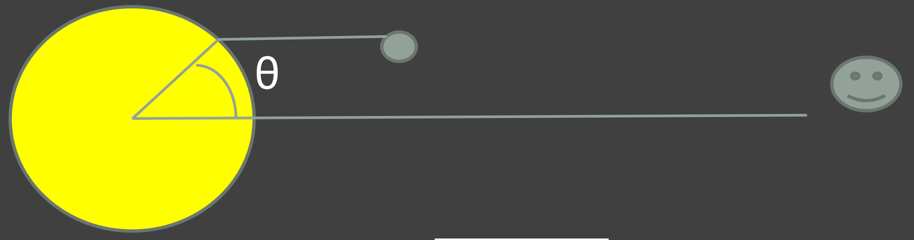

$$\mu = \cos\theta = \sqrt{1 - b^2}$$

$$I = I_0(1 - u(1 - \mu))$$

$$\frac{\Delta f}{f} = \frac{\pi R_{\mathrm{p}}^2 I_0 (1 - u + u\cos\theta)}{2\pi R_*^2 I_0 \int_0^{\pi/2} (1 - u + u\cos\theta)\sin\theta\cos\theta d\theta}$$
$$= \frac{3(1 - u + u\sqrt{1 - b^2})}{3 - u}\left(\frac{R_{\mathrm{p}}}{R_*}\right)^2.$$

Limb darkening can be taken into account in a more precise manner

$$\frac{I(\mu)}{I_0} = 1 - \sum_{n=1}^{4} u_n (1 - \mu^{n/2}).$$

Andrew Cameron (in Bozza et al. 2016)

Transit duration

$$\frac{t_{\rm tr}}{P} \simeq \frac{R_*}{a}\frac{\sqrt{(1+R_{\rm p}/R_*)^2-b^2}}{\pi}\frac{1+e\sin\omega}{1-e^2}.$$

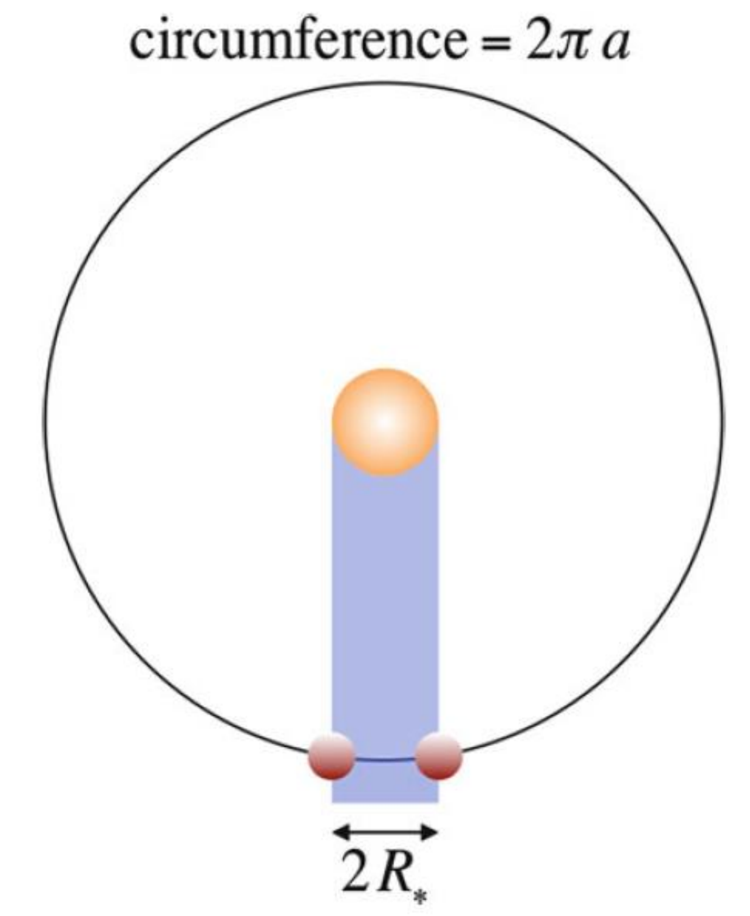

$$\frac{T}{P} = \frac{1}{\pi}\sin^{-1}\frac{R_*}{a}$$

$$\frac{T}{P} = \frac{1}{\pi}\sin^{-1} R_*\left(\frac{4\pi^2}{GM_*P^2}\right)^{1/3}$$

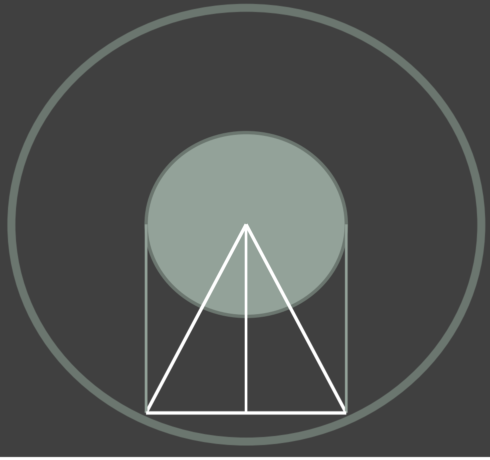

$$\frac{t_T}{P} = \frac{1}{\pi}\sin^{-1}\left(\frac{R_*}{a}\left\{\frac{[1+(R_{\rm p}/R_*)]^2-[(a/R_*)\cos i]^2}{1-\cos^2 i}\right\}^{1/2}\right)$$

t_T – from first to last contact

For $\cos i \ll 1$

$$\frac{t_T}{P} = \frac{R_*}{\pi a}\sqrt{\left(1+\frac{R_{\rm p}}{R_*}\right)^2 - b^2}.$$

System parameters

$$T \simeq 3\mathrm{h}\left(\frac{P}{4\mathrm{d}}\right)^{1/3}\left(\frac{\rho_*}{\rho_\odot}\right)^{-1/3}$$

Stellar density estimate

$$\frac{dv_\mathrm{r}}{dt} = \frac{2\pi K}{P} = \frac{GM_\mathrm{p}}{a^2} = g_\mathrm{p}\frac{R_\mathrm{p}^2}{a^2} = g_\mathrm{p}\frac{R_\mathrm{p}^2}{R_*^2}\frac{R_*^2}{a^2},$$

K – stellar velocity

$$g_\mathrm{p} = \frac{2\pi K}{P}\left(\frac{R_*}{R_\mathrm{p}}\right)^2\left(\frac{a}{R_*}\right)^2$$

Planet density

$$\rho_\mathrm{p} = \frac{3g_\mathrm{p}}{4\pi G R_\mathrm{p}} = \frac{3g_\mathrm{p}}{4\pi G R_*}\left(\frac{R_*}{R_\mathrm{p}}\right)$$

$$R_* = \theta d = \theta/\hat{\pi}:$$

$$\rho_\mathrm{p} = \frac{3g_\mathrm{p}\hat{\pi}}{4\pi G\theta}\left(\frac{R_*}{R_\mathrm{p}}\right)$$

Ground based searches with small cameras

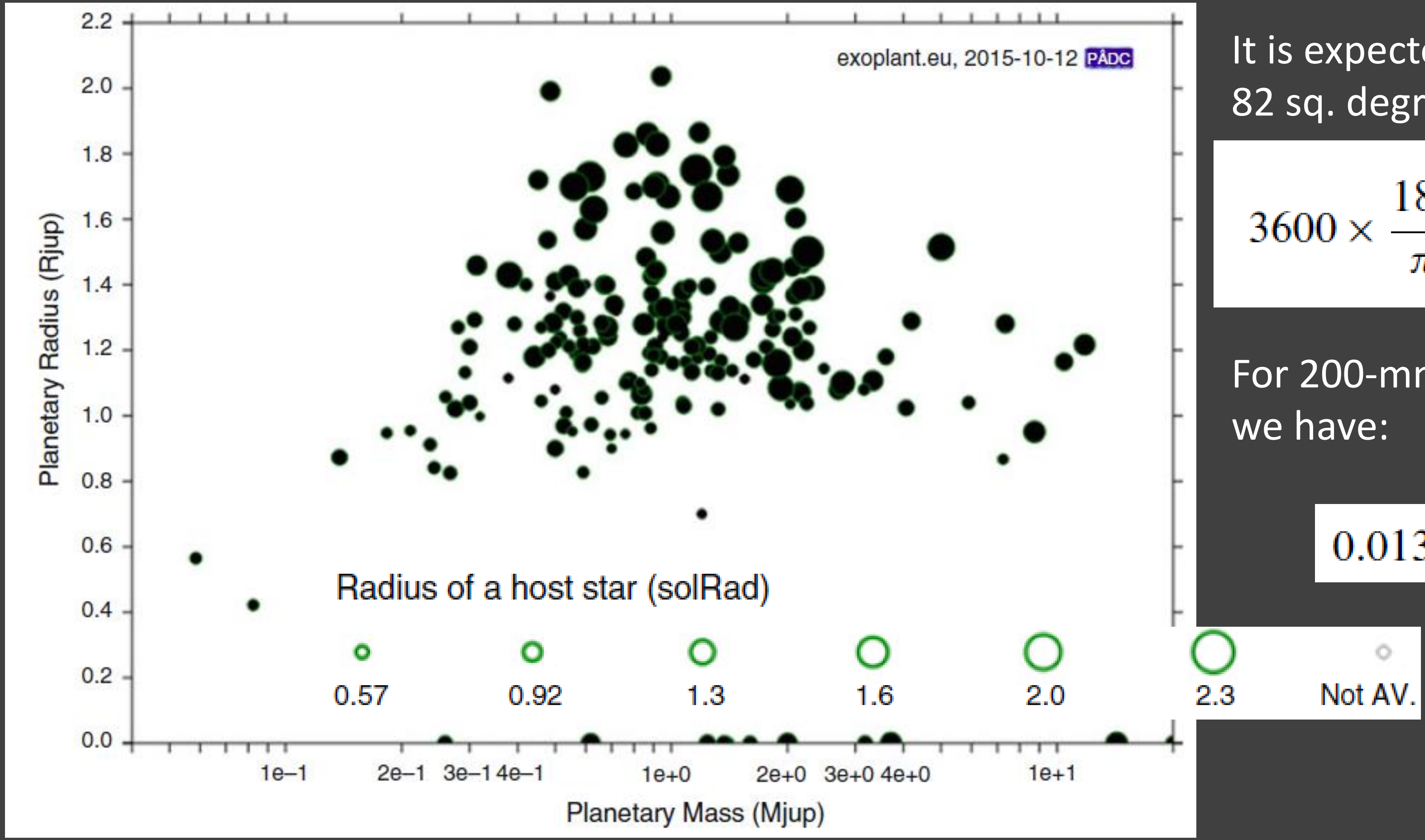

It is expected to have one hot Jupiter per 82 sq. degrees at V<12

$$3600 \times \frac{180}{\pi}\frac{1}{f} = \frac{206265}{f}\,\mathrm{arcsec/mm},$$

Thus one source per 82 sq.deg cooresponds to f=174 mm

For 200-mm camera we have:

$$3600 \times \frac{180}{\pi}\frac{1}{f} = 1031\,\mathrm{arcsec/mm},$$

$$0.0135 \times 1031 = 13.9\,\mathrm{arcsec/pixel}$$

FOV is:

$$\frac{2048 \times 13.9}{3600} = 7.9\,\mathrm{degrees},$$

which gives 52 sq. deg.

Space surveys vs. ground based

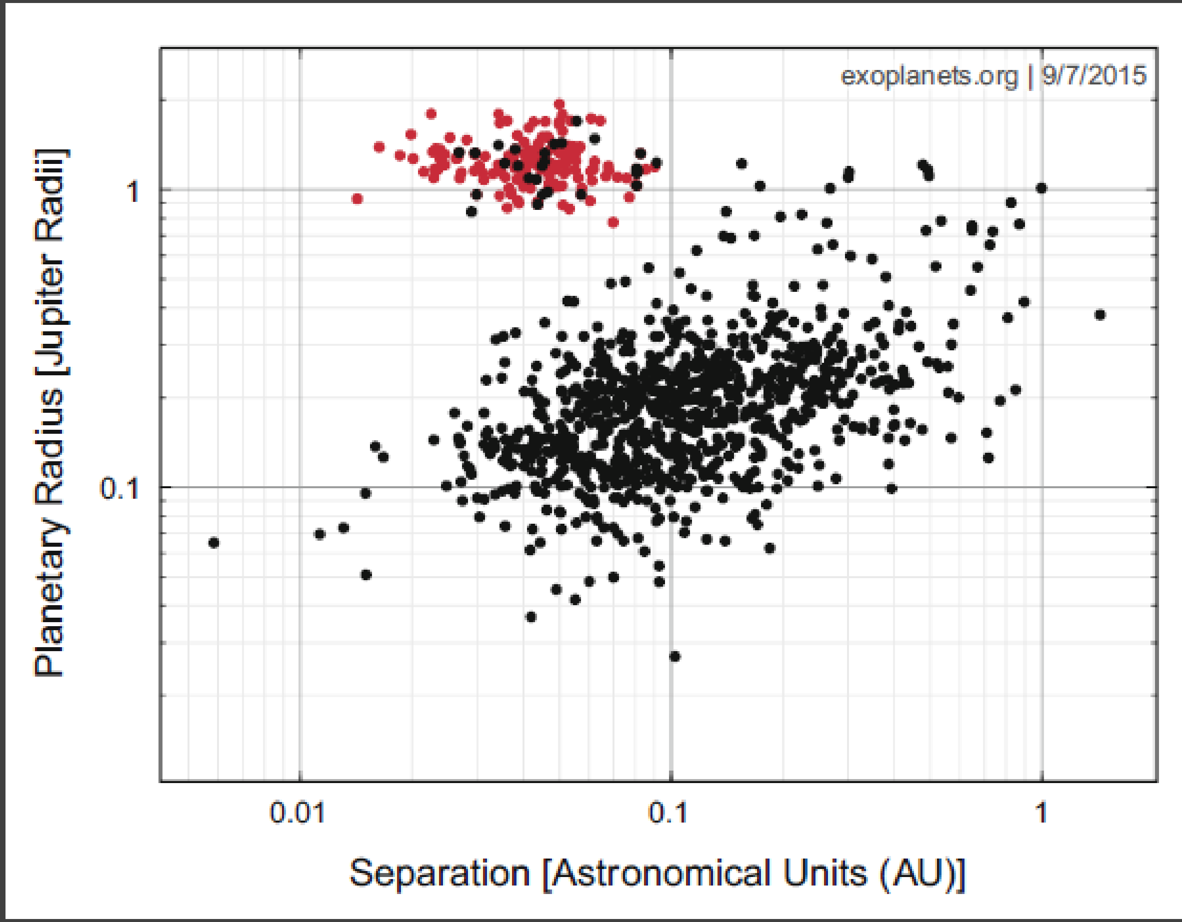

Hot jupiters are rare, but easy to detect from Earth. Space surveys (here – Kepler) show mostly different types of planets.

CoRoT

December 2006 – November 2012
27-cm telescope

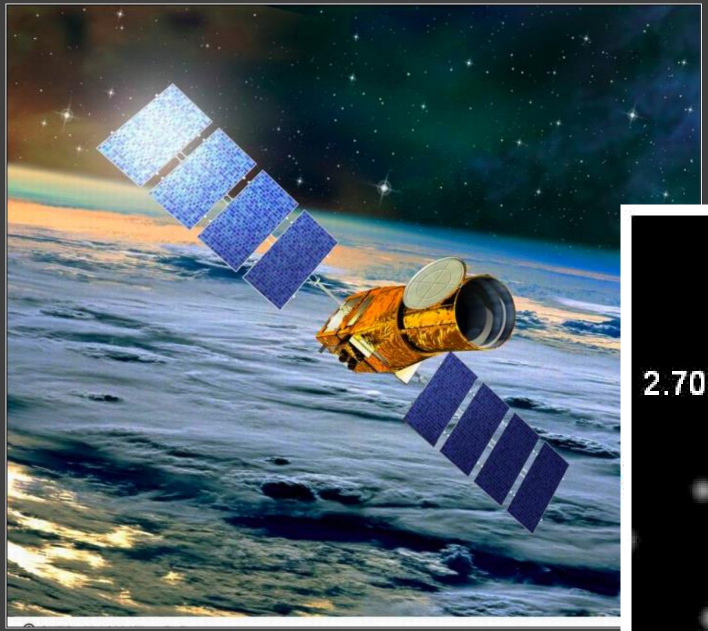

The satellite spent approximately 6 months per year observing in the center direction and
6 months per year observing in the anti-center direction.

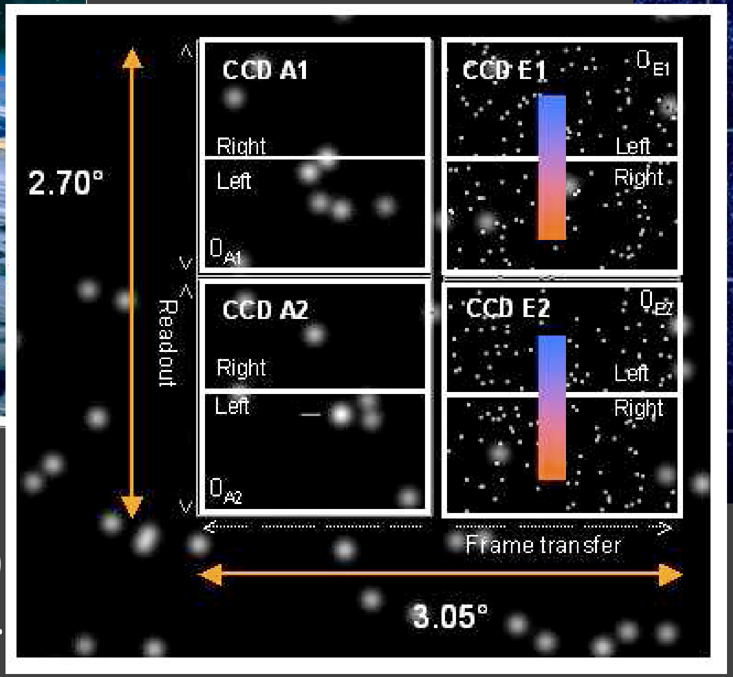

Focal planet arrangement
of the asteroseismology (A1, A2)
and the exoplanet (E1, E2) CCDs.

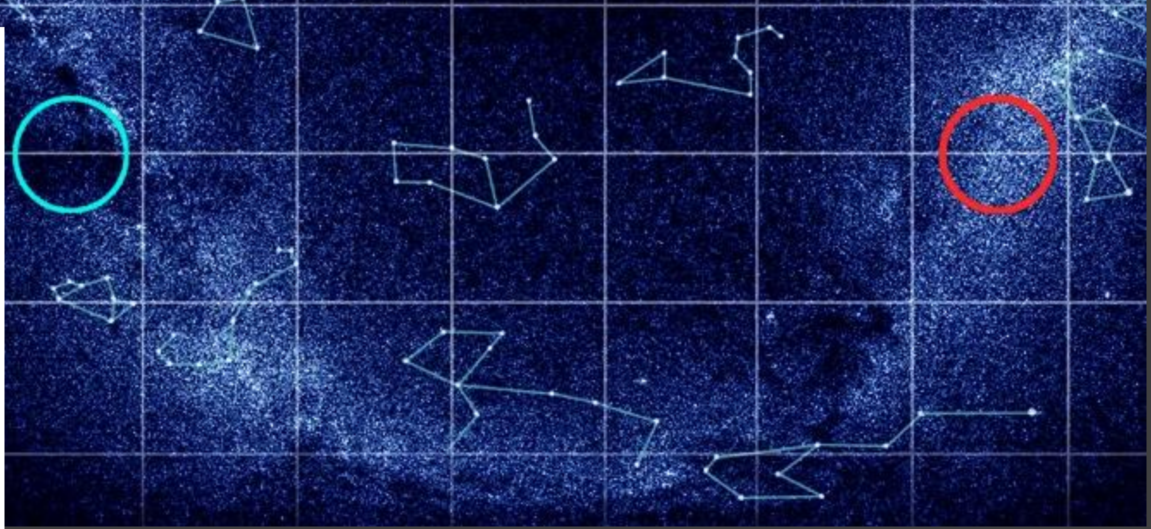

Position of the CoRoT eyes in the sky.
The blue and red circles represent the center and anti-center.

Kepler

2009-2013 + K2-mission
0.95 m telescope

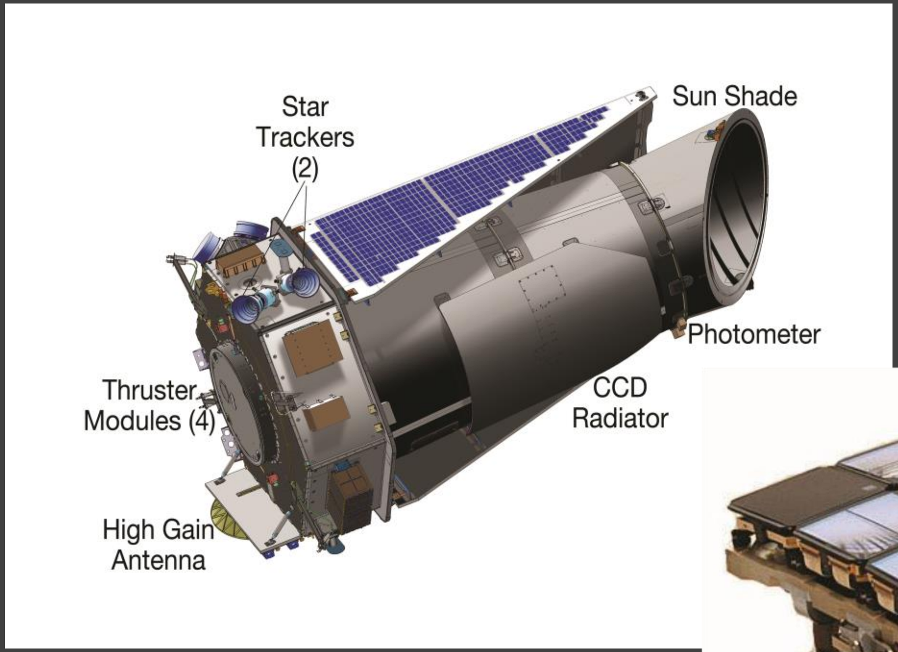

Monitoring of ~150 000 stars

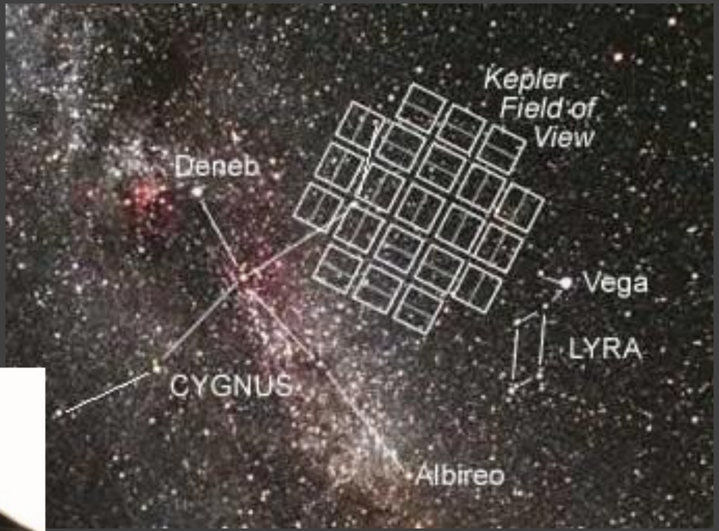

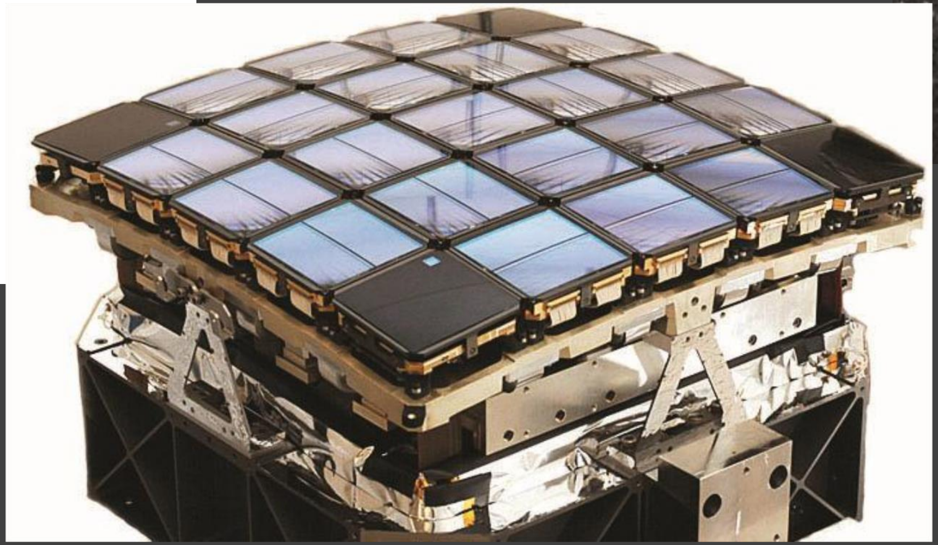

Field of view ~115 sq. degrees

Orbital elements

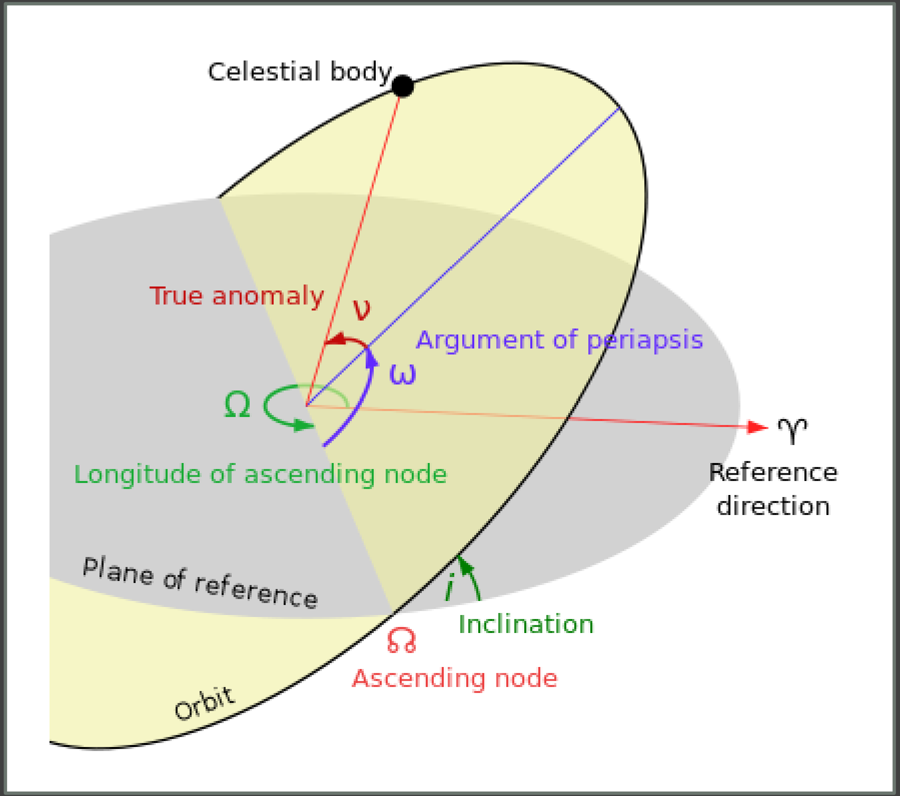

ν – true anomaly
ω – argument of periastron
E - eccentric anomaly
M – mean anomaly

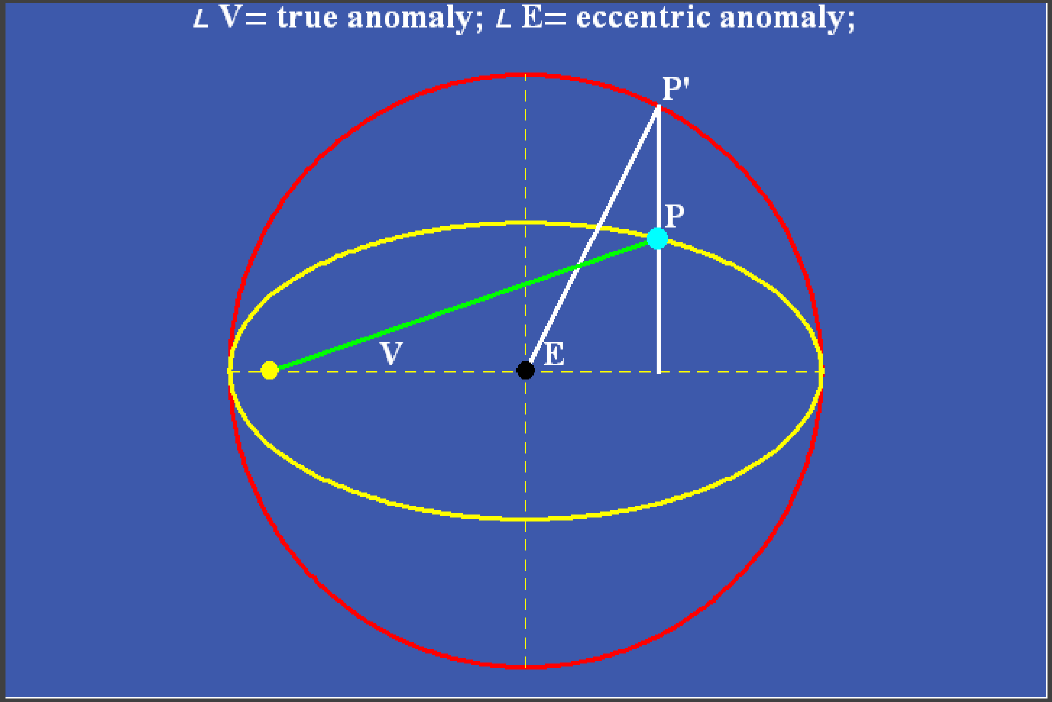

http://www.wlym.com/antidummies/part66.html

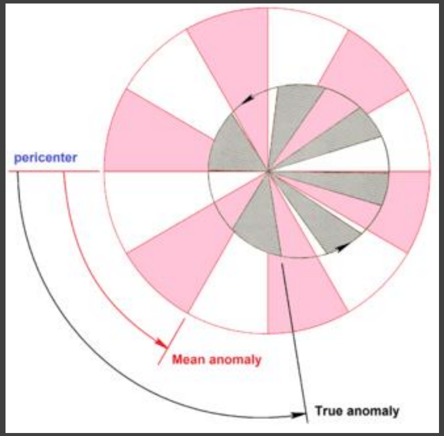

Orbital parameters

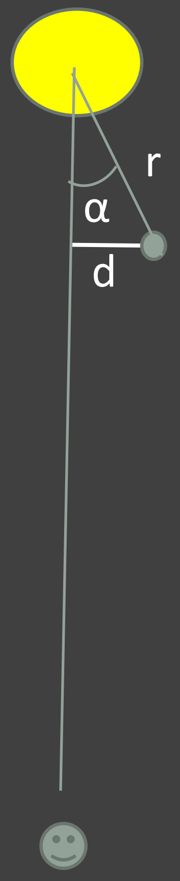

d=r sin α
z=d/R_{star}

p=R_p/R_{star}

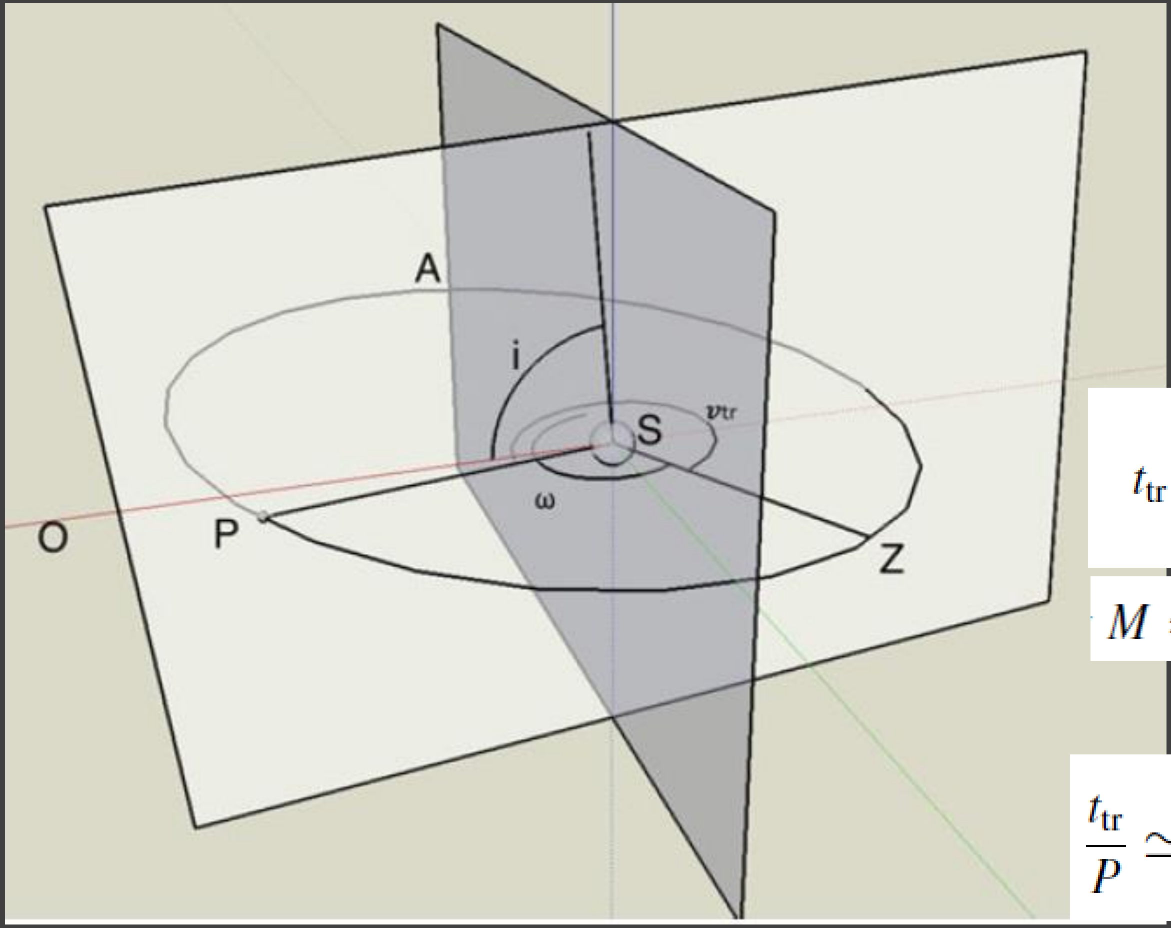

$$\nu_{\rm tr} = \frac{\pi}{2} - \omega \qquad \nu_{\rm occ} = \frac{3\pi}{2} - \omega,$$

$$E = 2\tan^{-1}\left[\sqrt{\frac{1-e}{1+e}}\tan\frac{\nu}{2}\right]$$

$$t_{\rm tr} - t_0 = \frac{P}{2\pi}M_{\rm tr} = \frac{P}{2\pi}(E_{\rm tr} - e\sin E_{\rm tr}).$$

$$M = E - e\sin E. \qquad E_{i+1} = M + e\sin E_i.$$

$$E_1 = M,$$

$$\frac{t_{\rm tr}}{P} \simeq \frac{R_*}{a}\frac{\sqrt{(1+R_{\rm p}/R_*)^2 - b^2}}{\pi}\frac{1+e\sin\omega}{1-e^2}.$$

Andrew Cameron (in Bozza et al. 2016)

Transits and transit-like events

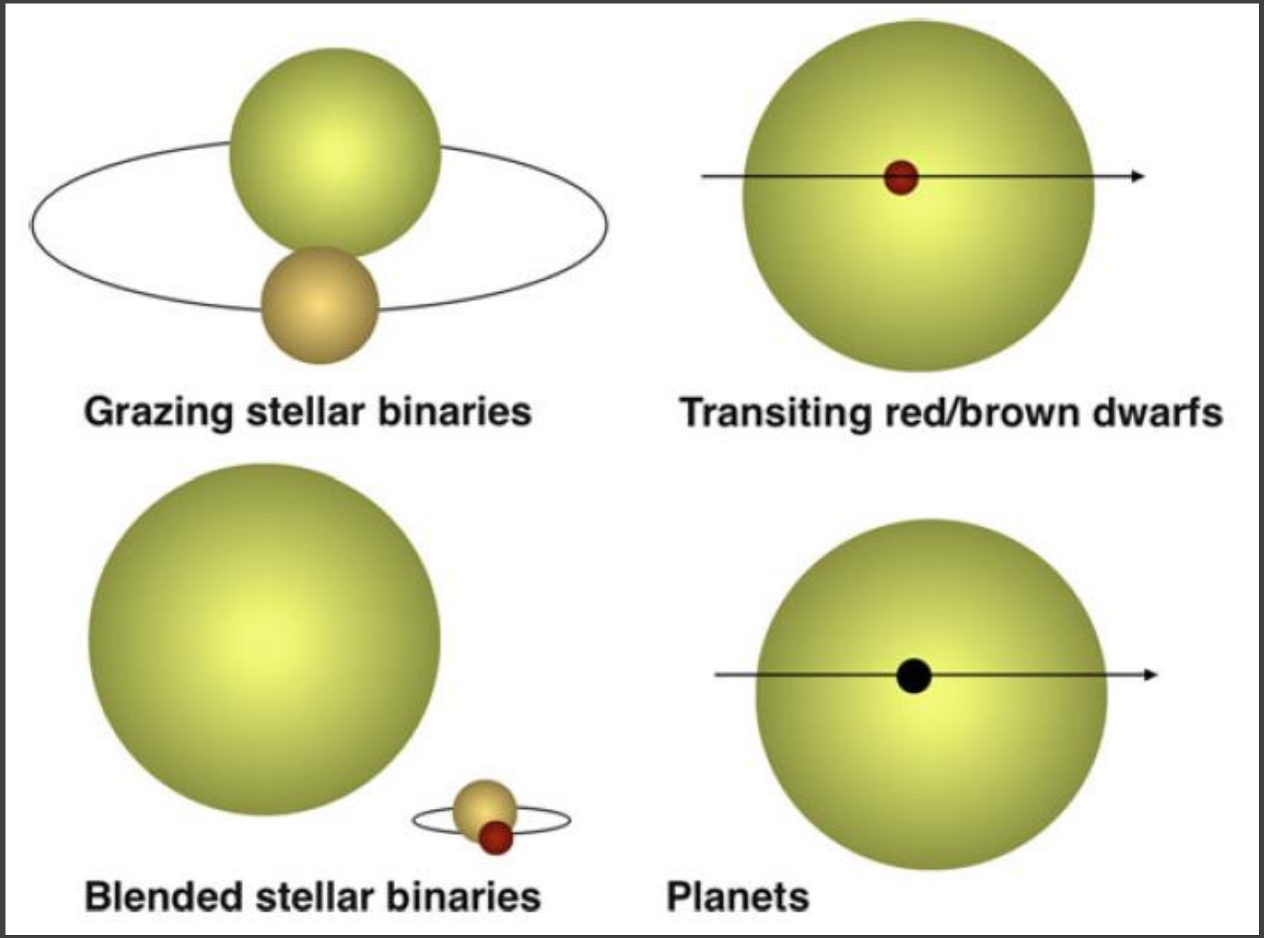

Andrew Cameron (in Bozza et al. 2016)

Spectral lines and planet/star mass ratio

$$\dot{v}_{\rm r} \simeq \frac{GM_*}{a^2} = \frac{2\pi K}{P}\frac{M_*}{M_{\rm p}}.$$

Observations of spectral line in the planet atmosphere can allow to measure important parameters of the system!

Measurements of the radial acceleration (due to observations of spectral lines in the planet atmosphere) allow to measure stellar mass.

$$\frac{T}{P} = \frac{1}{\pi}\sin^{-1}\frac{R_*}{a}$$

$$\delta v_{\rm r} \simeq \frac{P}{\pi}\frac{R_*}{a}\frac{2\pi K}{P}\frac{M_*}{M_{\rm p}}.$$

If narrow spectral lines in the planet atmosphere can be observed during transit then it is possible to derive M_{star}/M_{planet}

Andrew Cameron (in Bozza et al. 2016)

Rossiter–McLaughlin effect

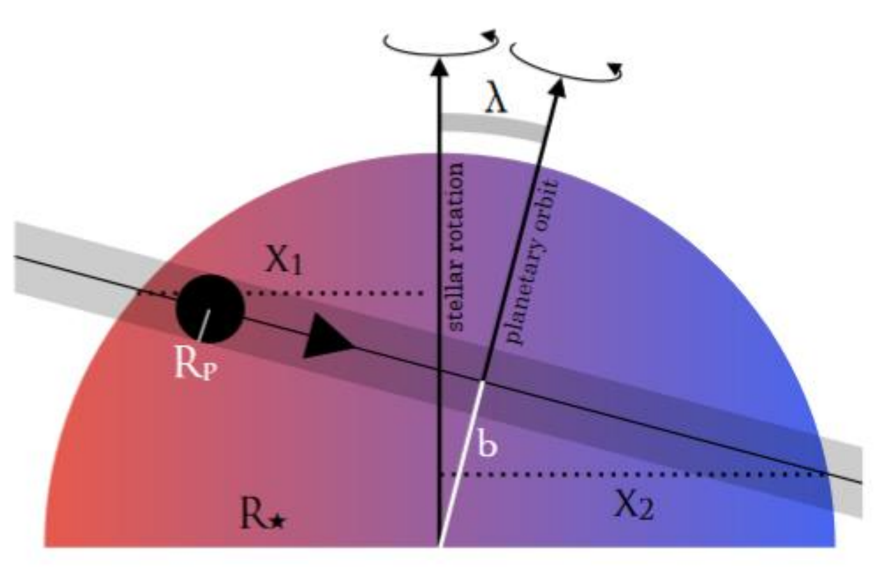

$$A_{\mathrm{RM}} \simeq \frac{2}{3} D v \sin i_\star \sqrt{1-b^2}$$

$$D = (R_p/R_\star)^2$$

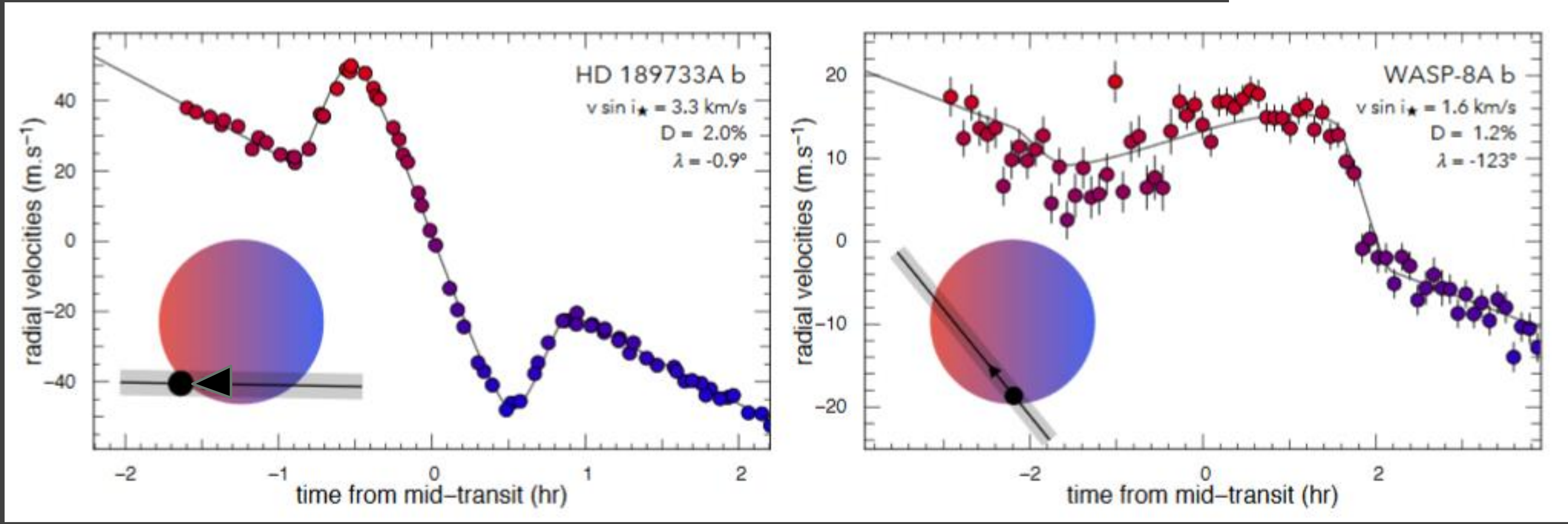

Transit timing variations

$$\delta t_1 = P_1 \frac{m_2}{m_0} f_{12}(\alpha_{12}, \theta_{12}),$$
$$\delta t_2 = P_2 \frac{m_1}{m_0} f_{21}(\alpha_{12}, \theta_{21}),$$

$$\alpha_{ij} = \min(a_i/a_j, a_j/a_i)$$

$$\theta_{ij} = (\lambda_i, e_i, \omega_i, I_i, \Omega_i, \lambda_j, e_j, \omega_j, I_j, \Omega_j)$$

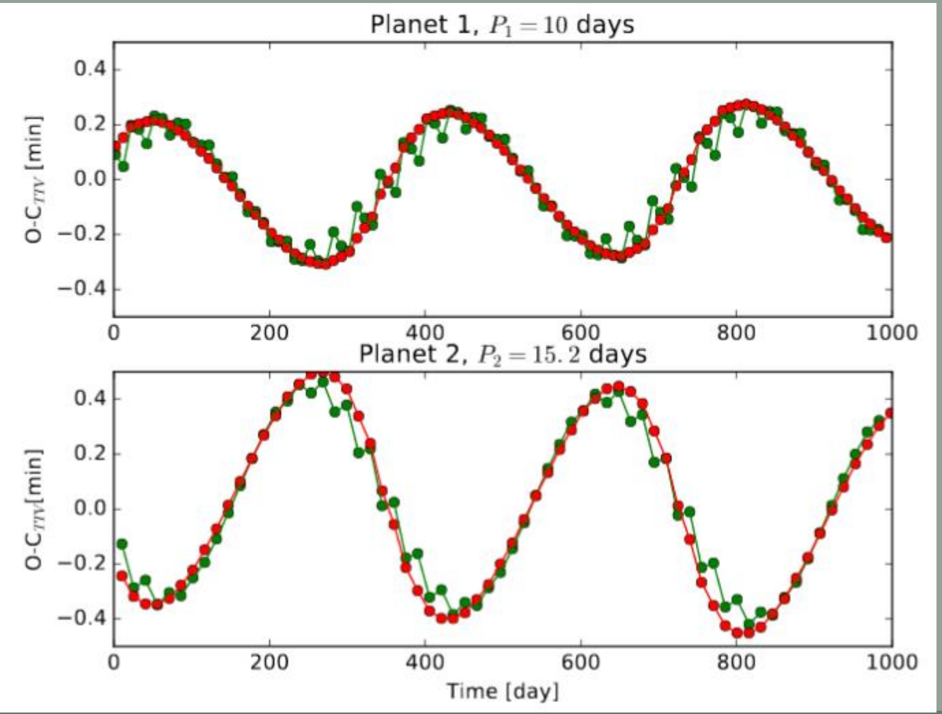

Transit-timing variations of two low-eccentricity planets with larger mass ratio (green) compared with two smaller mass planets with larger eccentricity $e_1=e_2=0.04$

Planets are nearly in 3:2 resonance.

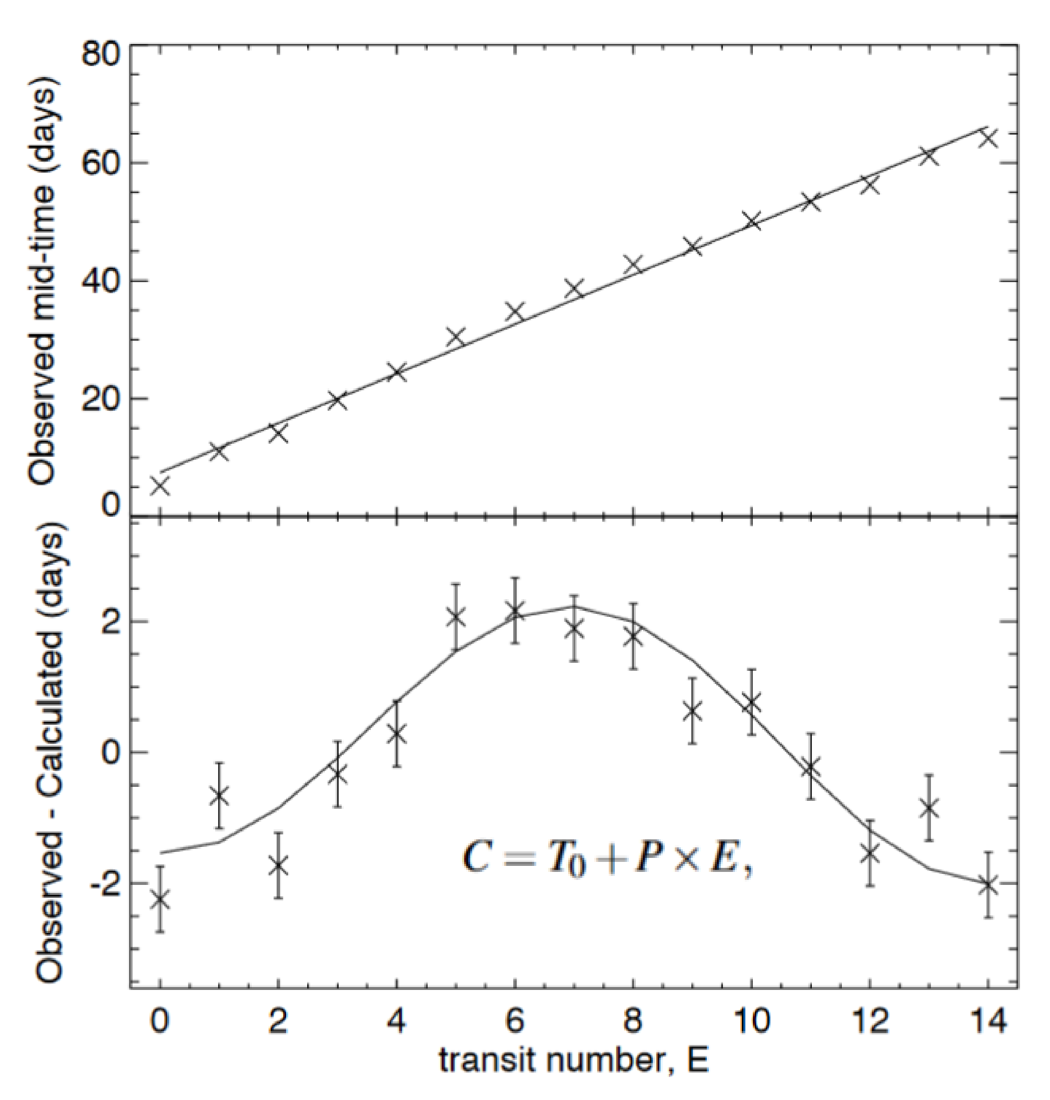

Transit timing variations (TTV)

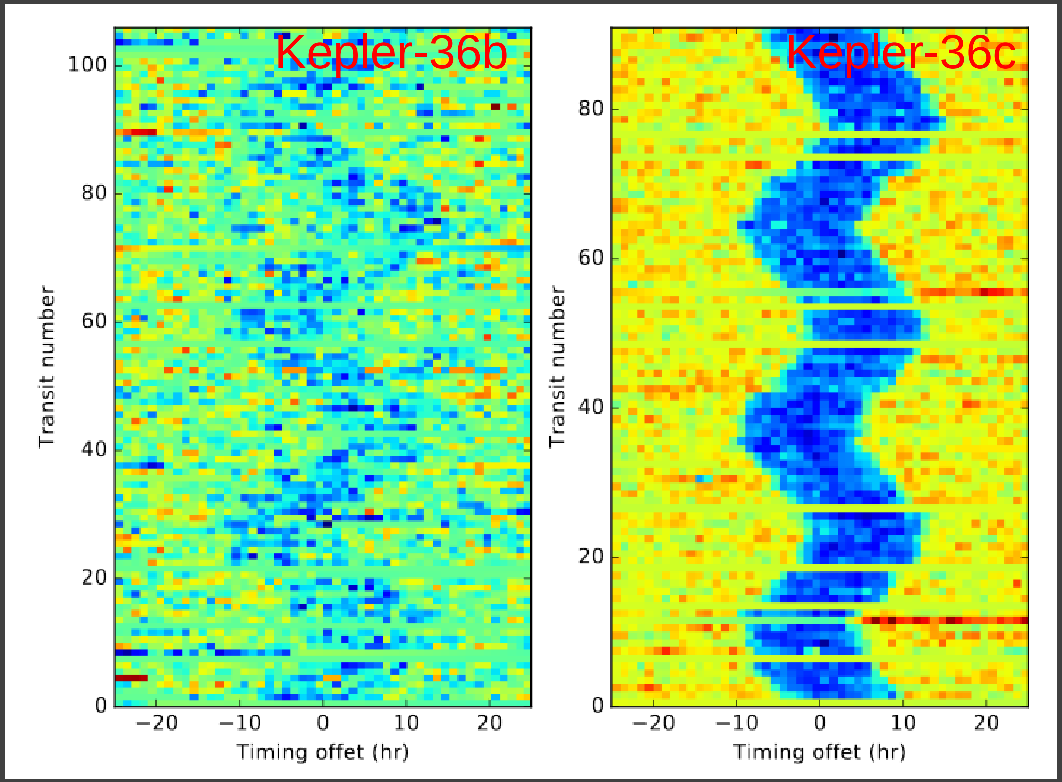

River plot

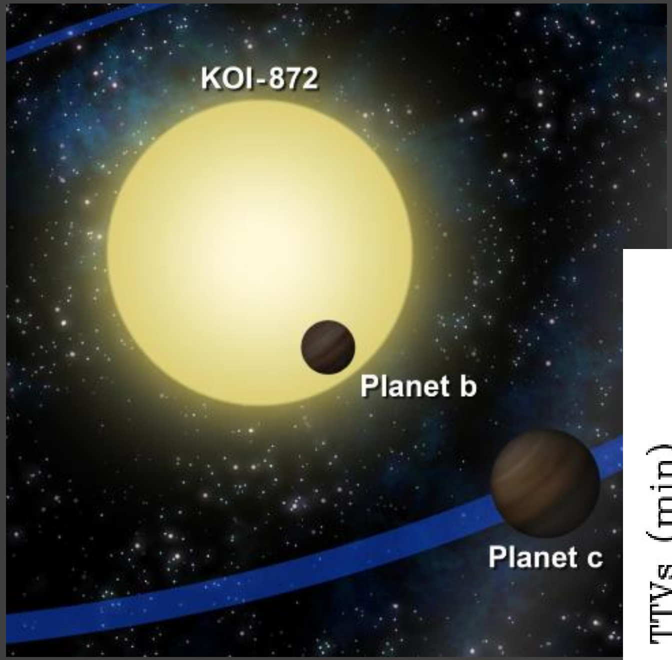

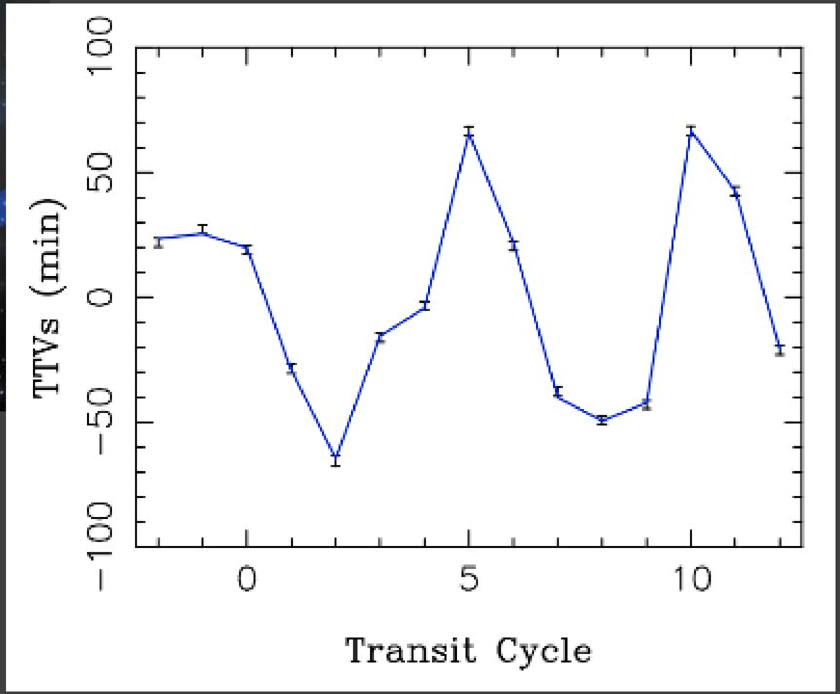

Transit duration variations (TDV)

1706.09849

- Torque due to the rotational oblateness of the star;
- Eccentricity variations due to a resonant interaction;
- Inclination changes due to secular precession of the orbital plane.

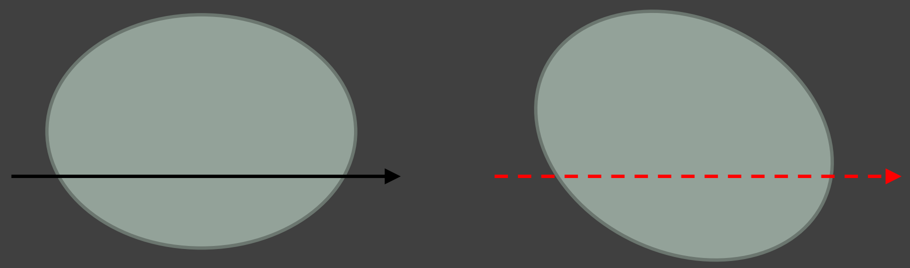

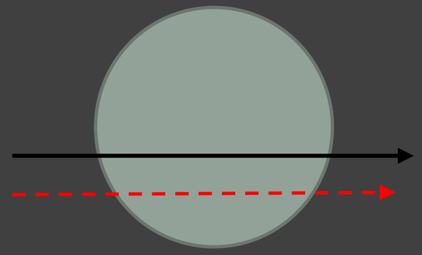

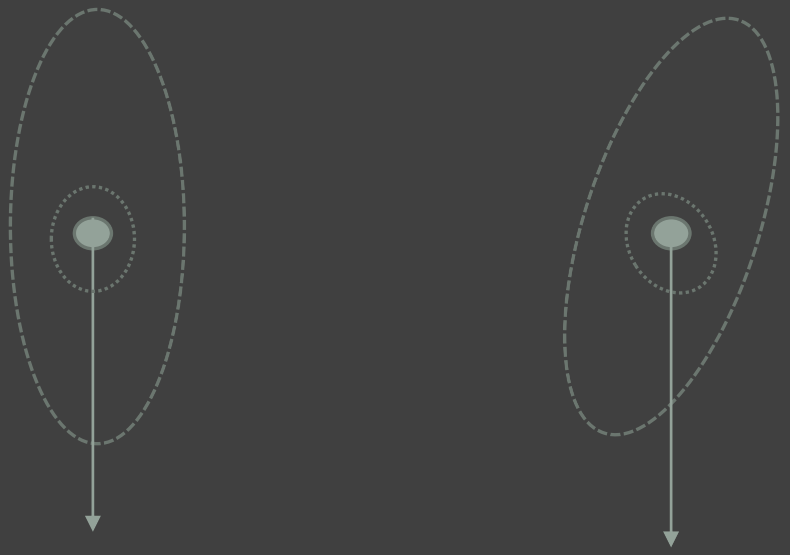

Calculations of transits in 3 body systems

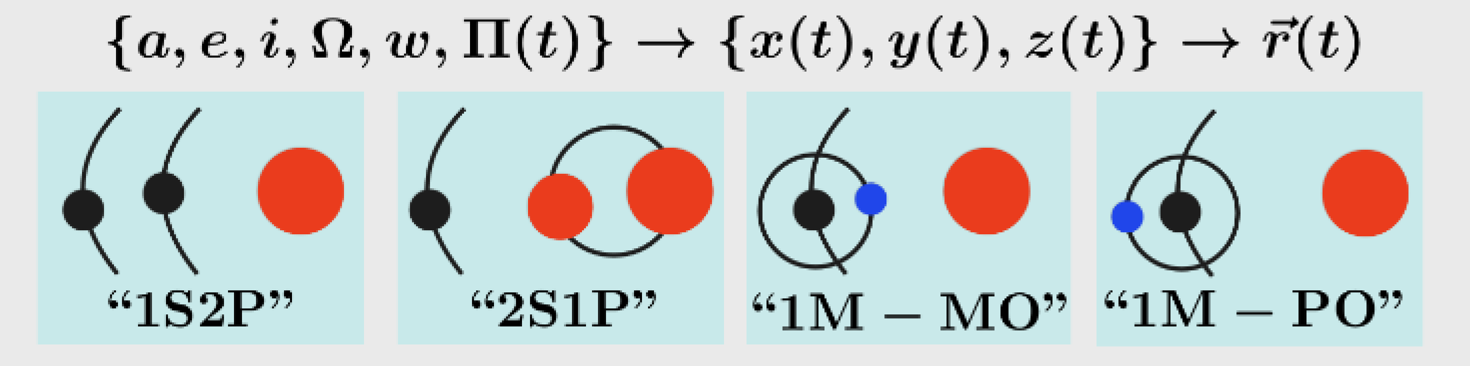

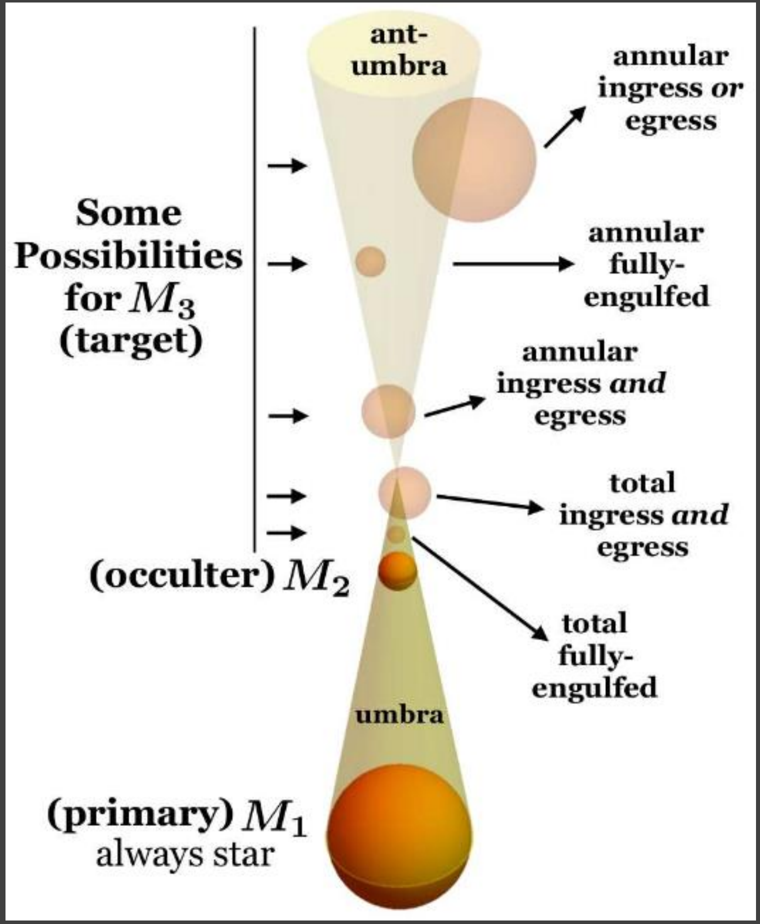

Microlensing

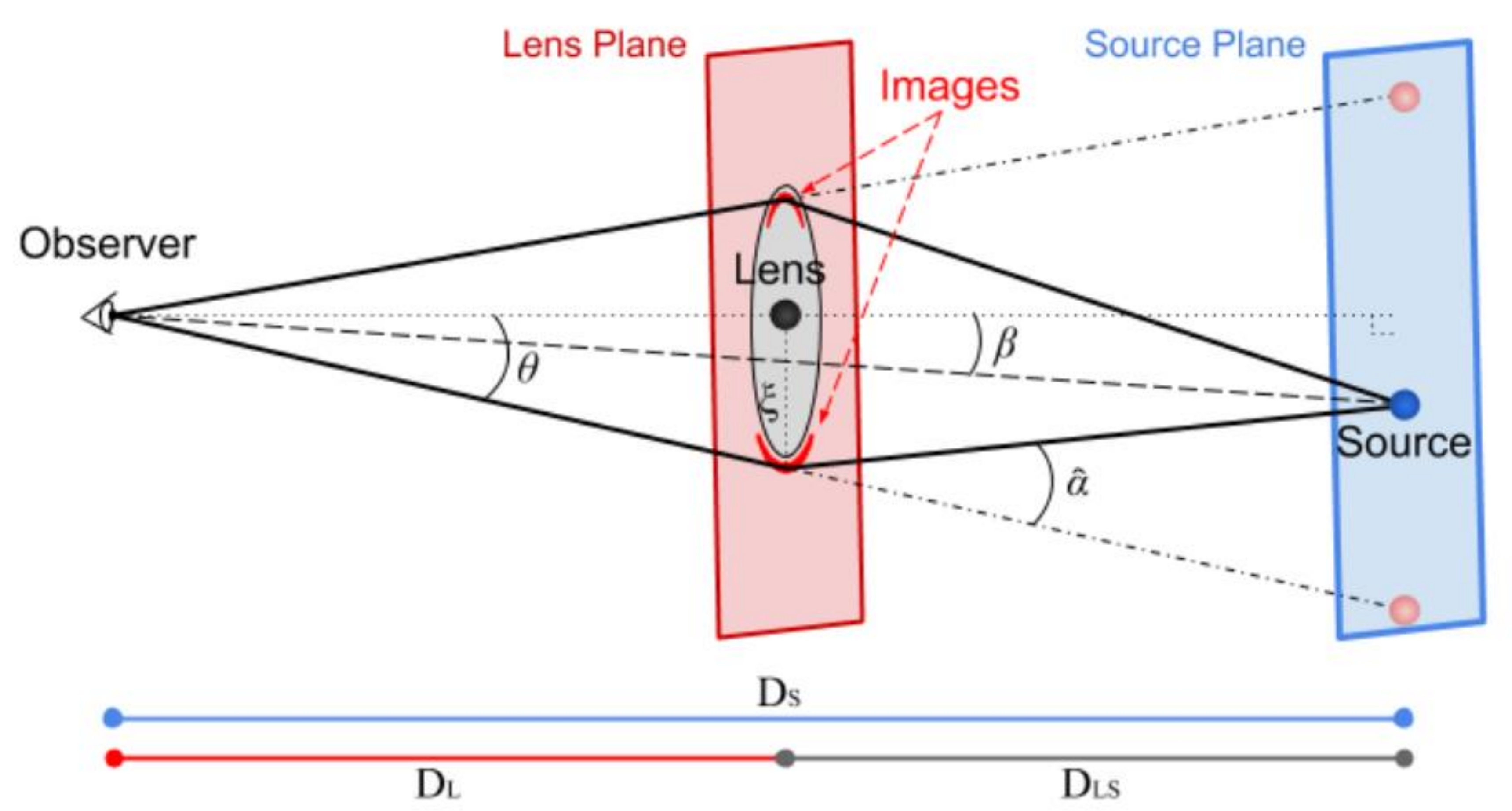

Exoplanet detection via microlensing

- Sensitive to low mass planets (down to 0.1 M_{earth})
- Sensitive to wide orbits (1-4 AU)
- Sensitive to free-floating planets

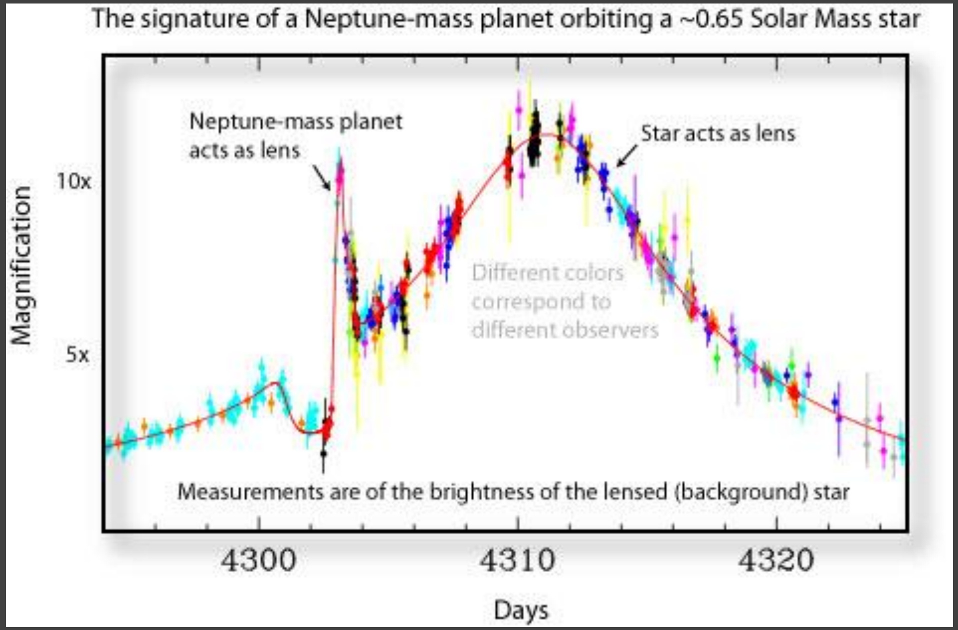

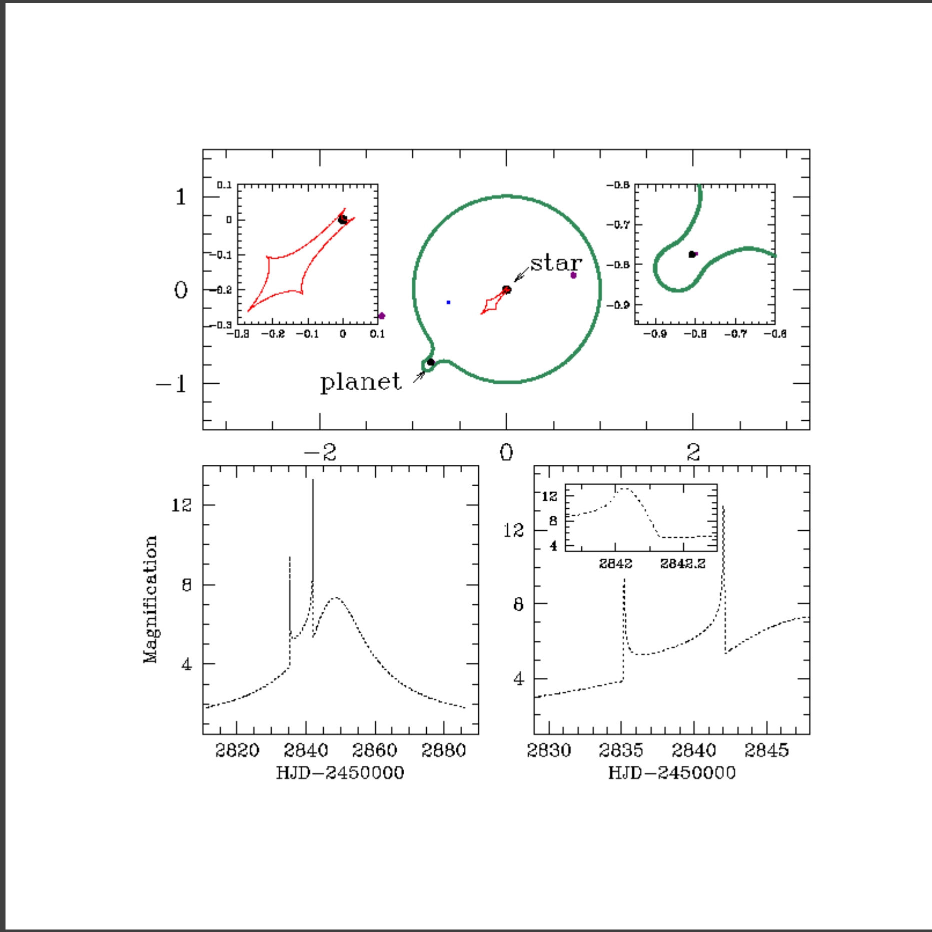

https://www3.nd.edu/~bennett/moa53-ogle235/technical.gif

See a review in Bennet 0902.1761

Gravitational microlensing - 1

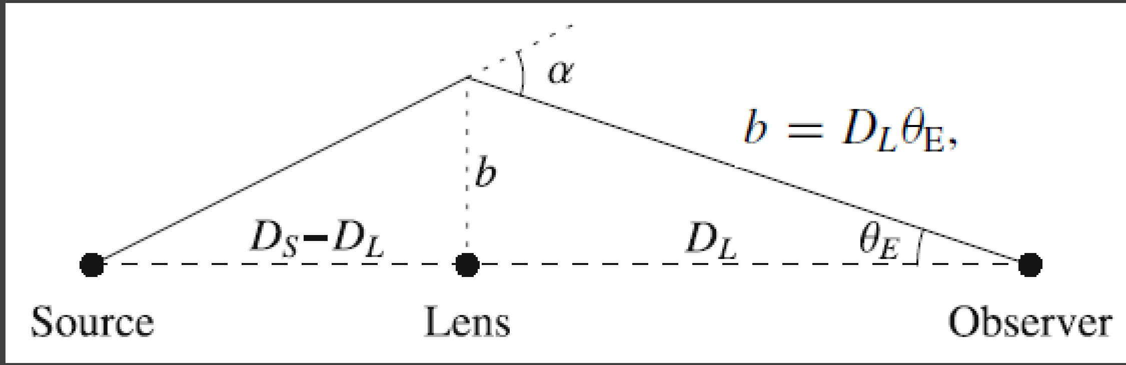

$$\alpha = b/D_L + b/(D_S - D_L).$$

$$\theta_E = \sqrt{\kappa M \pi_{rel}}; \qquad \kappa \equiv \frac{4G}{c^2 \mathrm{AU}} \simeq 8.14 \frac{\mathrm{mas}}{M_\odot},$$

$$\pi_{rel} = \mathrm{AU}(D_L^{-1} - D_S^{-1})$$

Probability of microlensing is small.
For stars it is ~10^{-5} – 10^{-6} per year.
For planets it is lower, as θ_E ~ $M^{1/2}$
and M_{planet}/M_{star}~10^{-4}

$$\tau = \int dD_L \pi (D_L\theta_E)^2 n(D_L) \sim \frac{4\pi GMn}{c^2} D^2 = \frac{4\pi G\rho}{c^2} D^2 \sim \frac{GM_{tot}}{Dc^2} \sim \frac{v^2}{c^2}$$

Gravitational microlensing - 2

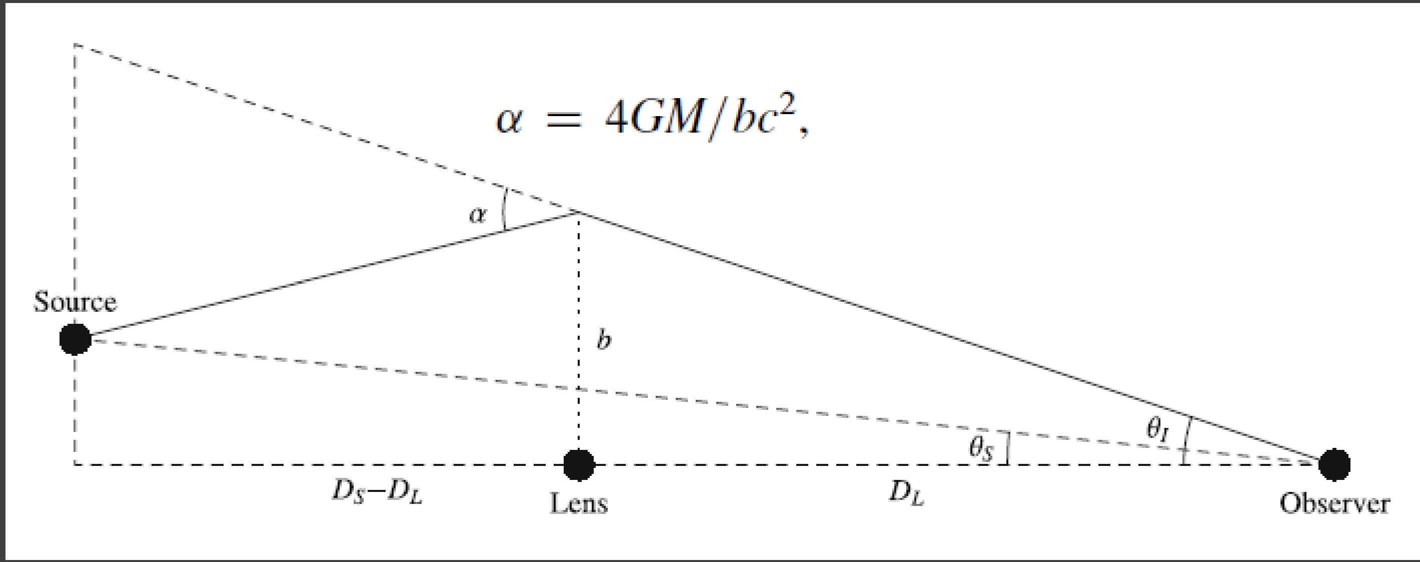

$$(\theta_I - \theta_S)D_S = \alpha(D_S - D_L)$$

$$\theta_I(\theta_I - \theta_S) = \frac{4GM\pi_{\rm rel}}{c^2 \mathrm{AU}} \equiv \theta_{\rm E}^2.$$

$$u_\pm = \frac{u \pm \sqrt{u^2+4}}{2}; \qquad u \equiv \frac{\theta_S}{\theta_{\rm E}} \qquad u_\pm \equiv \frac{\theta_{I,\pm}}{\theta_{\rm E}}.$$

$$A_\pm = \pm \frac{u_\pm}{u}\frac{\partial u_\pm}{\partial u} = \frac{A \pm 1}{2}$$

$$A = \frac{u^2+2}{u\sqrt{u^2+4}} = (1 - Q^{-2})^{-1/2}; \qquad Q \equiv 1 + \frac{u^2}{2},$$

Light curves for point lenses

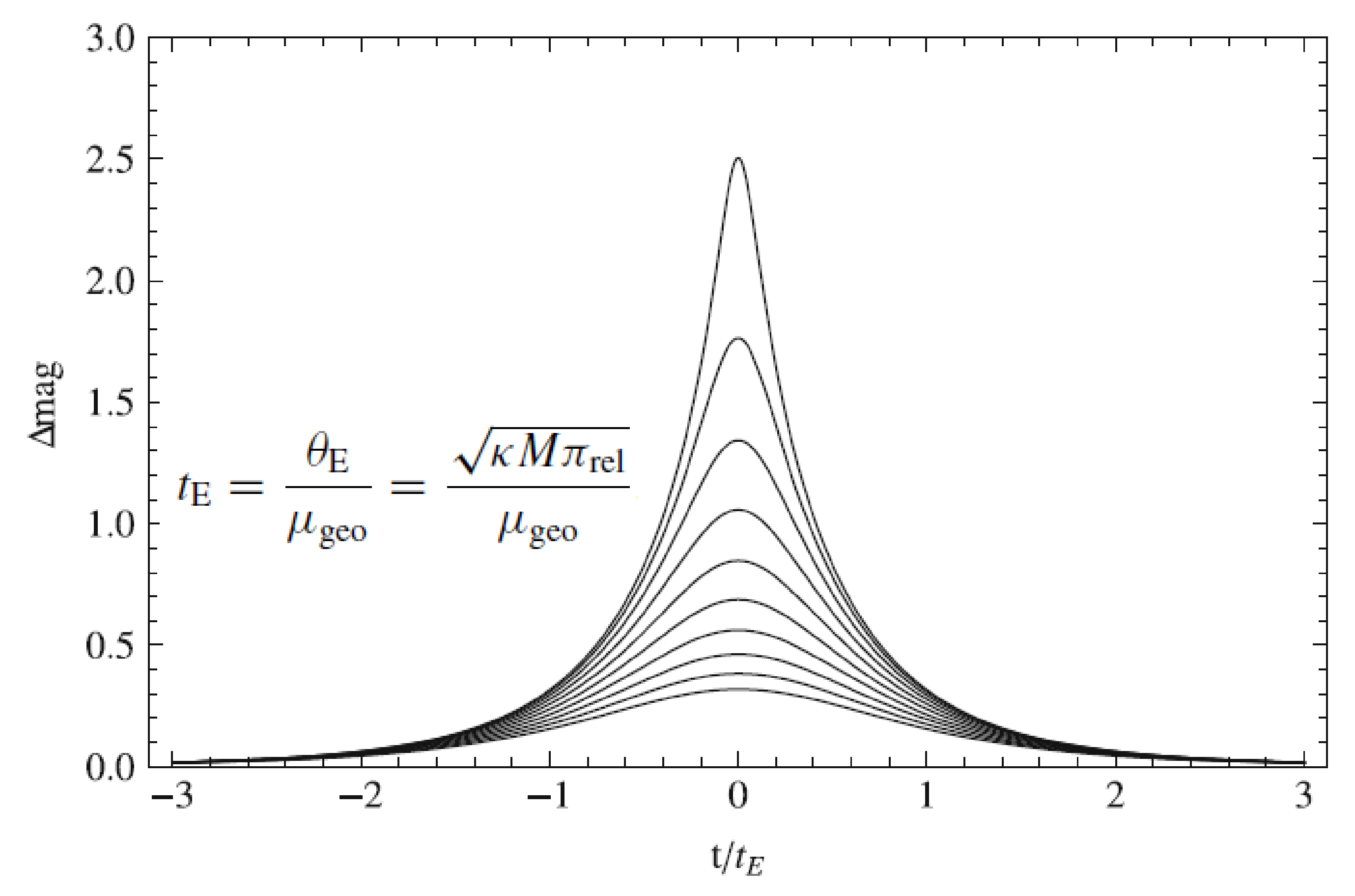

$$t_{\rm E} = \frac{\theta_{\rm E}}{\mu_{\rm geo}} = \frac{\sqrt{\kappa M \pi_{\rm rel}}}{\mu_{\rm geo}}$$

$$F(t) = f_s A(\mathbf{u}(t; t_0, u_0, t_{\rm E}), \rho) + f_b;$$

$$\mathbf{u}(t; t_0, u_0, t_{\rm E}) = (\tau(t), \beta) = \left(\frac{t - t_0}{t_{\rm E}}, u_0\right).$$

Andrew Gould (in Bozza et al. 2016)

Finite size lense

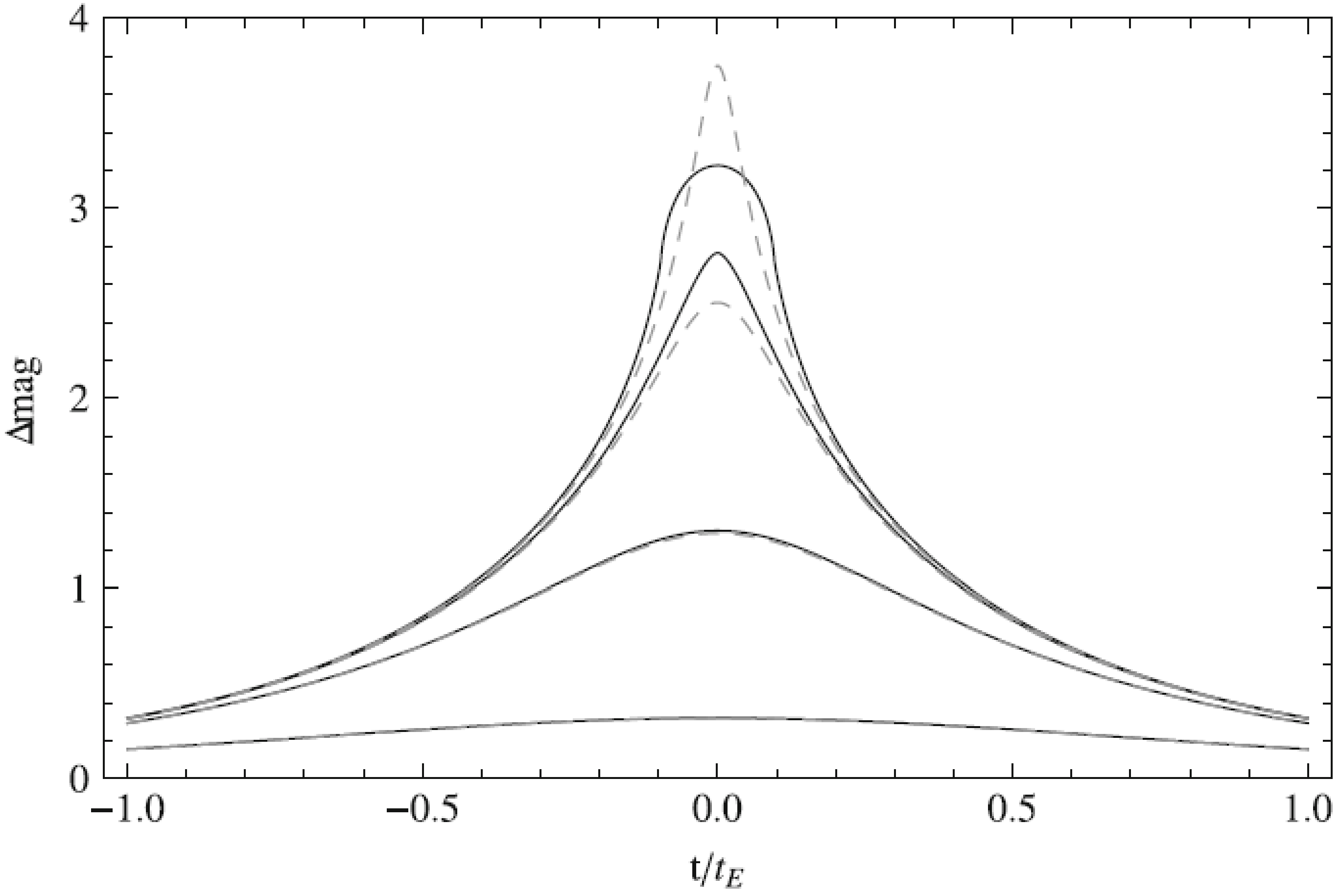

Fig. 3.4 Magnification as a function of time in microlensing events for an impact parameters $u_0 = 10^{-n}$ with $n \in \{-1.5, -1, -0.5, 0\}$. The angular source size is $0.1\theta_E$. Note that when the impact parameter is greater than the source radius, the magnification is higher than the corresponding Paczynski curve (*dashed*). When the impact parameter is smaller than the source radius (source passing right behind the lens), the magnification saturates

Andrew Gould (in Bozza et al. 2016)

Light curves form different trajectories

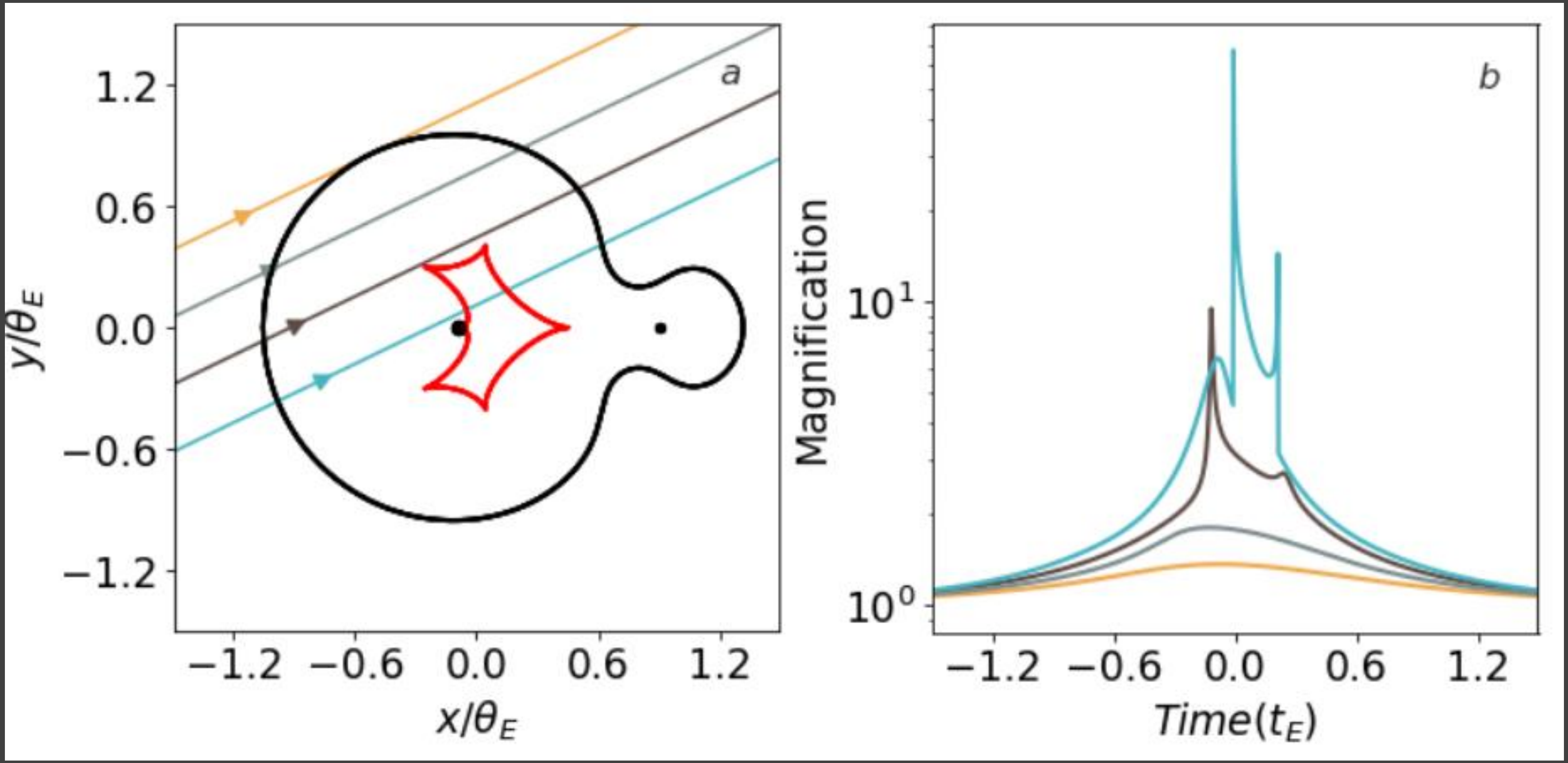

Binary lense

s – separation of components in units of the Einstein radius θ_E.
q - mass ratio.

$$r_\perp = s\theta_E D_L,$$

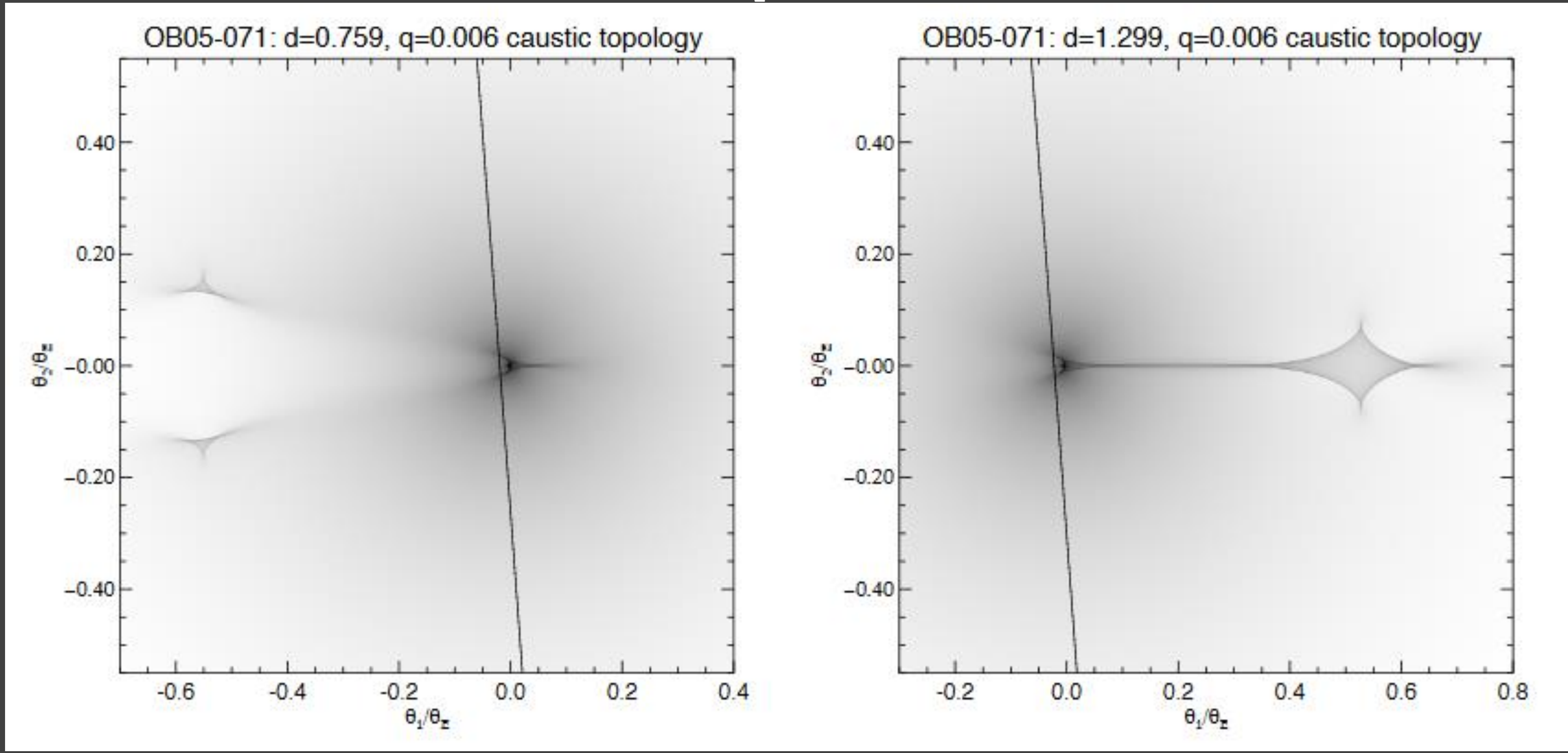

0902.1761

Light curves

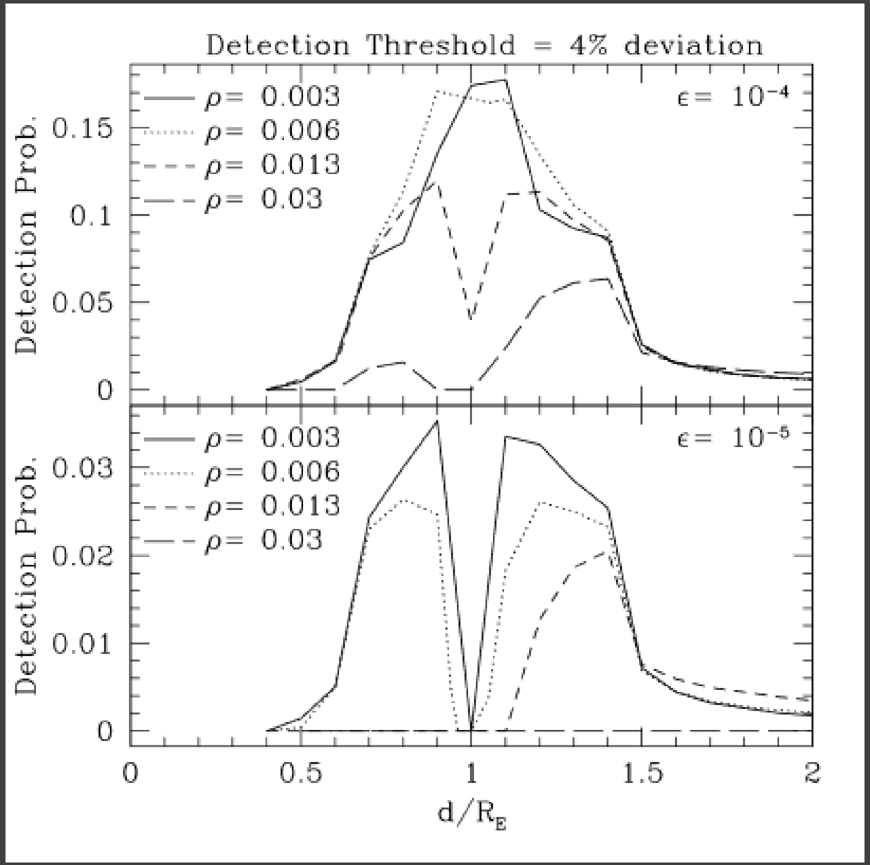

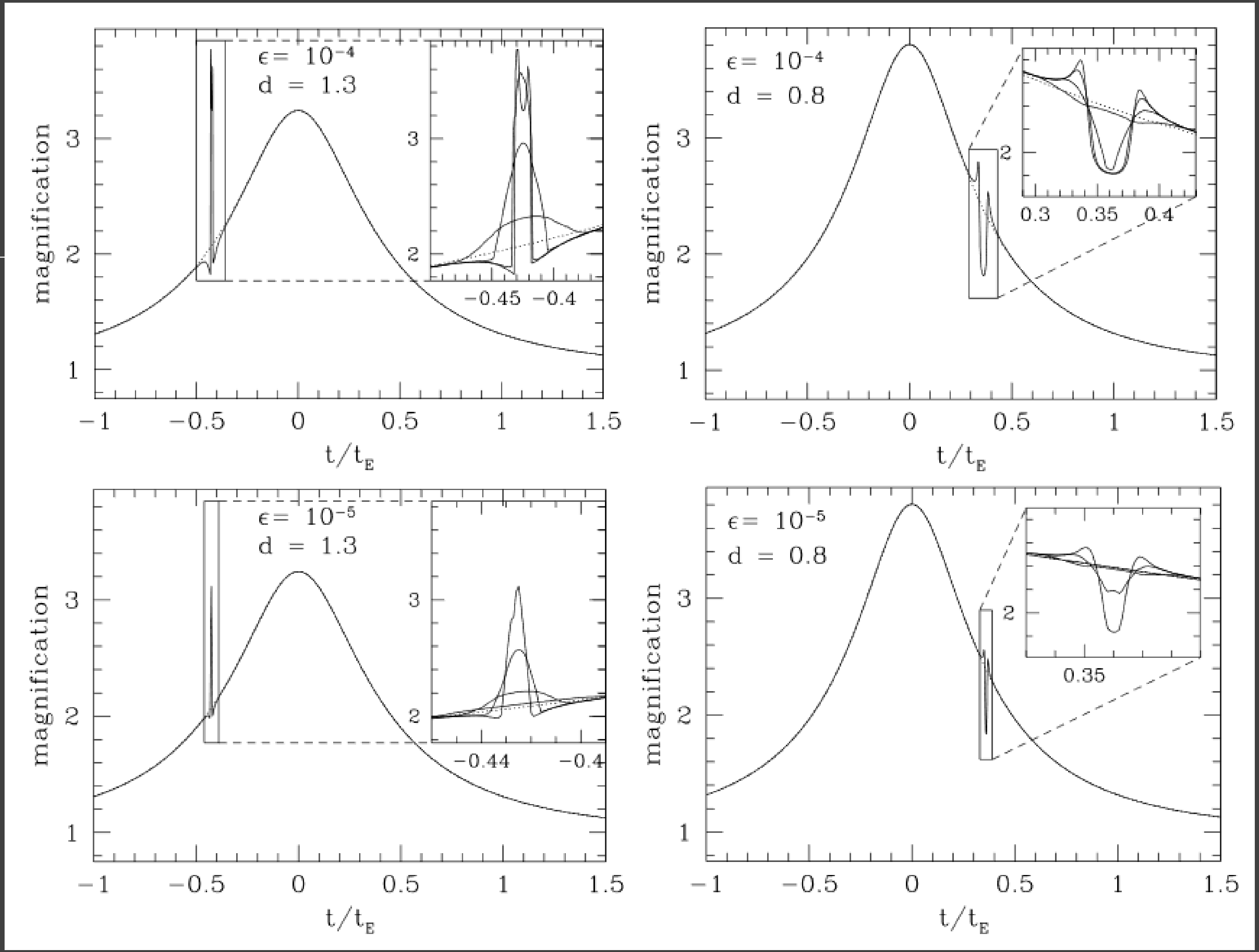

0902.1761

Cold Neptune

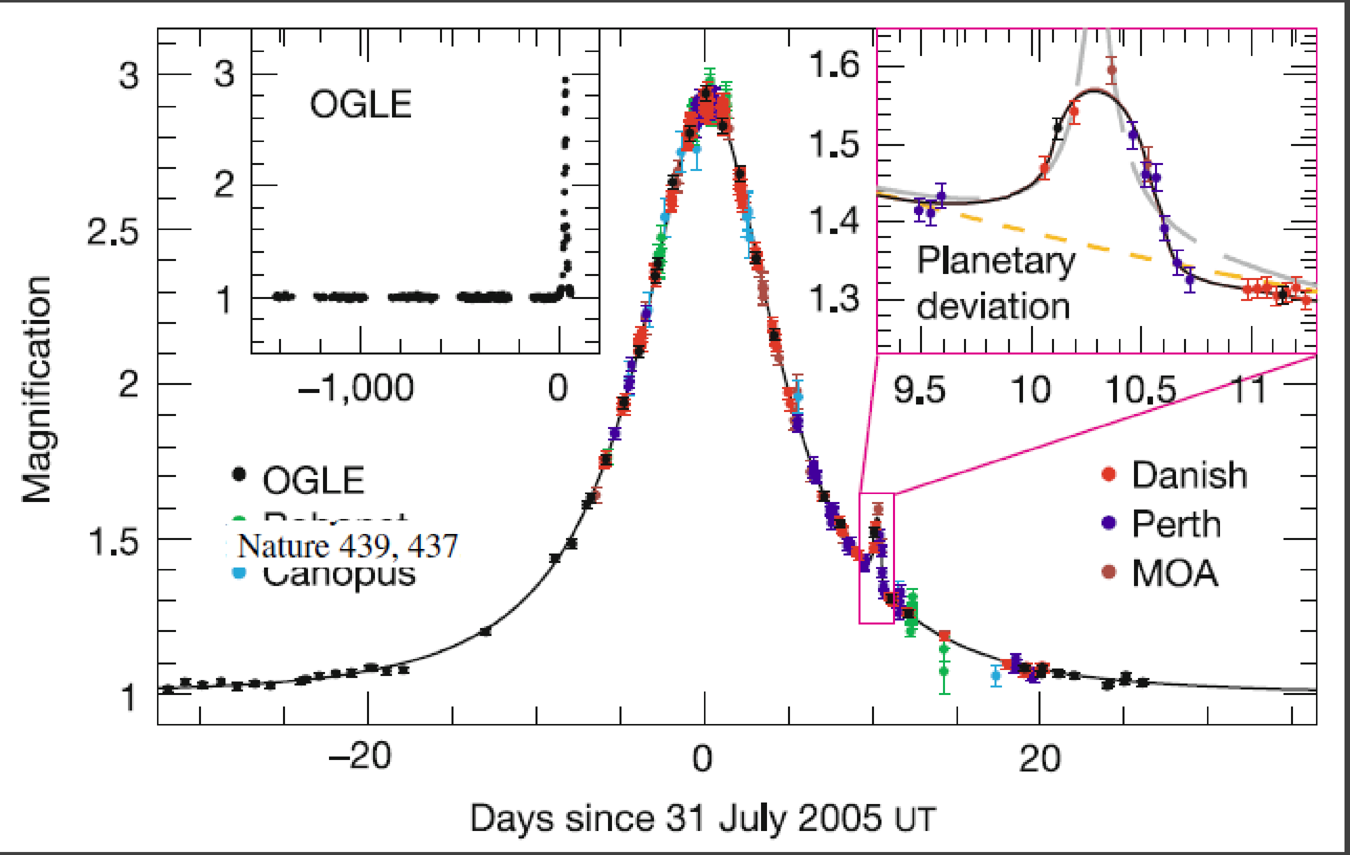

$$A_p = \frac{2}{\rho_p^2} = 2\left(\frac{\theta_{E,p}}{\theta_*}\right)^2$$

$$\frac{t_p}{t_E} = \frac{\theta_*}{\theta_E}.$$

$$q = \frac{m_p}{M} = \frac{\theta_{E,p}^2}{\theta_E^2} = \frac{\theta_{E,p}^2}{\theta_*^2}\frac{\theta_*^2}{\theta_E^2} = \frac{A_p}{2}\frac{t_p^2}{t_E^2} \simeq 1.0 \times 10^{-4}.$$

$$r_\perp = s\theta_E D_L = 2.2\,\mathrm{AU}\frac{D_L}{8\,\mathrm{kpc}}.$$

Andrew Gould (in Bozza et al. 2016)

Solar system – like system

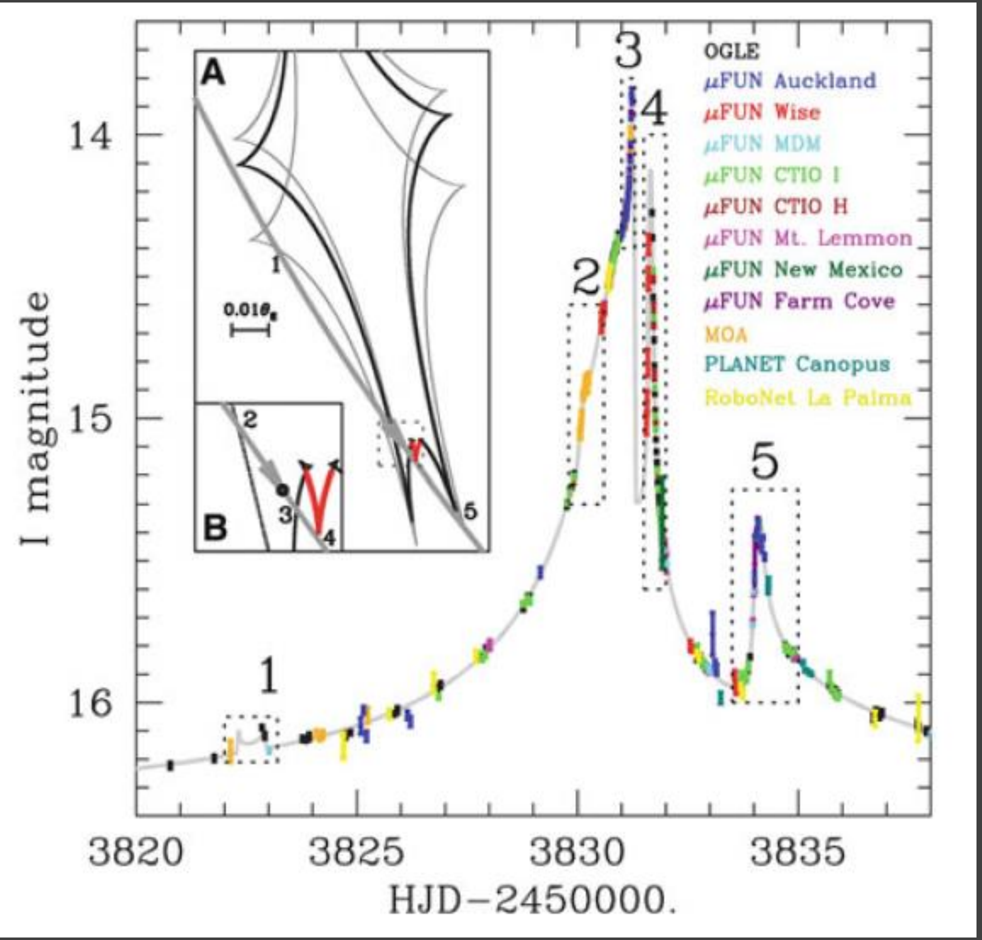

Jupiter and Saturn analogues. Distances are slightly smaller consistent with smaller mass of the host star.

Dips due to planets

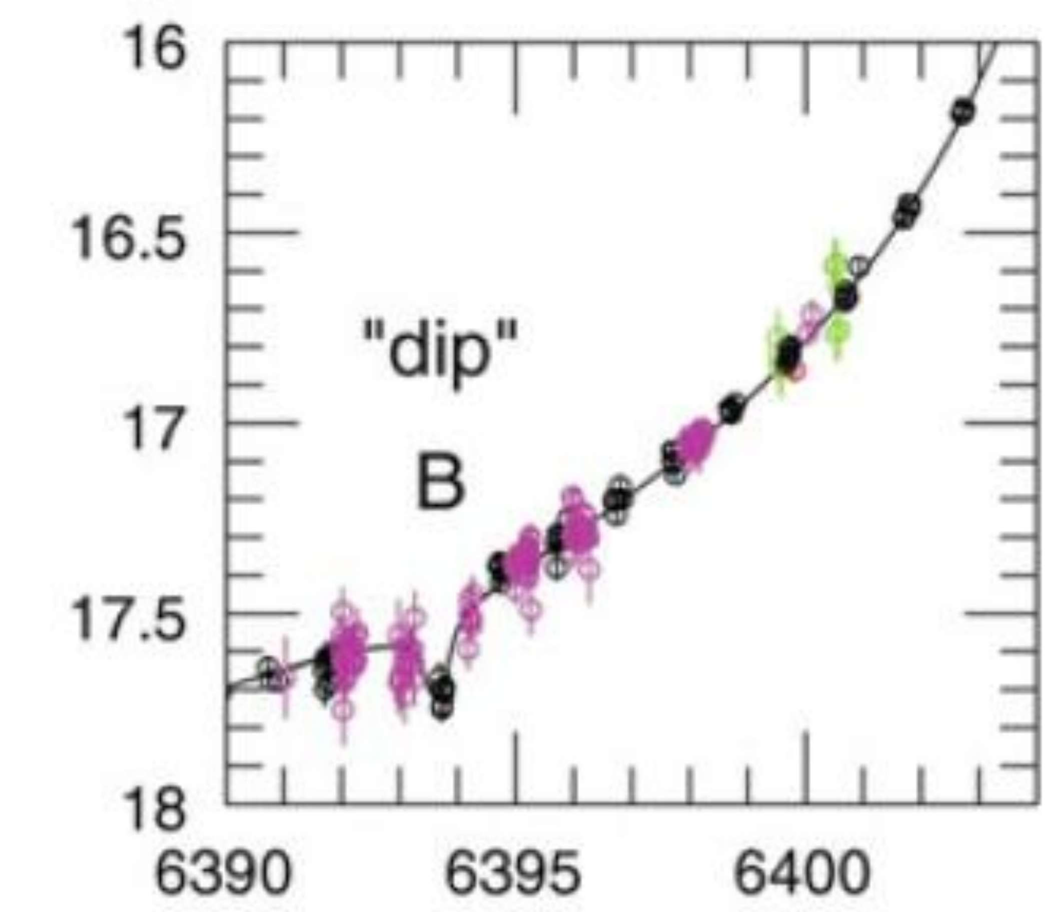

A terrestrial-mass planet in a binary. The planet orbits a red dwarf (1 AU), which orbits another star (15 AU)

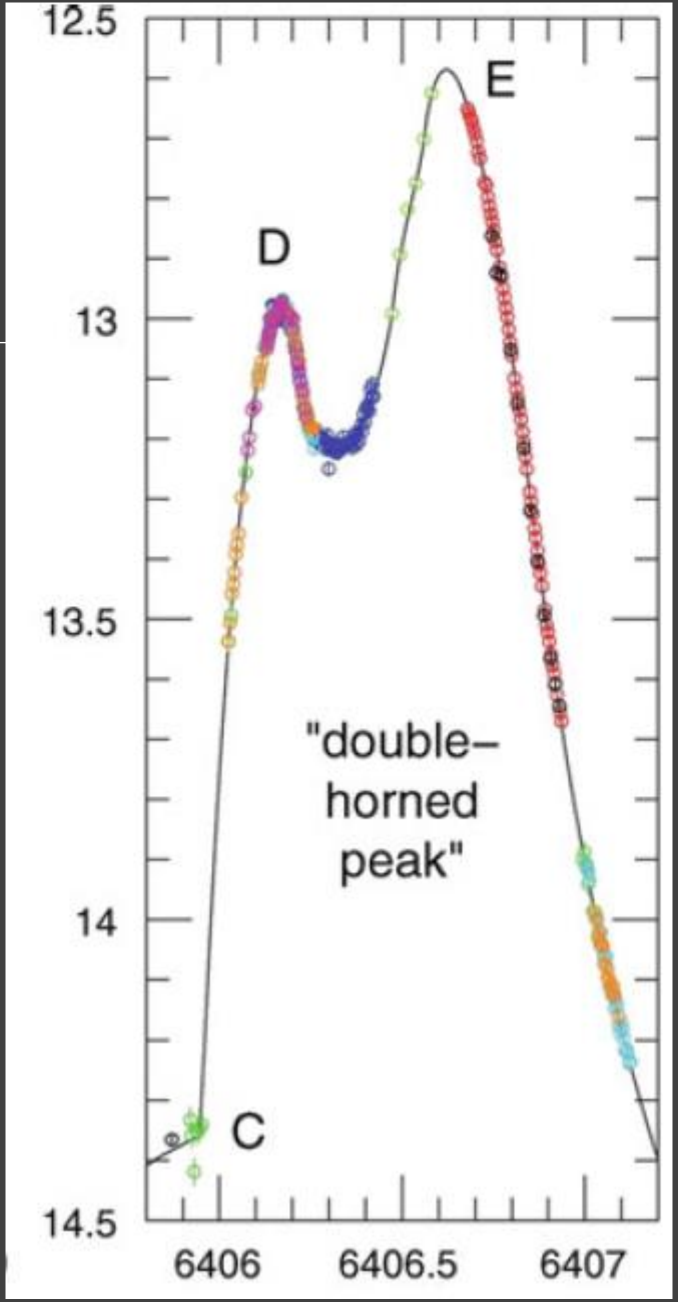

Comparison of three methods

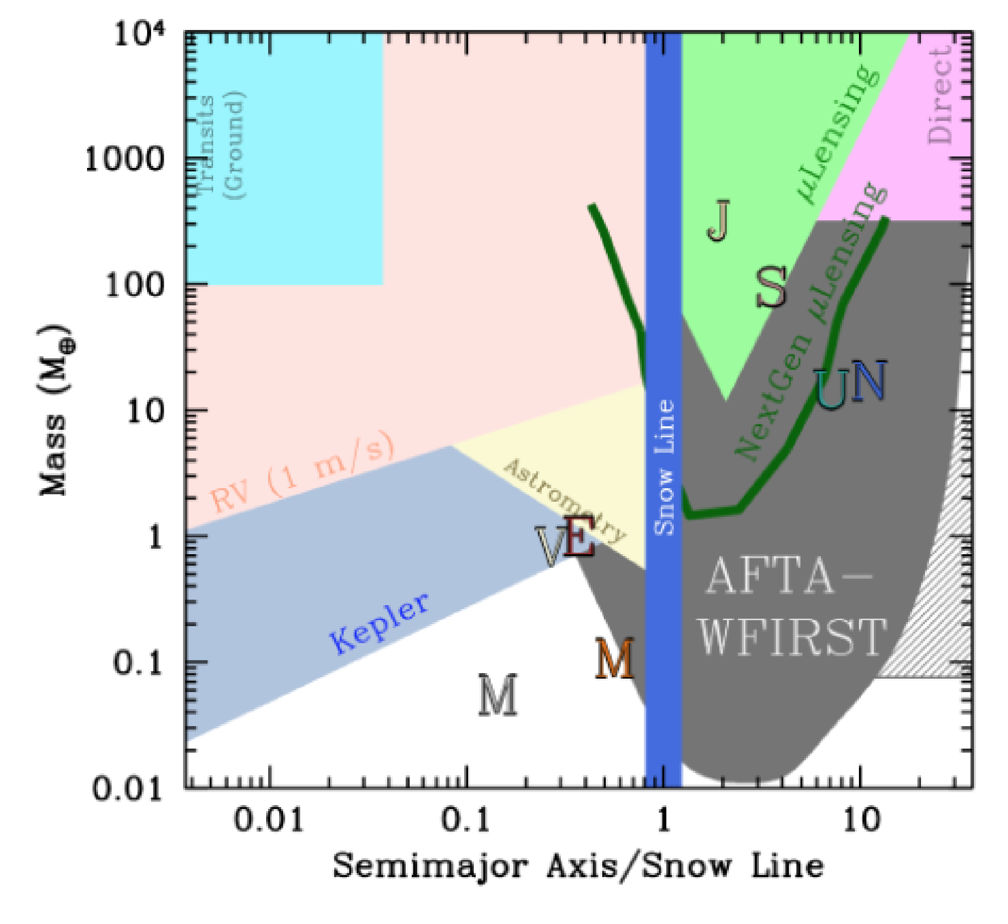

1505.06869

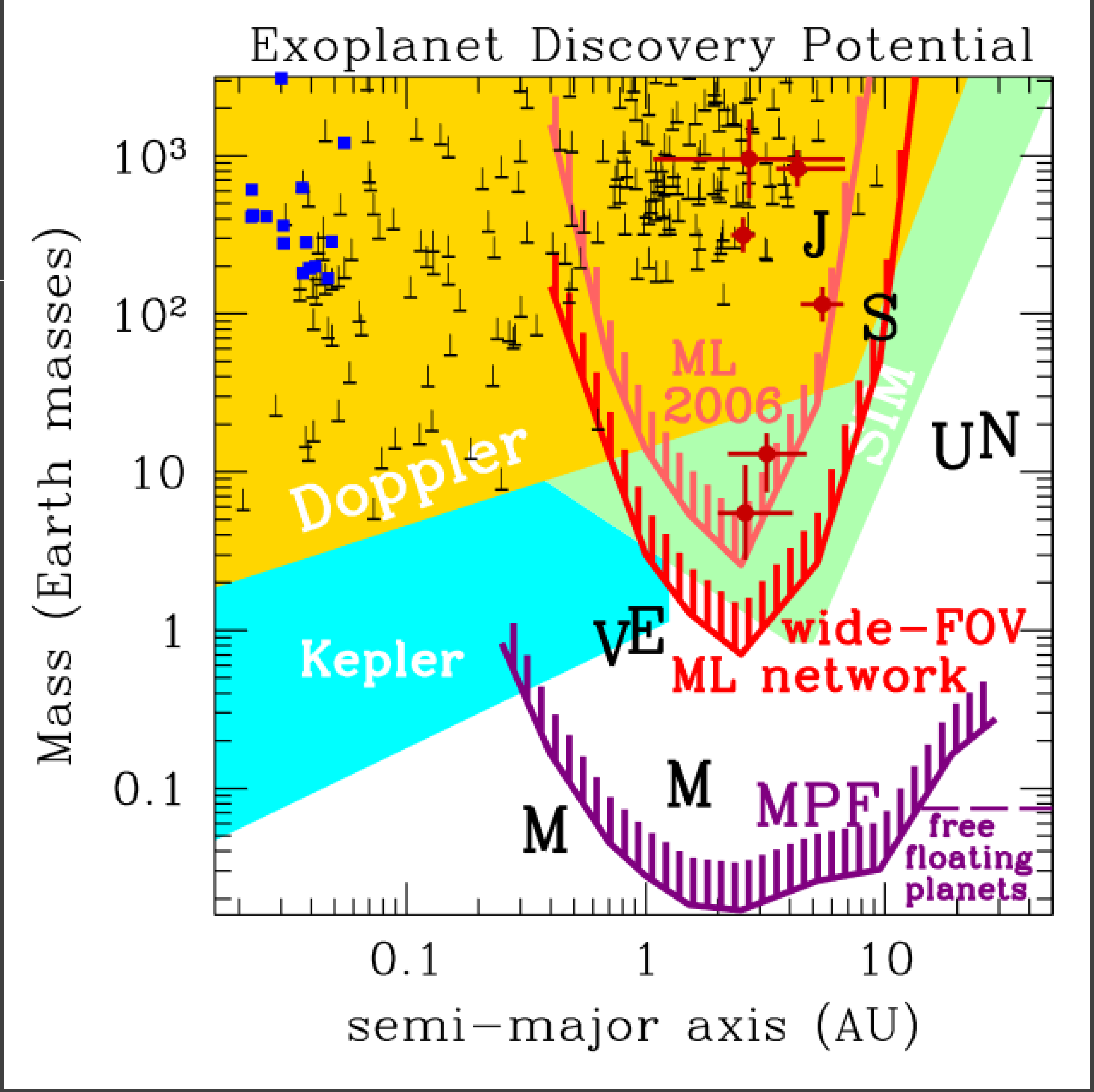

0902.1761

Discoveries by different methods

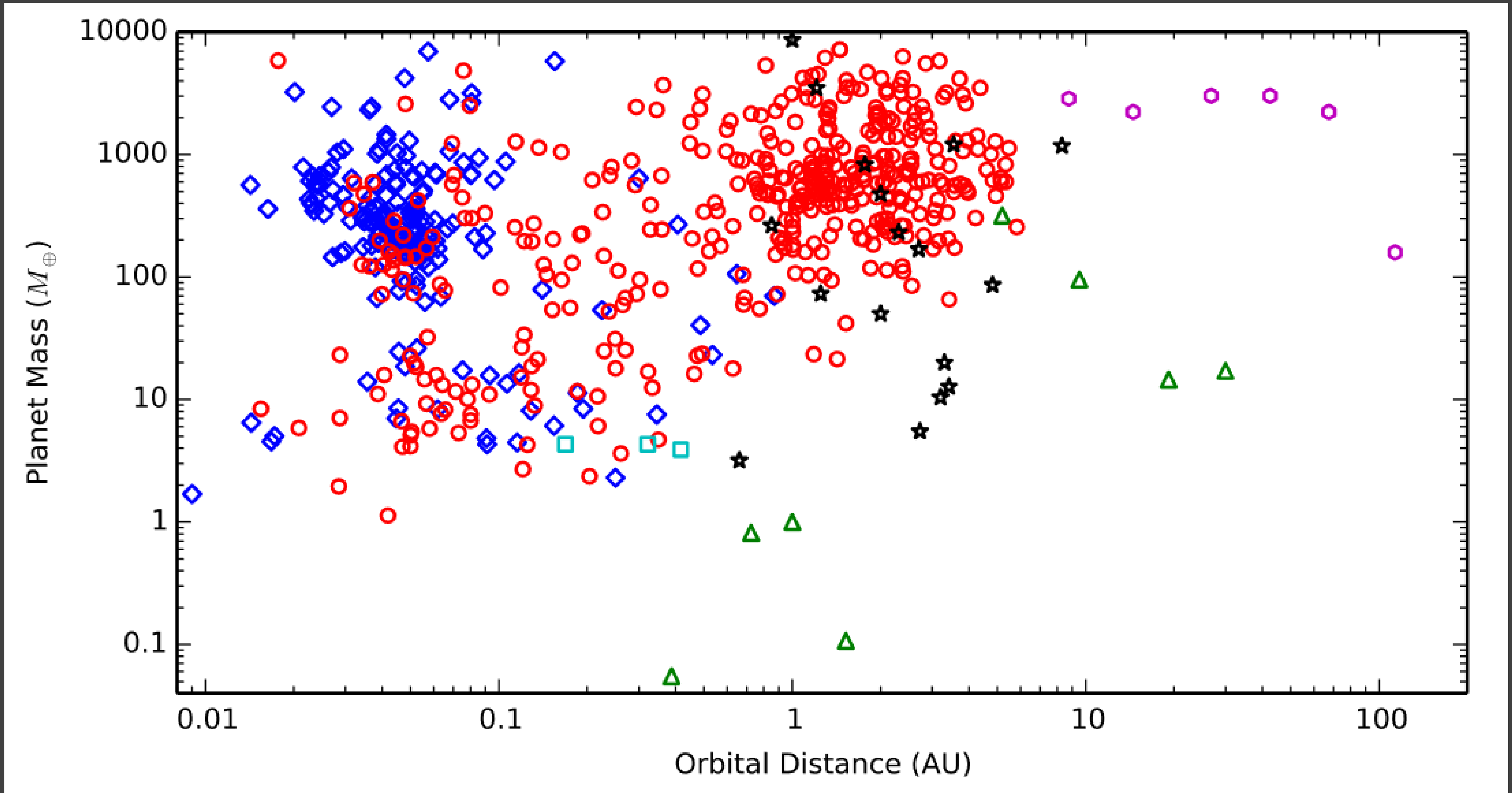

RV = red circles,
transit = blue diamonds,
imaging = magenta hex.,
gravlens = black stars,
psr time = cyan squares.

Planets in the Solar System are green triangles.

Blue- RV
Red – Trans.
Green – lense
Orange – imaging

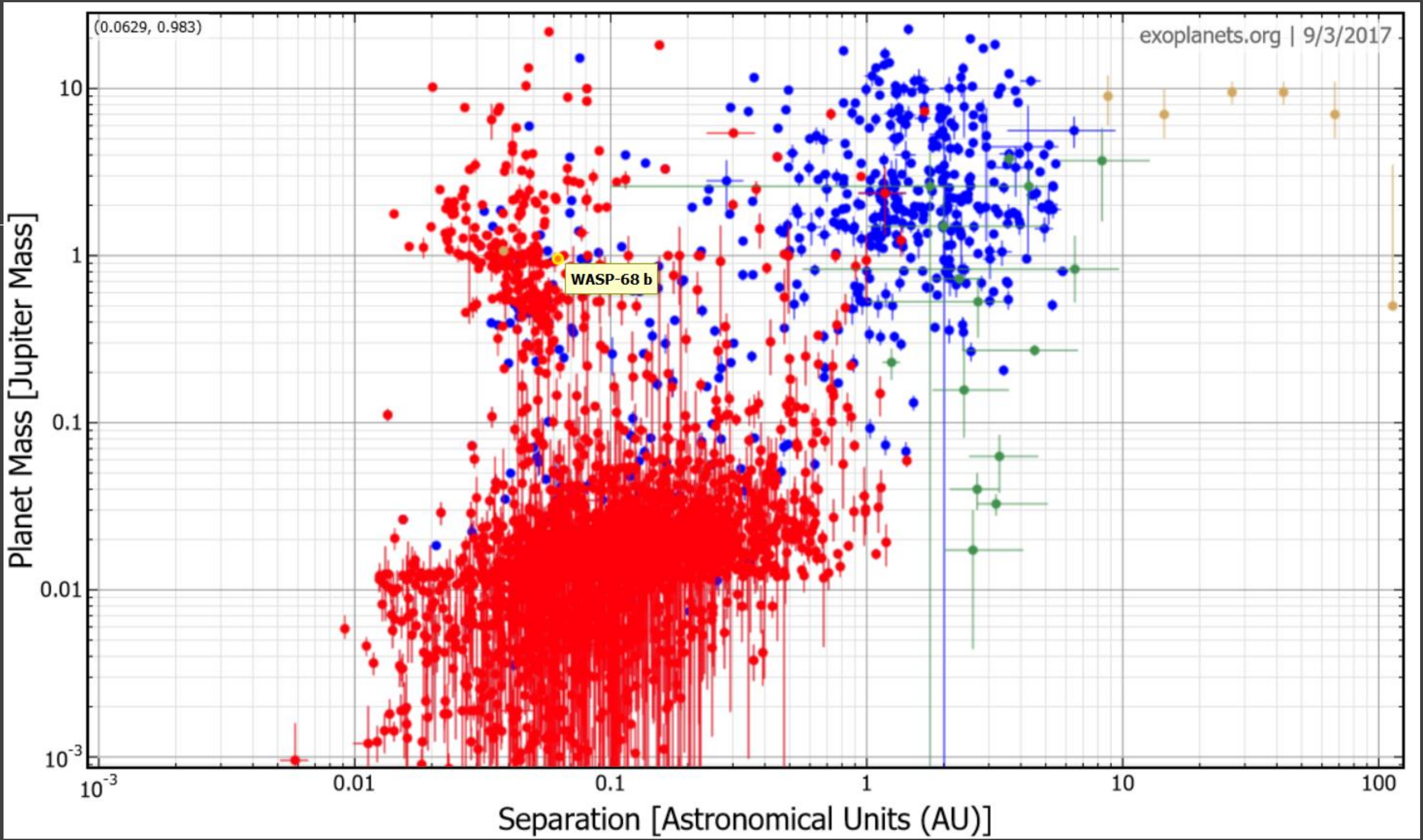

http://exoplanets.org/plots

Microlensing wins in distance!

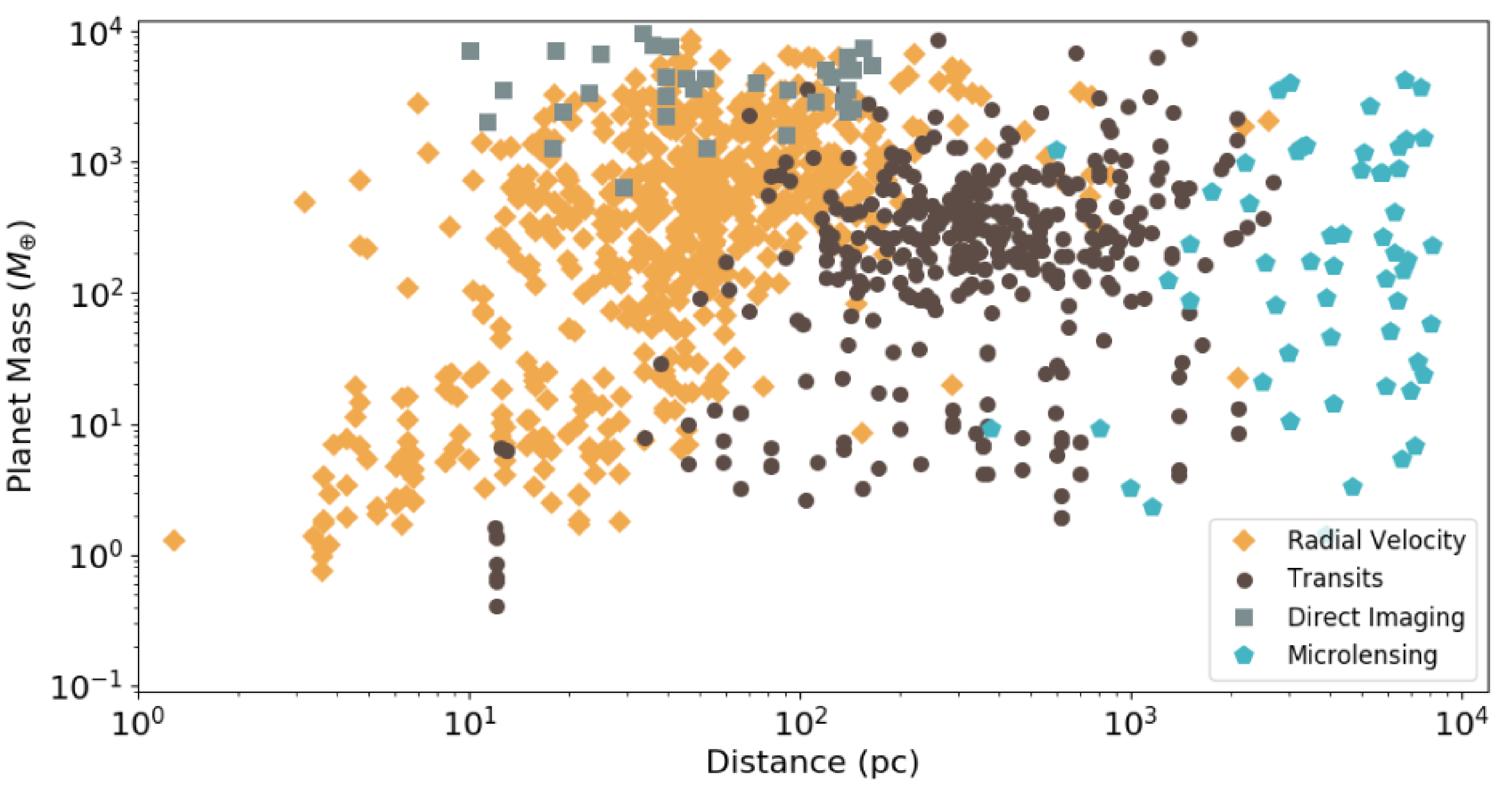

1810.02691

Extragalactic planets

Free-floating planets detected due to microlensing in X-rays: observations of FeKα from QSOs with Chandra.

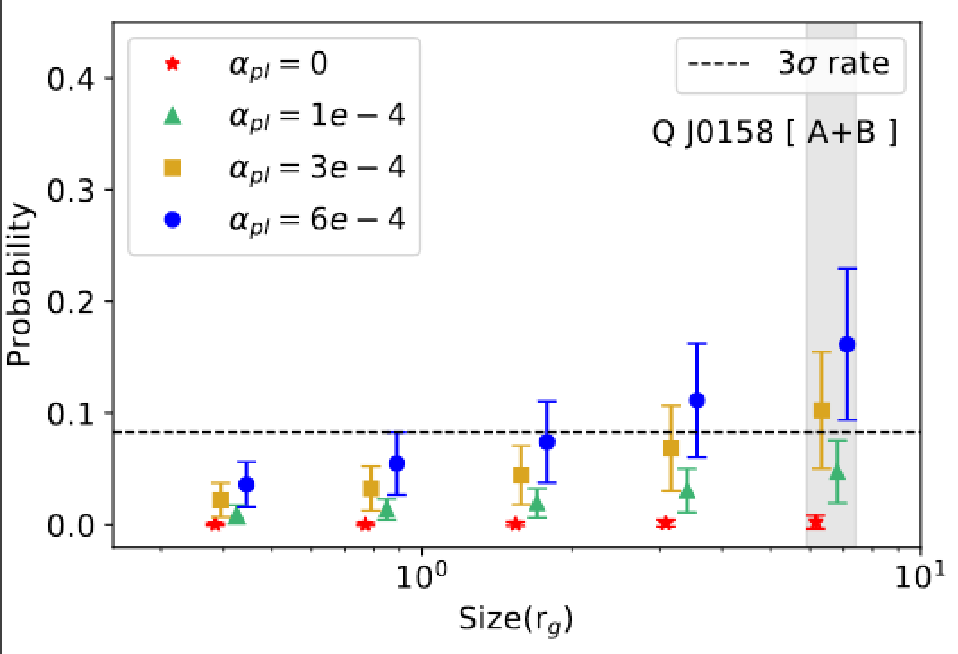

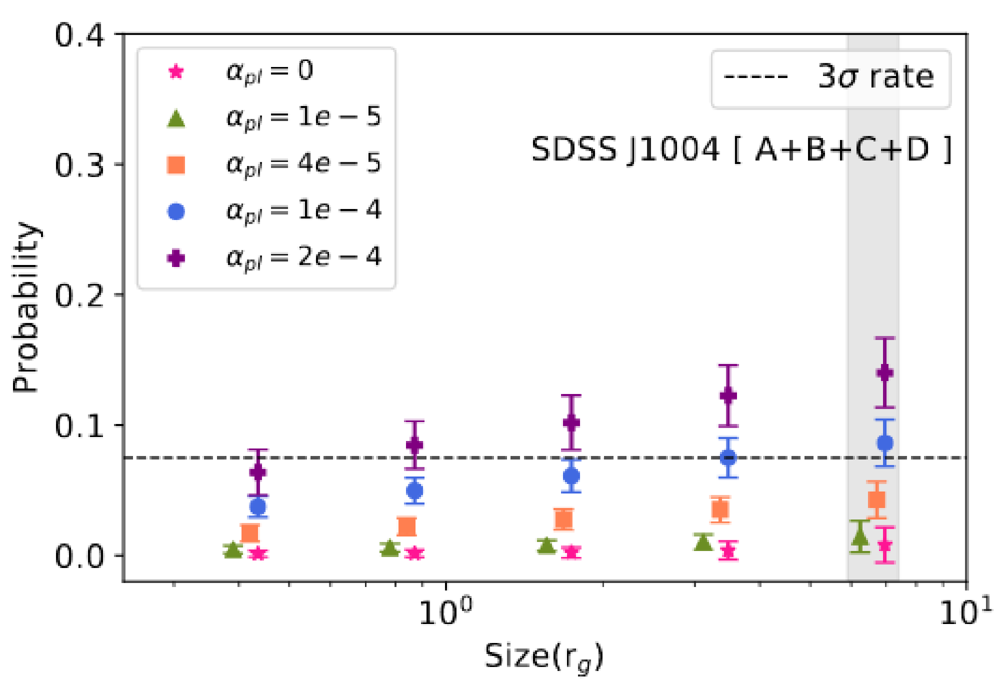

Timing

Observations of a periodic process
(radio pulsar, binary system, pulsating star)
allows to identify a perturber

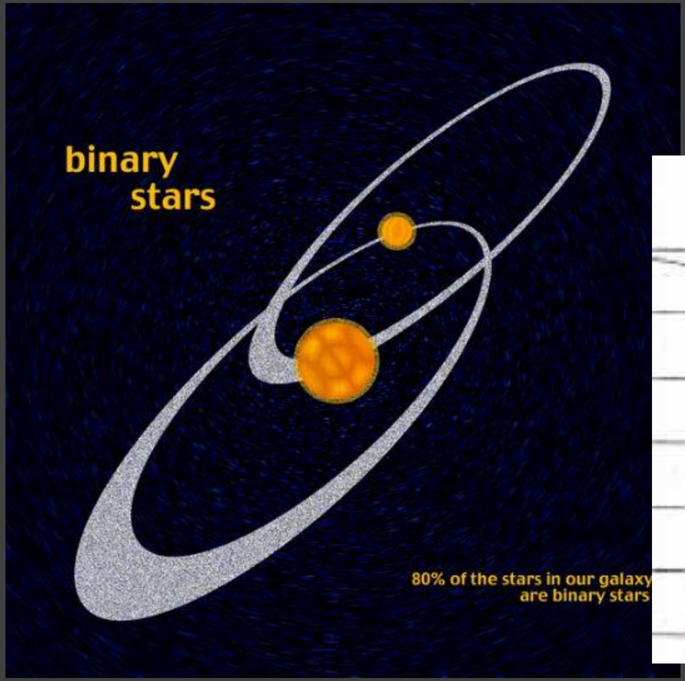

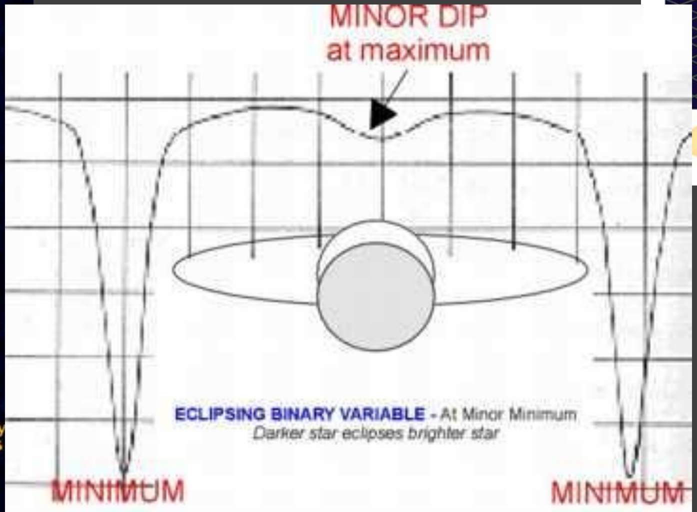

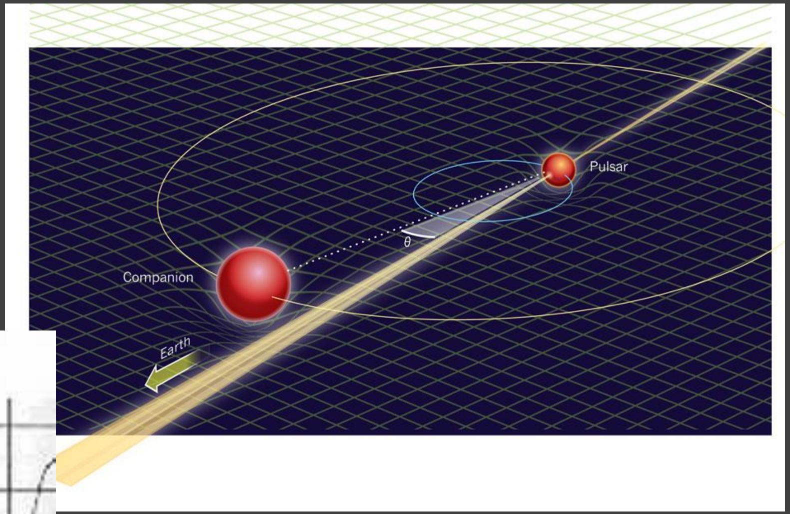

Planets around a radio pulsar

Wolszczan, Frail 1992

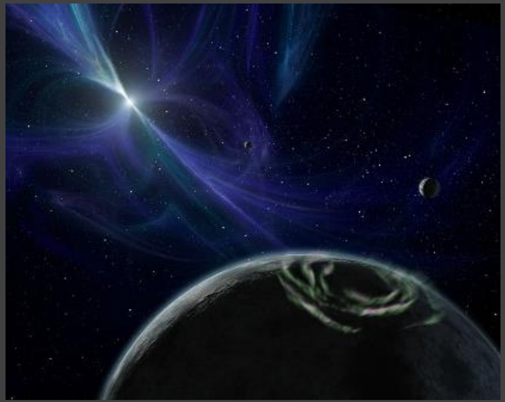

PSR B1257+12
Millisecond pulsar

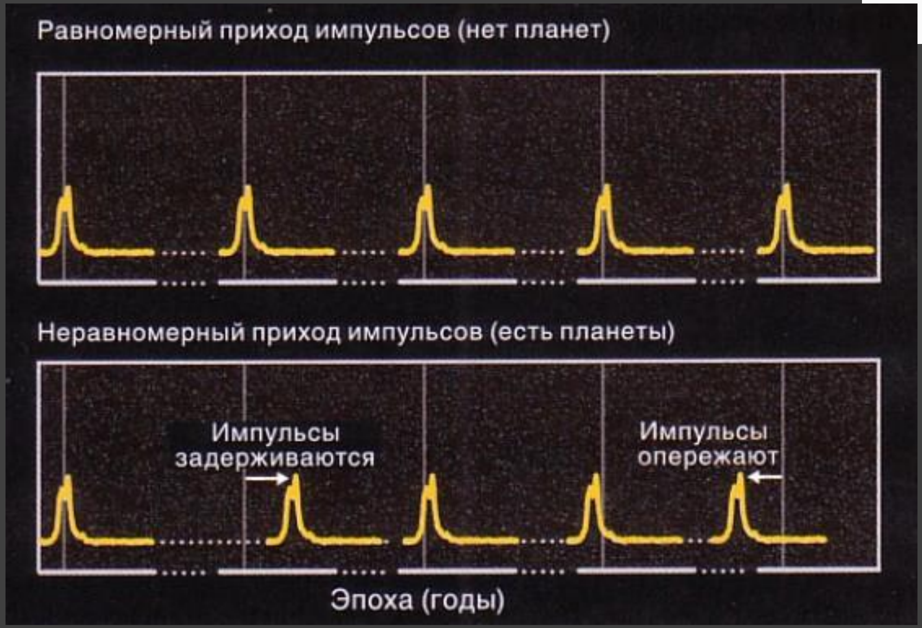

Three light planets

Companion (in order from star)	Mass	Semimajor axis (AU)	Orbital period (days)
A (b)	$0.020 \pm 0.002\ M_\oplus$	0.19	25.262 ± 0.003
B (c)	$4.3 \pm 0.2\ M_\oplus$	0.36	66.5419 ± 0.0001
C (d)	$3.9 \pm 0.2\ M_\oplus$	0.46	98.2114 ± 0.0002

Time delay $A \simeq \frac{a \sin i}{c} \frac{m_p}{M_\star}$,

$$\tau(t) = -\frac{1}{c} \int_0^t v_{\rm rad}(t')\,{\rm d}t'$$

$$v_{\rm rad}(t) = -c\frac{{\rm d}\tau}{{\rm d}t}$$

See 1708.00896, details in 1404.5649

Time delays for KIC 7917485

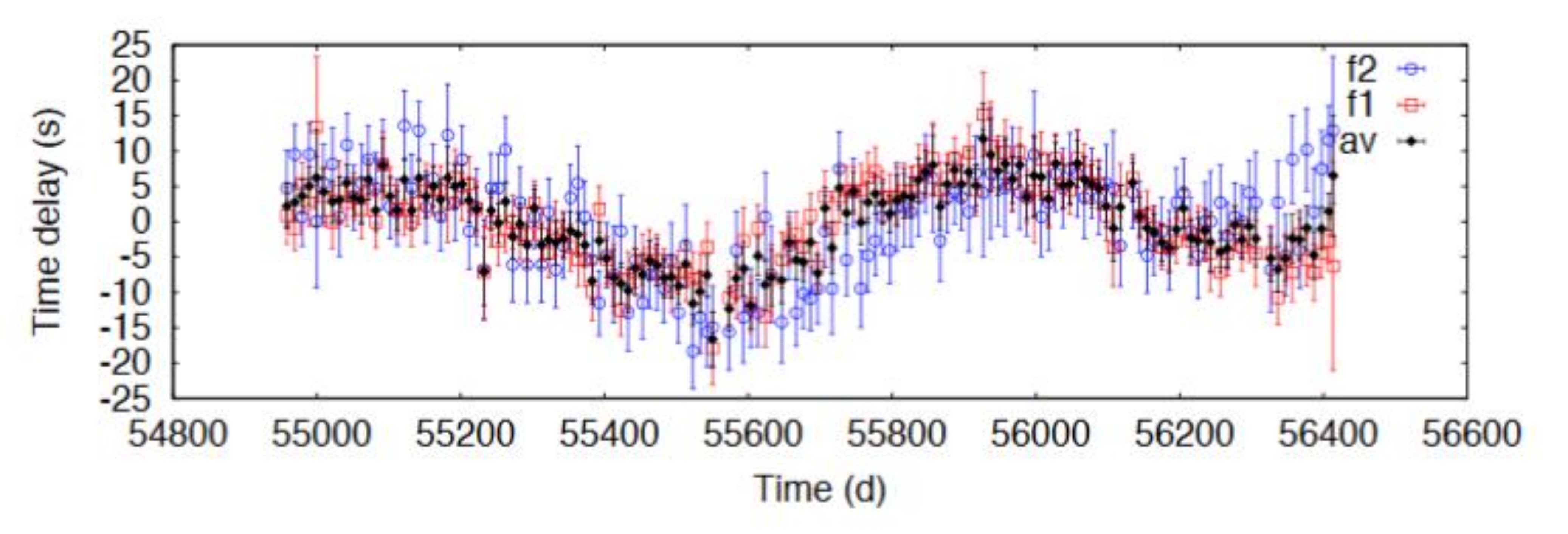

δ Scuti-type star
Planet: M~11 M_{Jup}
Porb ~ 840 days

Pulsations 1.18 and 1.56 hours.
Δt~ 7 sec
Habitable zone!

Direct imaging

Now it is possible to see self-luminous planets (10^{-5} in flux) at >~1 arcsec.
For comparison: Solar system analogue at 10 pc gives for Jupiter 10^{-9} in flux and 0.5 arcsec.

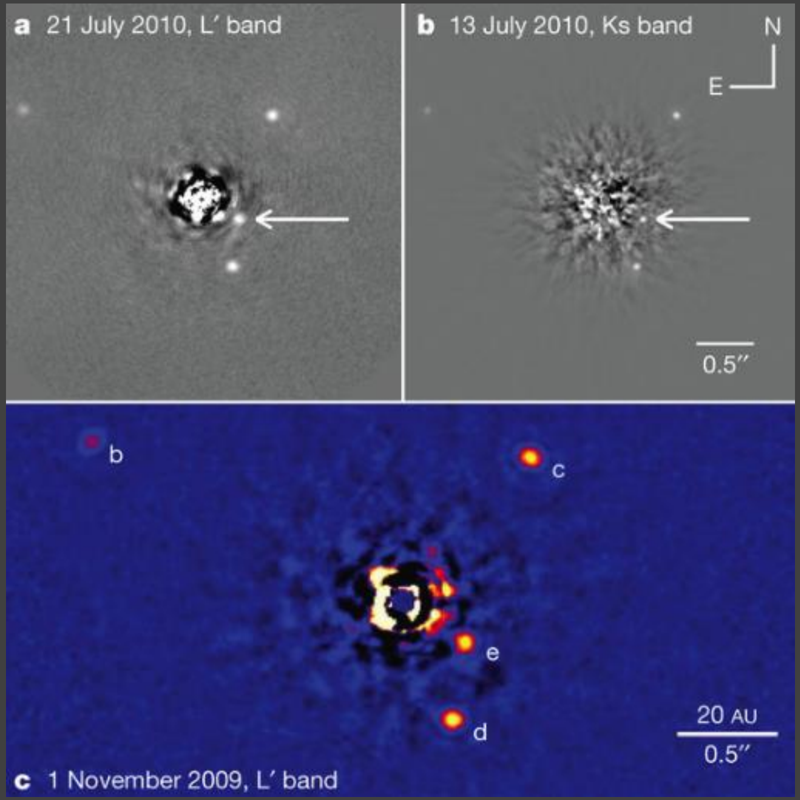

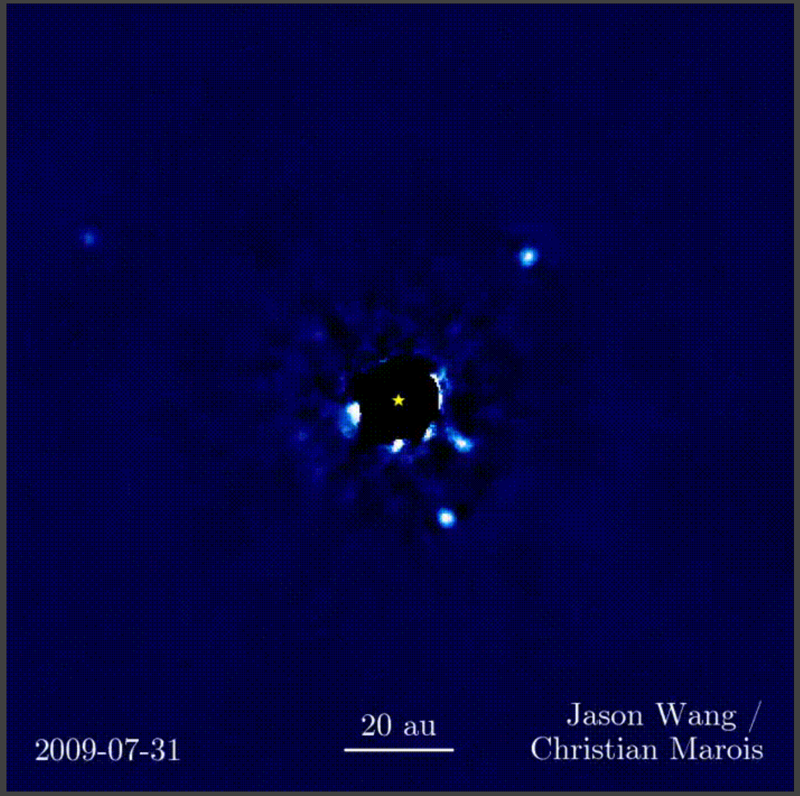

Distant planet

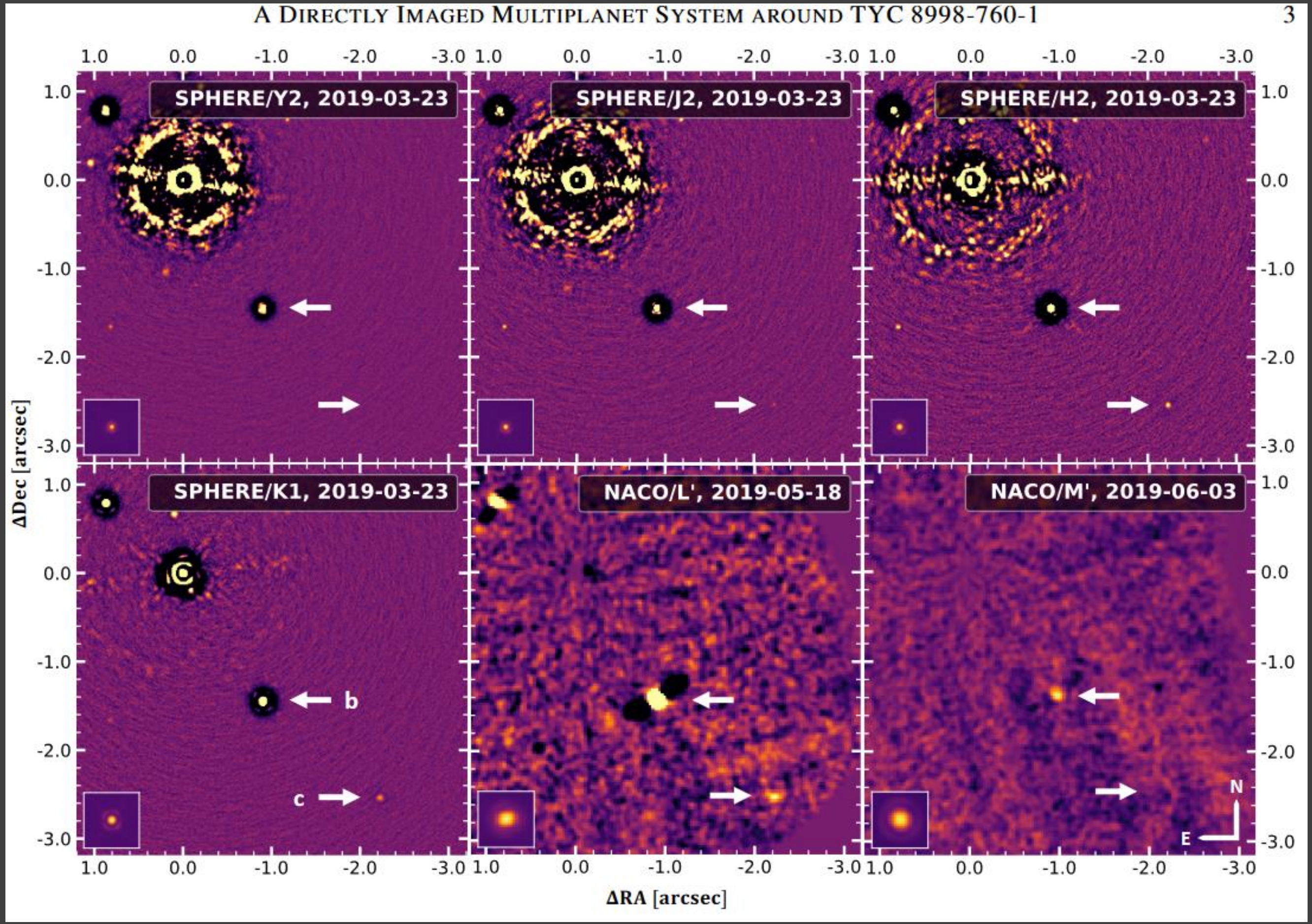

160 and 320 AU

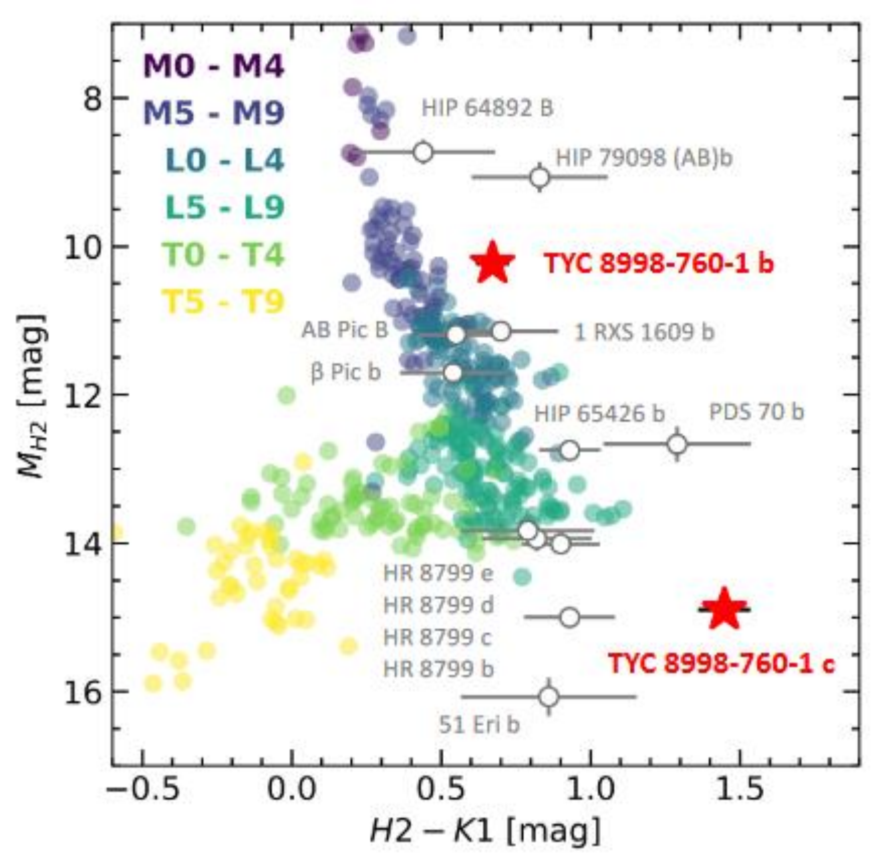

Telescope properties

Instrument	Telescope	Wavelength (µm)	Ang. resol. (mas)	Coronagraph
ACS	HST	0.2–1.1	20–100	Lyot
STIS	HST	0.2–0.8	20–60	Lyot
NAOS–CONICA	VLT	1.1–3.5	30–90	Lyot/FQPM
VISIR	VLT	8.5–20	200–500	–
SINFONI–SPIFFI	VLT	1.1–2.45	28–62	–
SPHERE	VLT	0.95–2.32	24–62	Lyot/APLC/FQPM
PUEO	CFHT	0.75–2.5	4–140	Lyot
CIAO	SUBARU	1.1–2.5	30–70	Lyot
OSIRIS	Keck I	1.0–2.4	20–100	–
AO–NIRC2	Keck II	0.9–5.0	20–100	Lyot
ALTAIR–NIRI	Gemini N.	1.1–2.5	30–70	Lyot
GPI	Gemini S.	0.9–2.4	24–62	Lyot/APLC
PALM-3000 PHARO	Hale 200″	1.1–2.5	60–140	Lyot/FQPM
PALM-3000 Project1640	Hale 200″	1.06–1.76	43–71	APLC
AO–IRCAL	Shane 120″	1.1–2.5	100–150	–

$\Theta=(a/d)(1+e) =$

$= 1 \text{ arcsec } (a/AU)(d/pc)^{-1} (1+e)$

GPIES survey (300 stars)

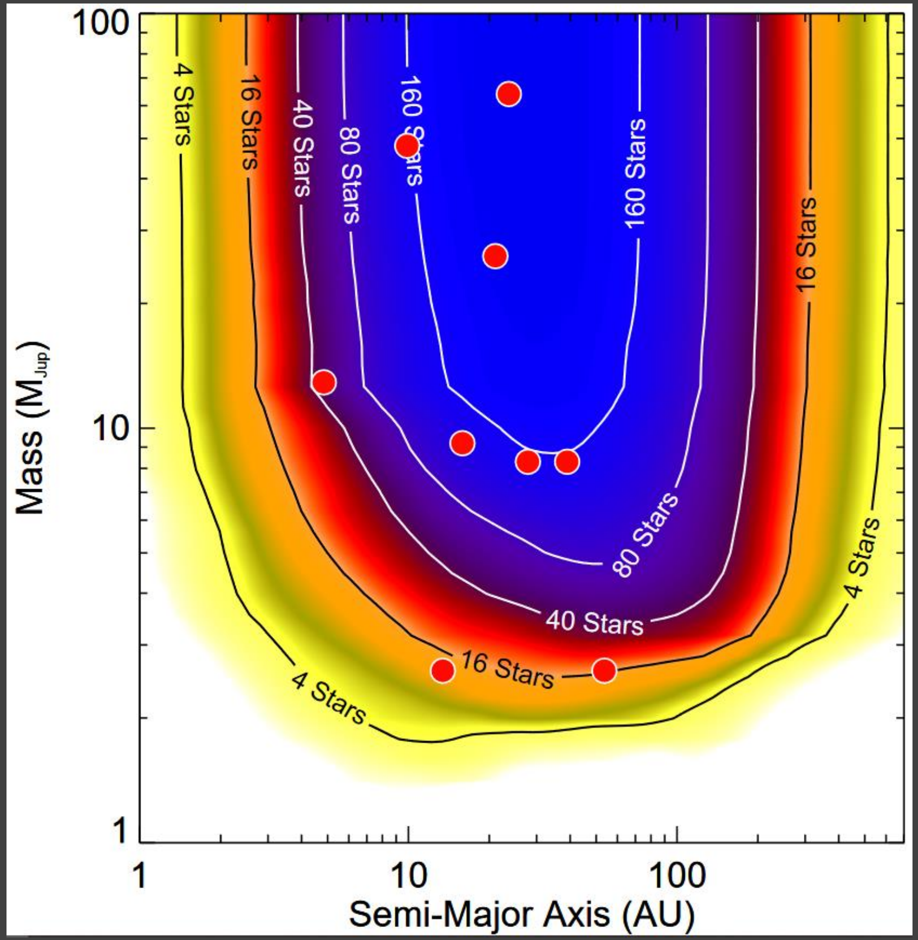

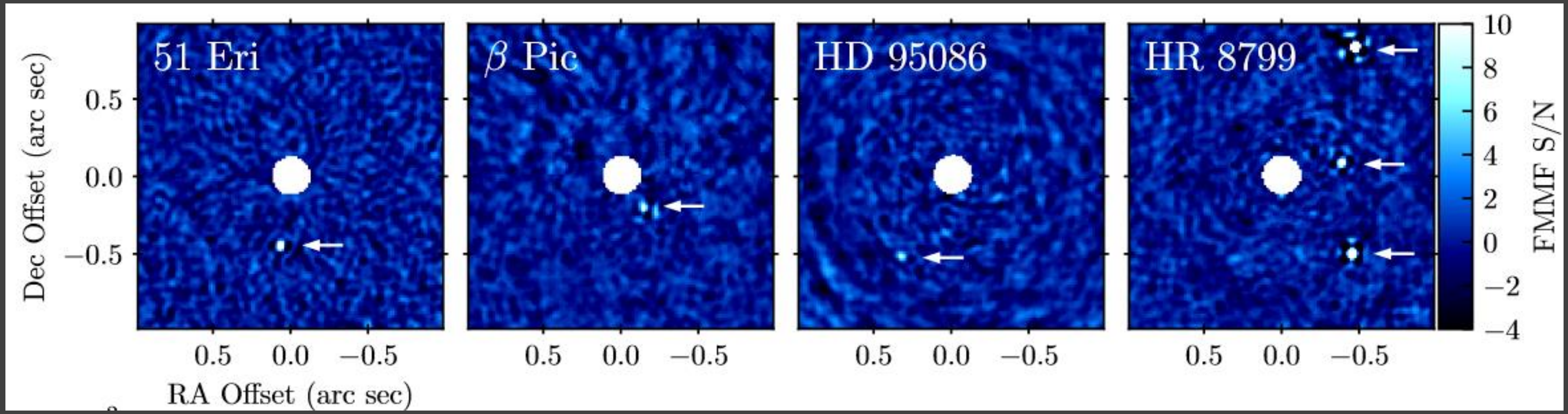

Gemini Planet Imager Exoplanet Survey

10-100 AU

6 planets + 3 brown dwarfs detected

Direct imaging: present and future

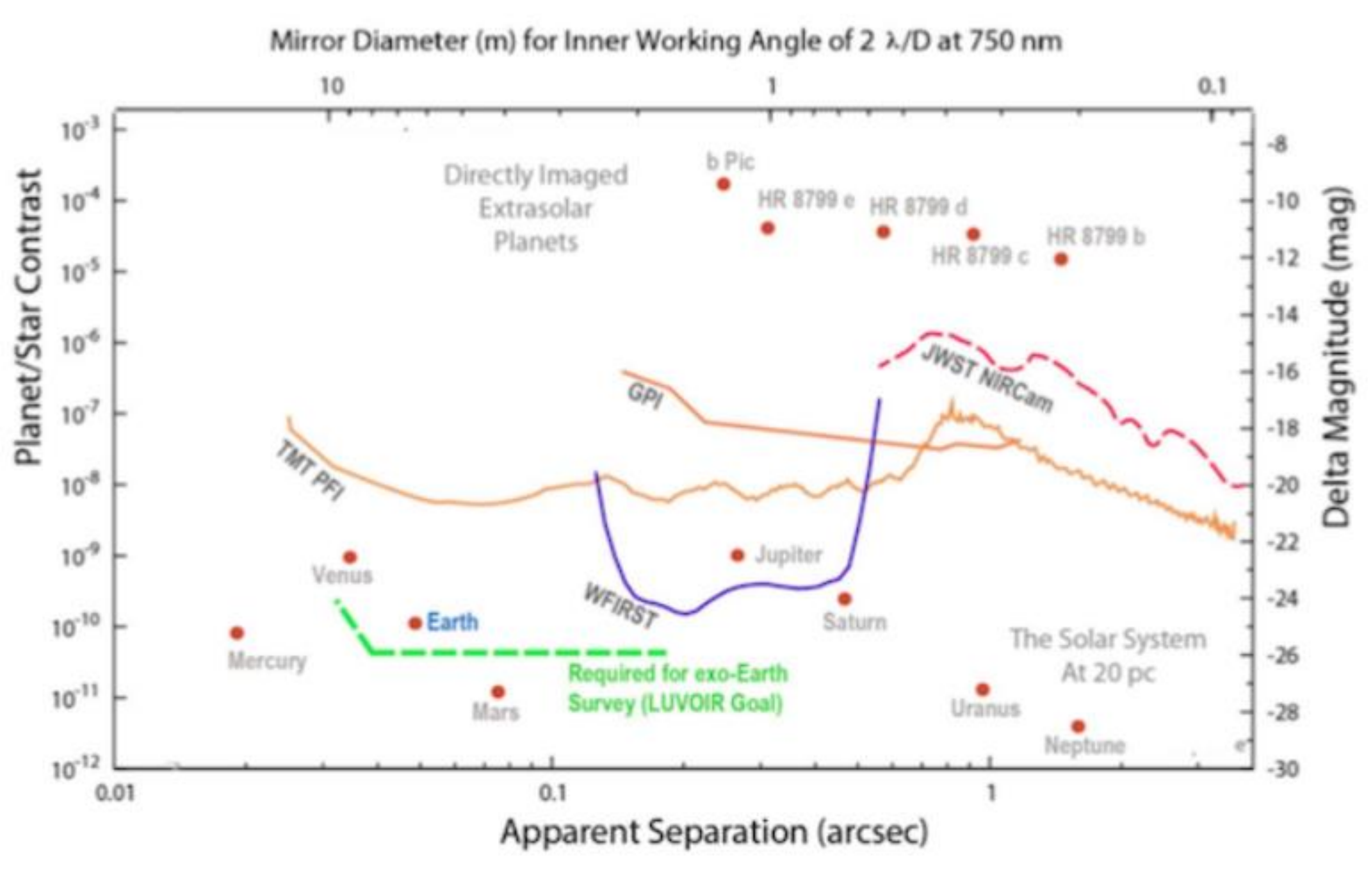

Ground optical interferometers

Instrument	Interf.	Baseline (m)	Bands	Ang. res. (mas)	Spec. res.	Aperture
AMBER	VLTI	16–200	J,H,K	0.6–14	35–15,000	3
MIDI	VLTI	16–200	N	4–80	20–220	2
PIONIER	VLTI	16–200	H,K	1.5–45	15	4
V2	Keck I	85	H,K,L	2–5	25–1800	2
Nuller	Keck I	85	N	10–16	40	2
Mask	Keck	1–10	J to L	13–400	None	2
Classic	CHARA	34–330	H,K	0.5–7	None	2
FLUOR	CHARA	34–330	K	0.7–7	None	2
MIRC	CHARA	34–330	J,H	0.4–5	40–400	4
BLINC	MMT	4	N	250	None	2
LMIRCAM	LBTI	14–23	L,M	27–72	None	2
NOMIC	LBTI	14–23	N	72–200	None	2

Better resolution,
but smaller aperture

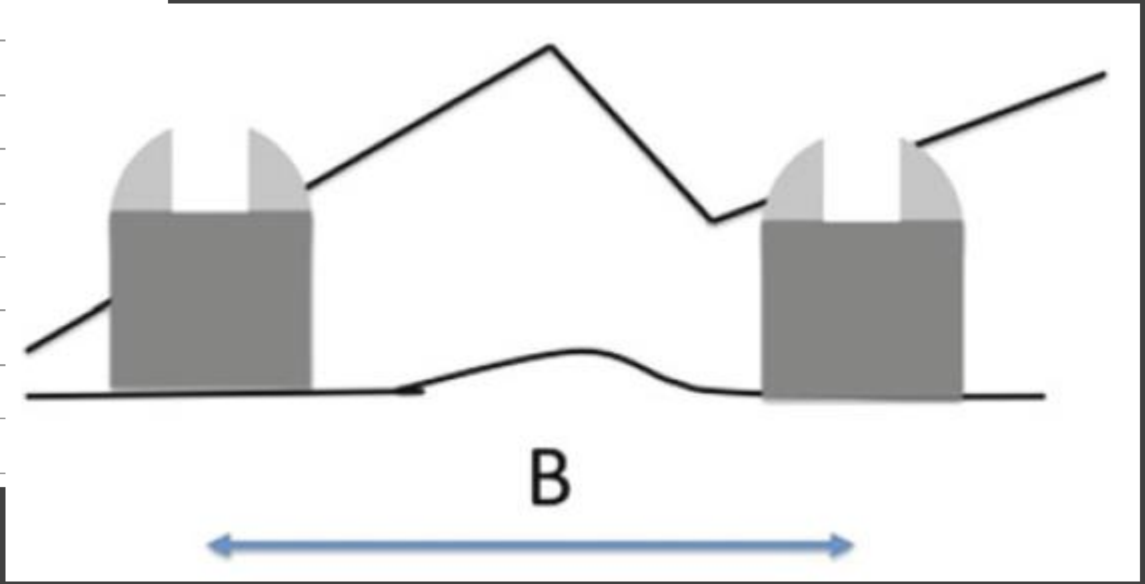

Riccardo Claudi (in Bozza et al. 2016)

Coronagraphs

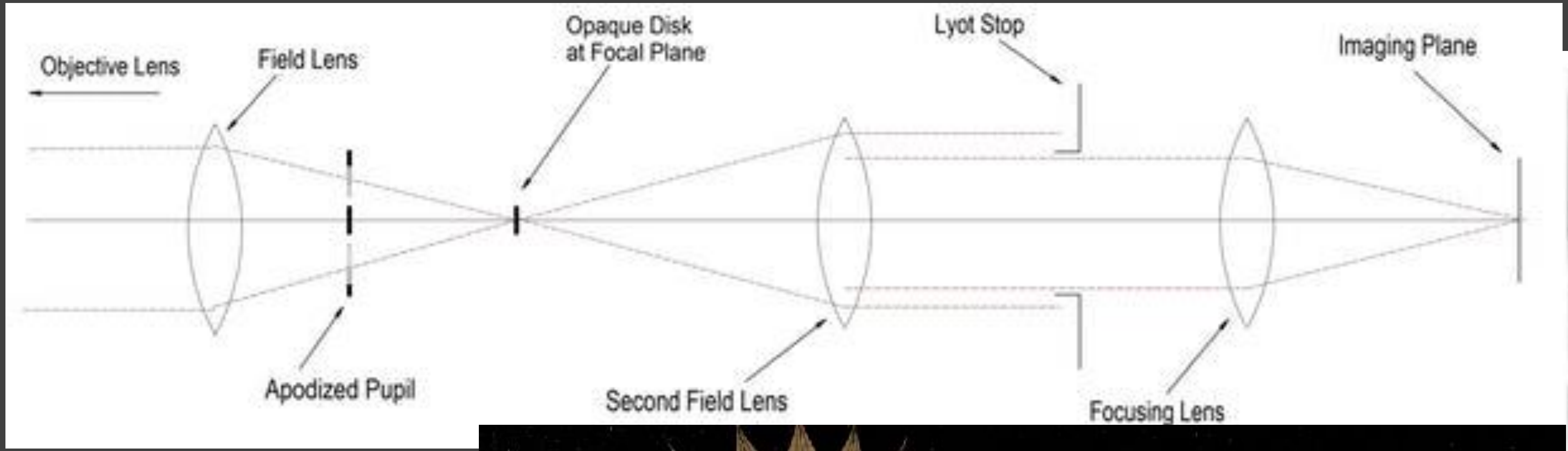

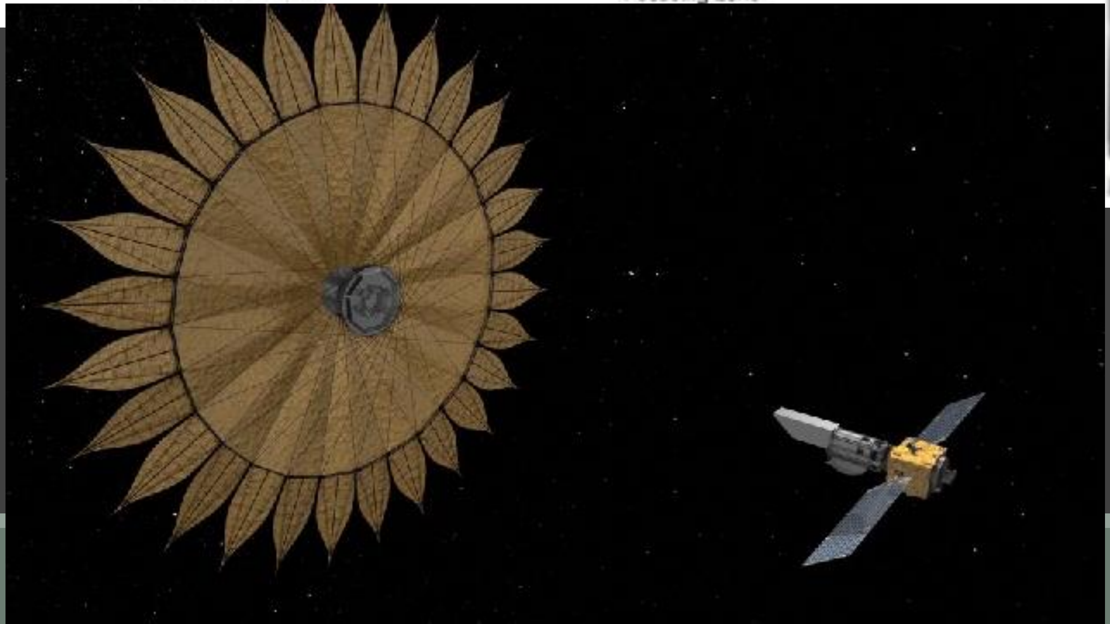

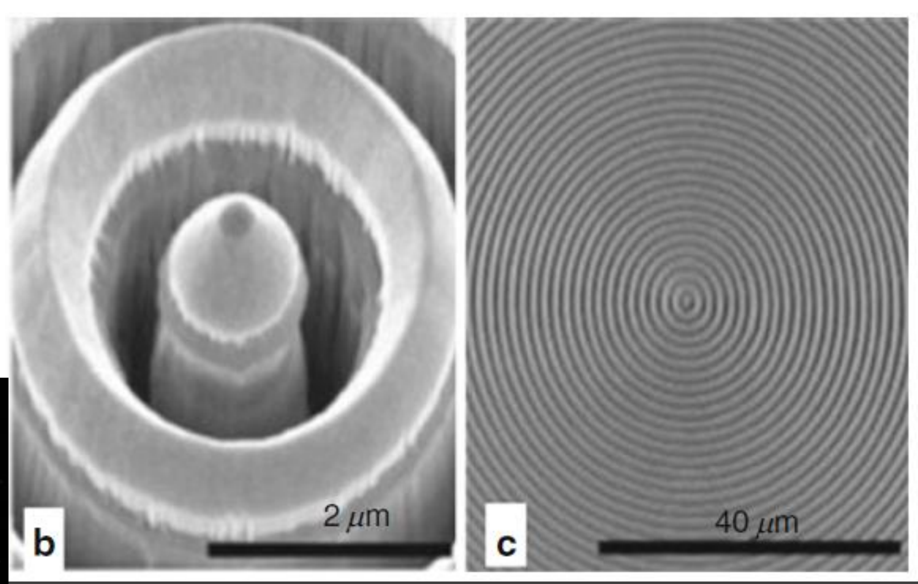

To obtain planet images different kinds of coronagraphs are used.

Riccardo Claudi (in Bozza et al. 2016)

Imaging vs. other methods

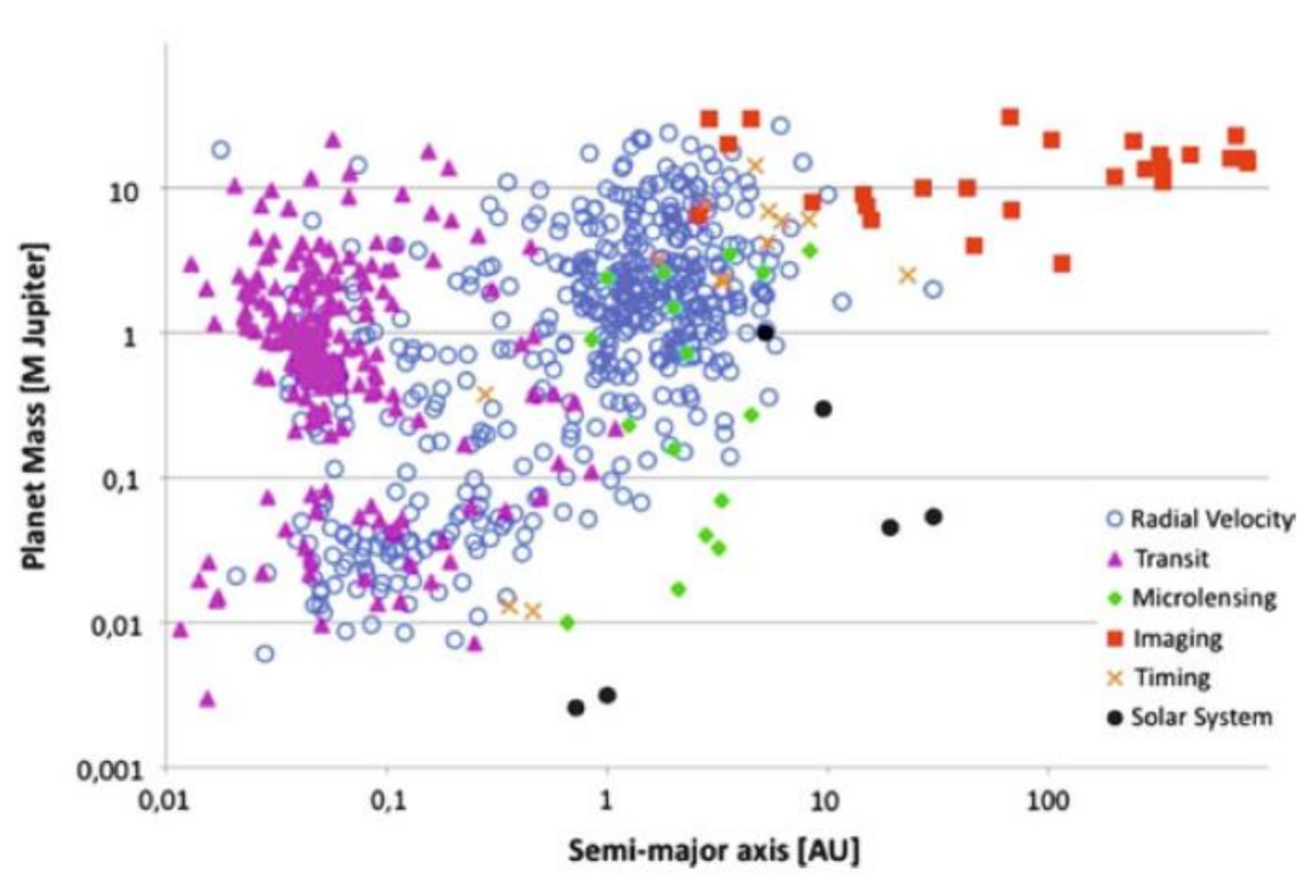

Riccardo Claudi (in Bozza et al. 2016)

Solar system

Notice, how much better planets are visible in IR.
Especially Jupiter at 20-30 micrometers.

Reflected flux

$$F_{\mathrm{p,Vis}} = A(\lambda, t)\phi(t)\frac{R_{\mathrm{p}}^2}{4a^2}B(\lambda, T_{\mathrm{eff}})R_{\star}^2,$$

(A – albedo, a – semimajor axis, ϕ - phase)

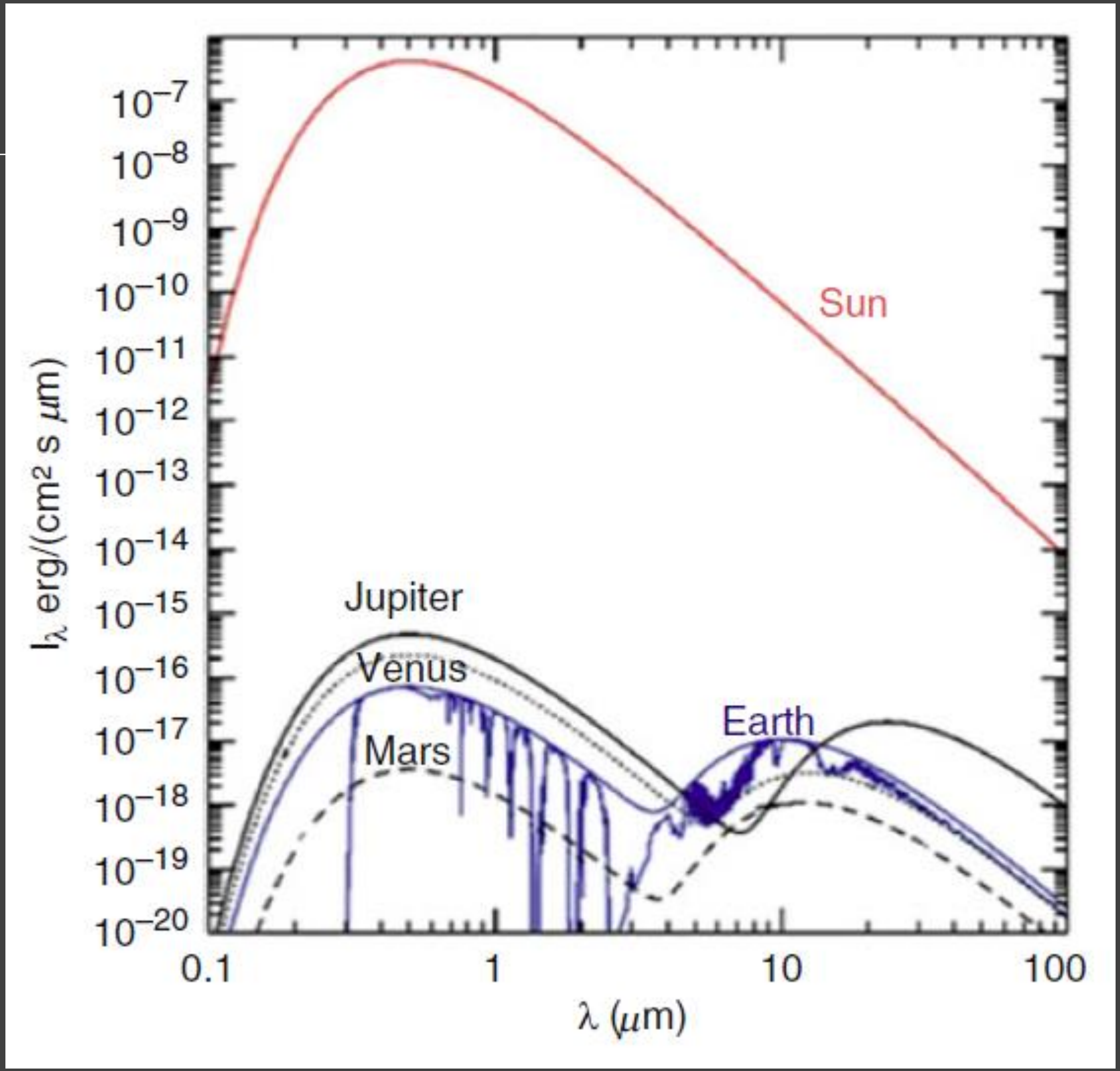

Young planets are hotter

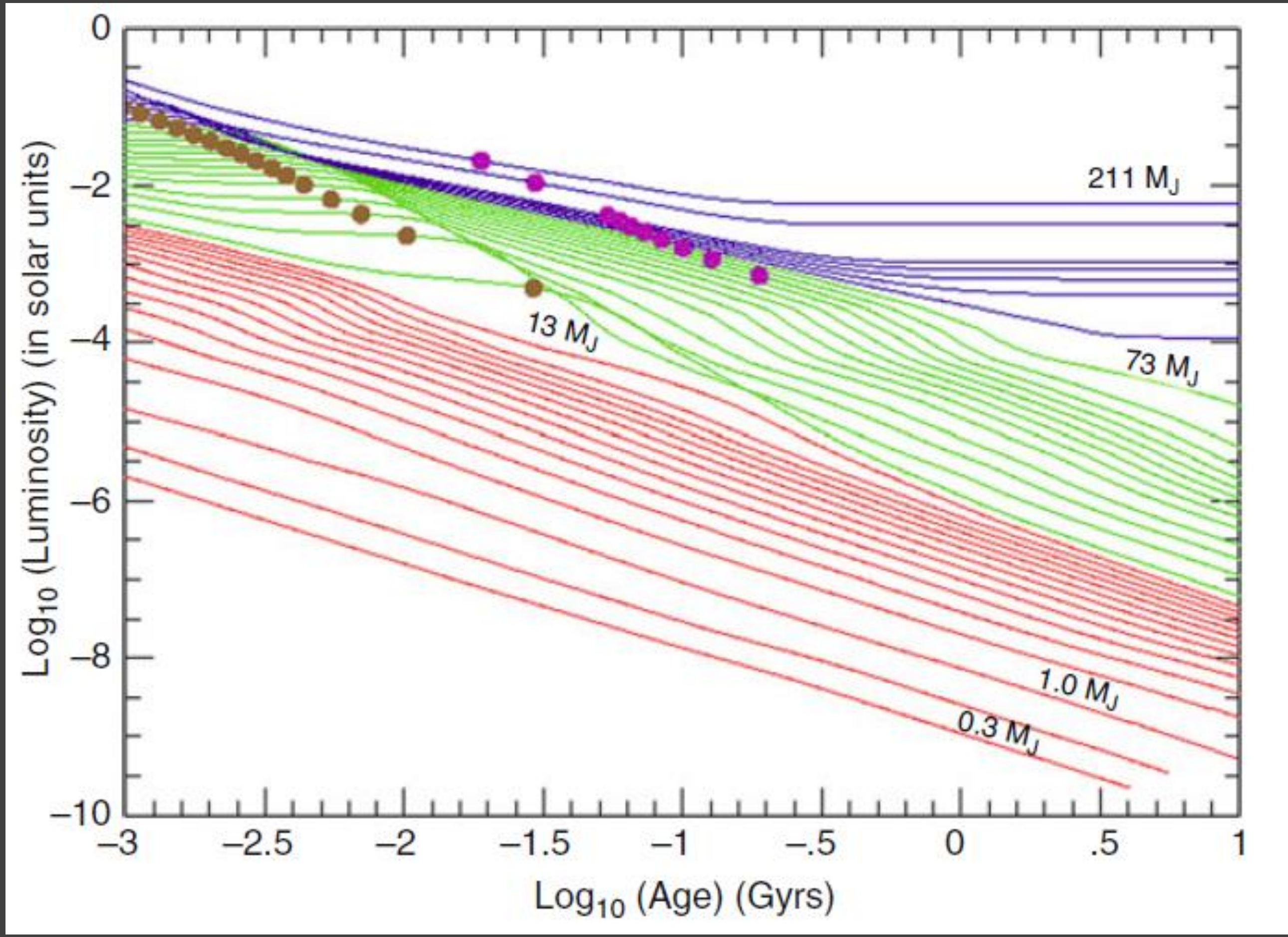

Planet light identification

Kepler-70b,c

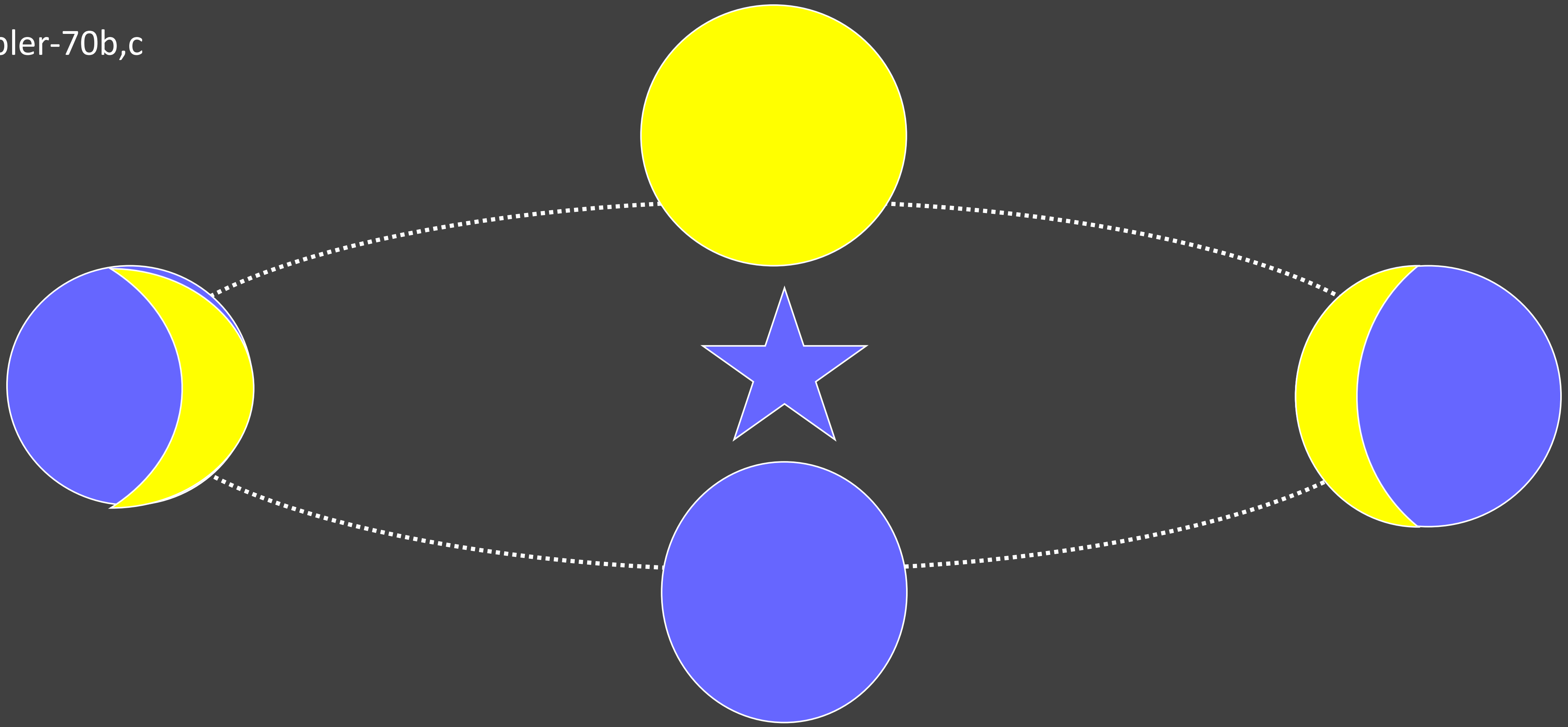

IR light

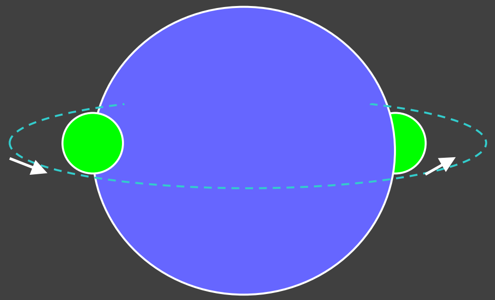

55 Cnc e
Mass: 7-8 Earth mass
Semi-major axis: 0.016 AU
Orbital period: 0.74 days

Temperature 2000-2600K

Occultation light curve

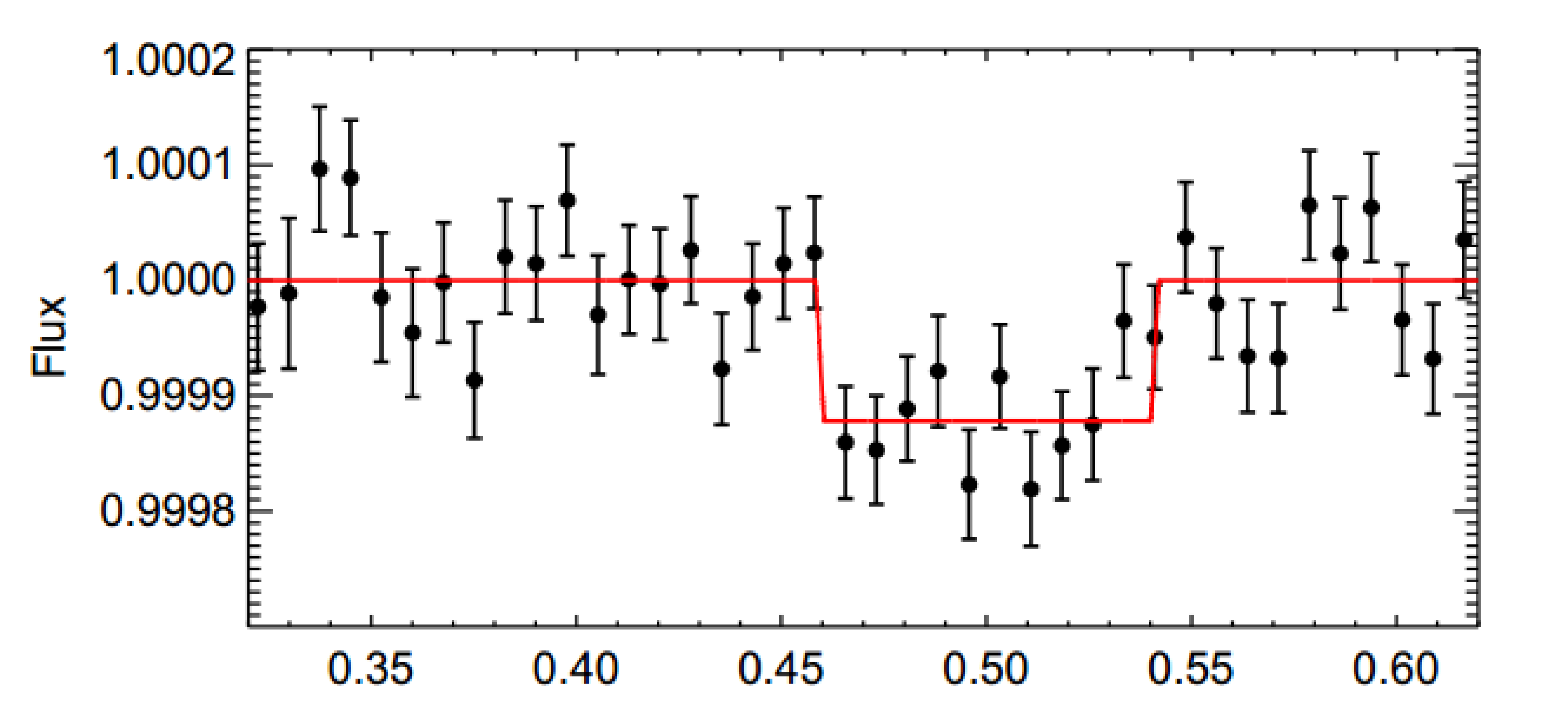

Astrometric detection

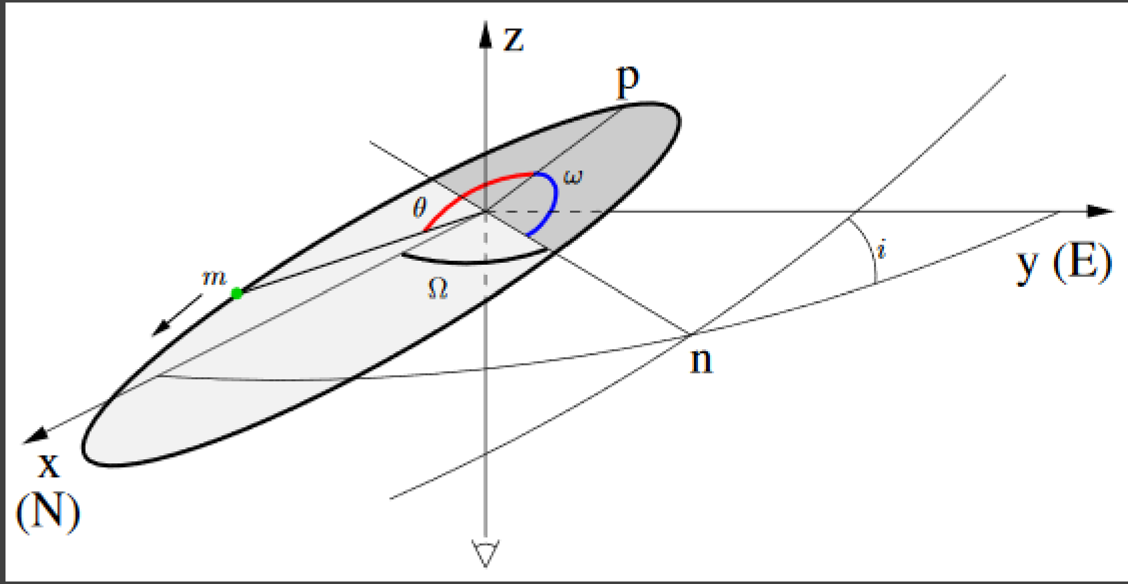

$$4\pi^2 \frac{\bar{a}_1^3}{P^2} = G \frac{M_P^3}{(M_* + M_P)^2},$$

It is easier to detect massive long period planets on eccentric orbits.

Astrometry allows to determine $M^3_{planet}/(M_{star}+M_{planet})^2$

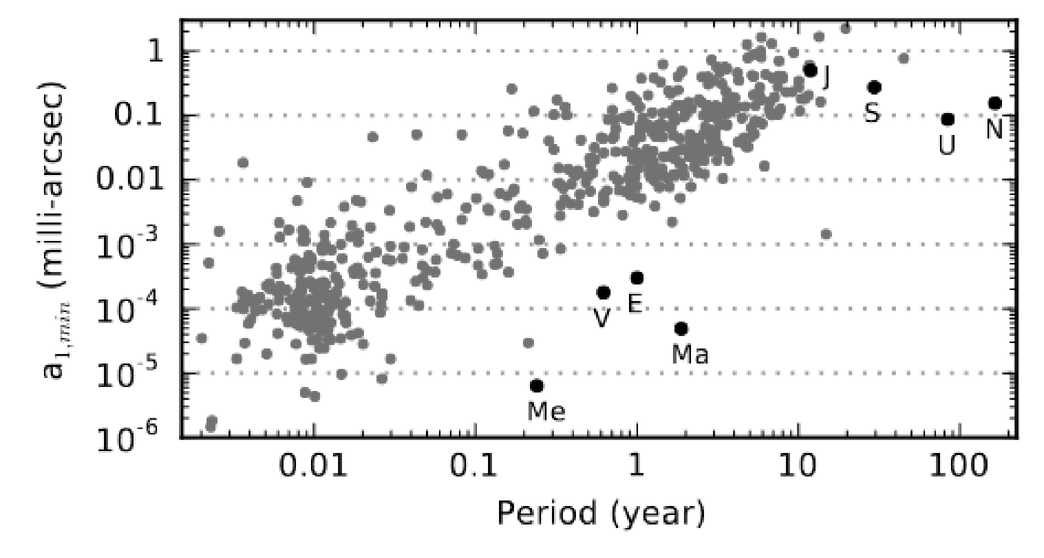

Data on 570 stars with planets are shown.
Solar system data is scaled for a star at 10 pc.

1505.06869, see a review in astro-ph/0507115

A former candidate

Came out to be a brown dwarf with 28 M_{jup}.

Now waiting for Gaia data.

Fig. 15.— The barycentric orbit of the L1.5 dwarf DENIS-P J082303.1-491201 caused by a 28 Jupiter mass companion in a 246 day orbit discovered through ground-based astrometry with an optical camera on an 8 m telescope (Sahlmann et al., 2013a).

Few other candidates have been mentioned by Muterspaugh et al. (2010)

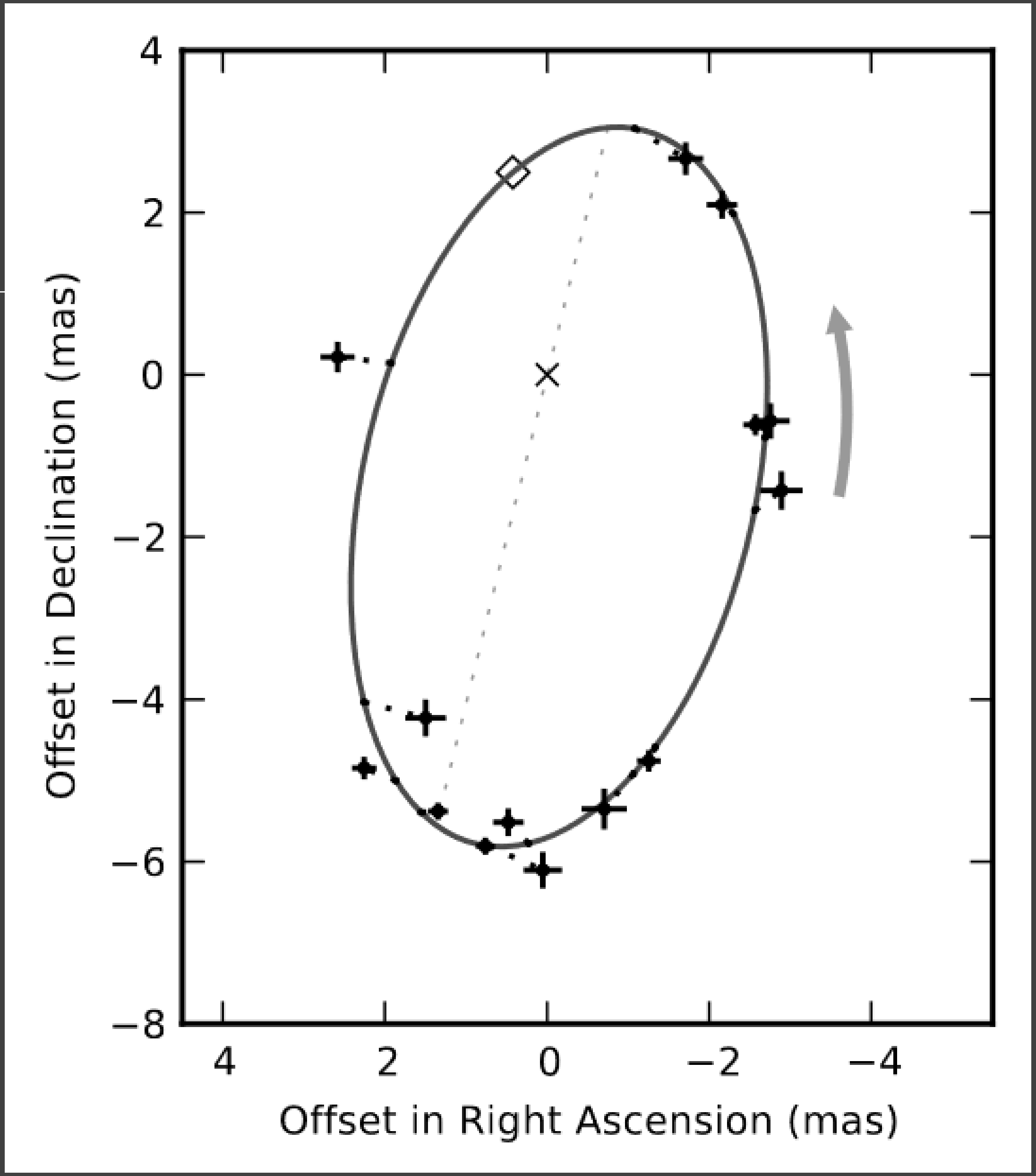

Fomalhaut B candidate

Fomalhaut is a binary system
(may be even triple).
Fomalhaut B (TW PsA)
is a red dwarf (K4Ve)
on a wide (light year) orbit.

Astrometry of Fomalhaut B
suggests a substellar component
due to measured acceleration.

Direct search puts a limit M<2 M_{jup}.

But situation is still uncertain.

Can be searched for with JWST and WFIRST.

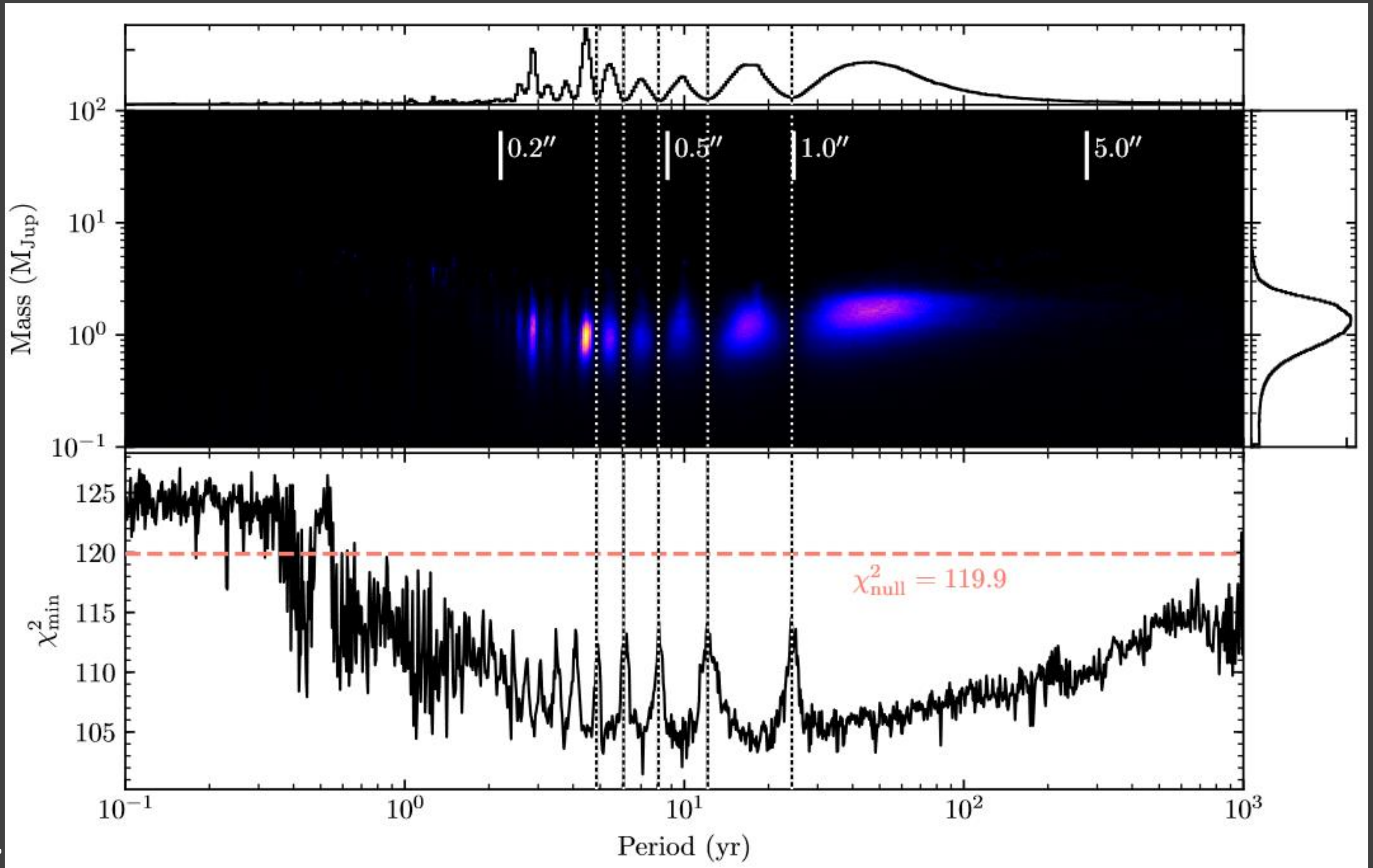

Astrometry in radio!

Saturn mass planet at ~0.3 AU from M9-dwarf.

VLBA observations.

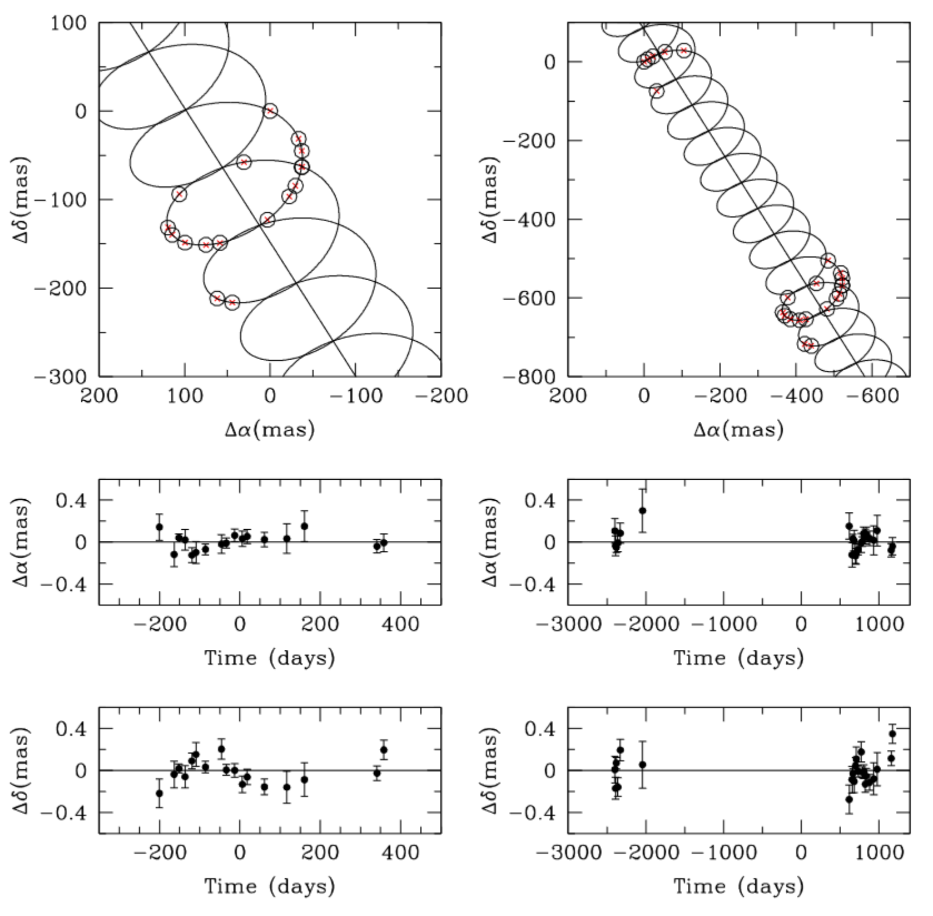

Gaia and astrometric microlensing

$$\alpha = \left(\frac{M_p}{M_\star}\right)\left(\frac{a_p}{1\ \mathrm{AU}}\right)\left(\frac{d}{1\ \mathrm{pc}}\right)^{-1} \mathrm{arcsec}$$

Precision of Gaia
is ~30 microarcsec
(see also 1704.02493).

Optimistic estimates:
tens of thousand planets
(~20000-30000).

Mostly massive and
with long orbital periods
up to ~500 pc distance.

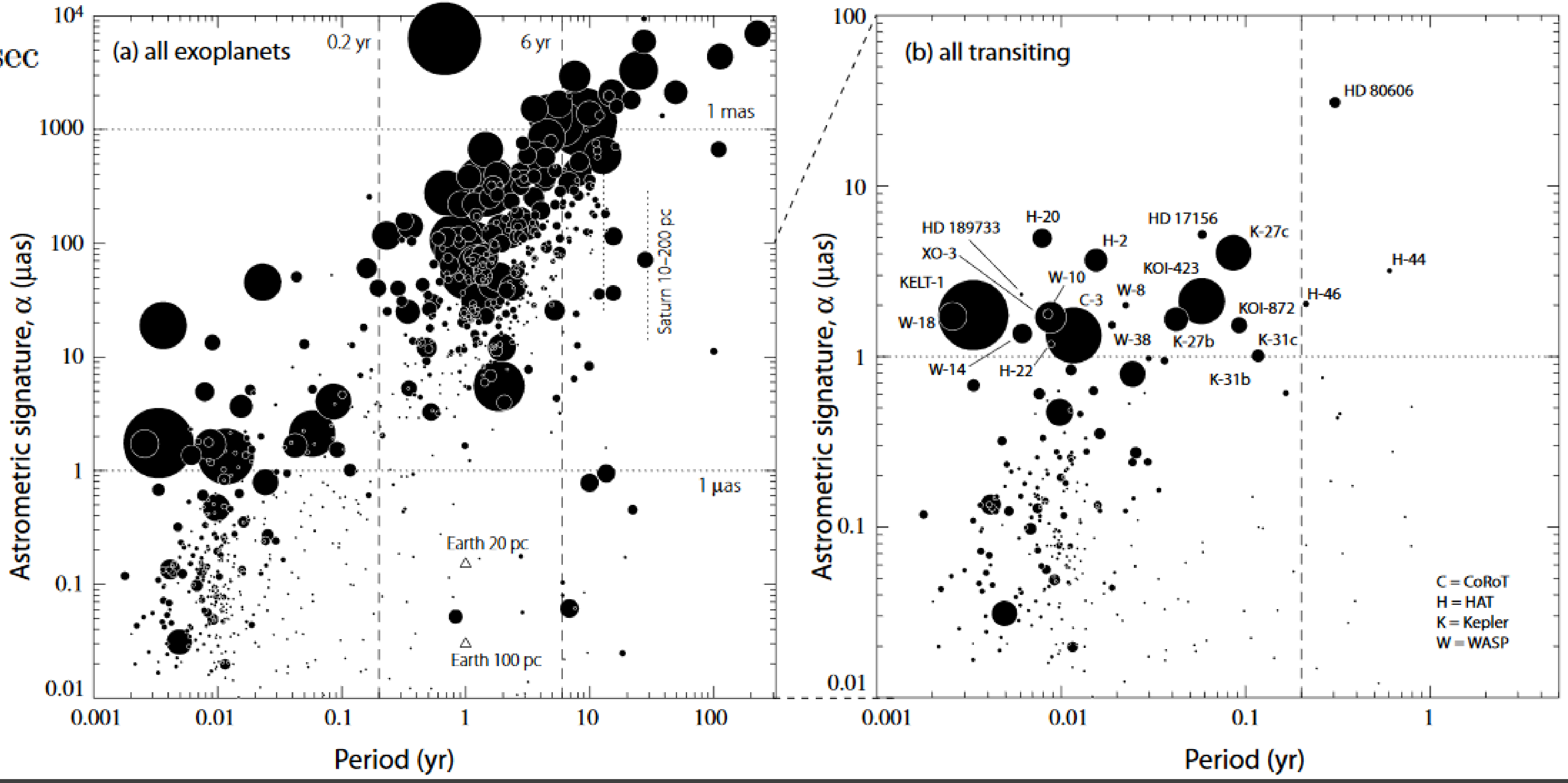

Astrometric microlensing

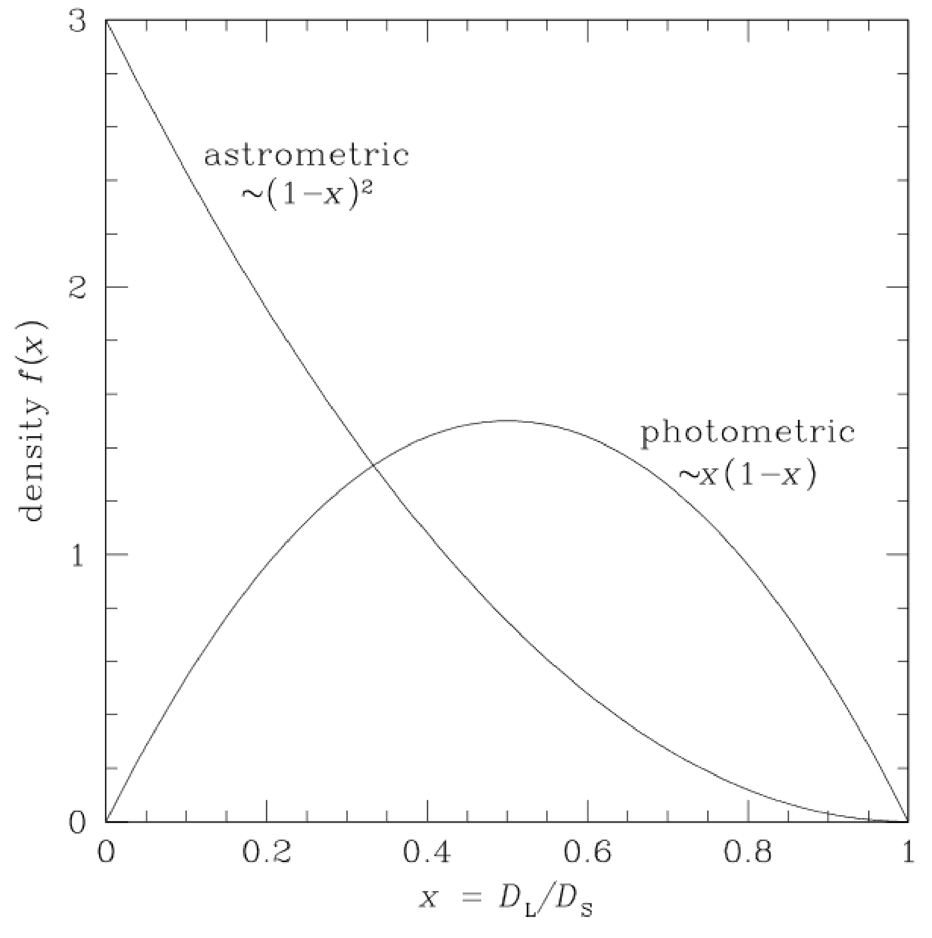

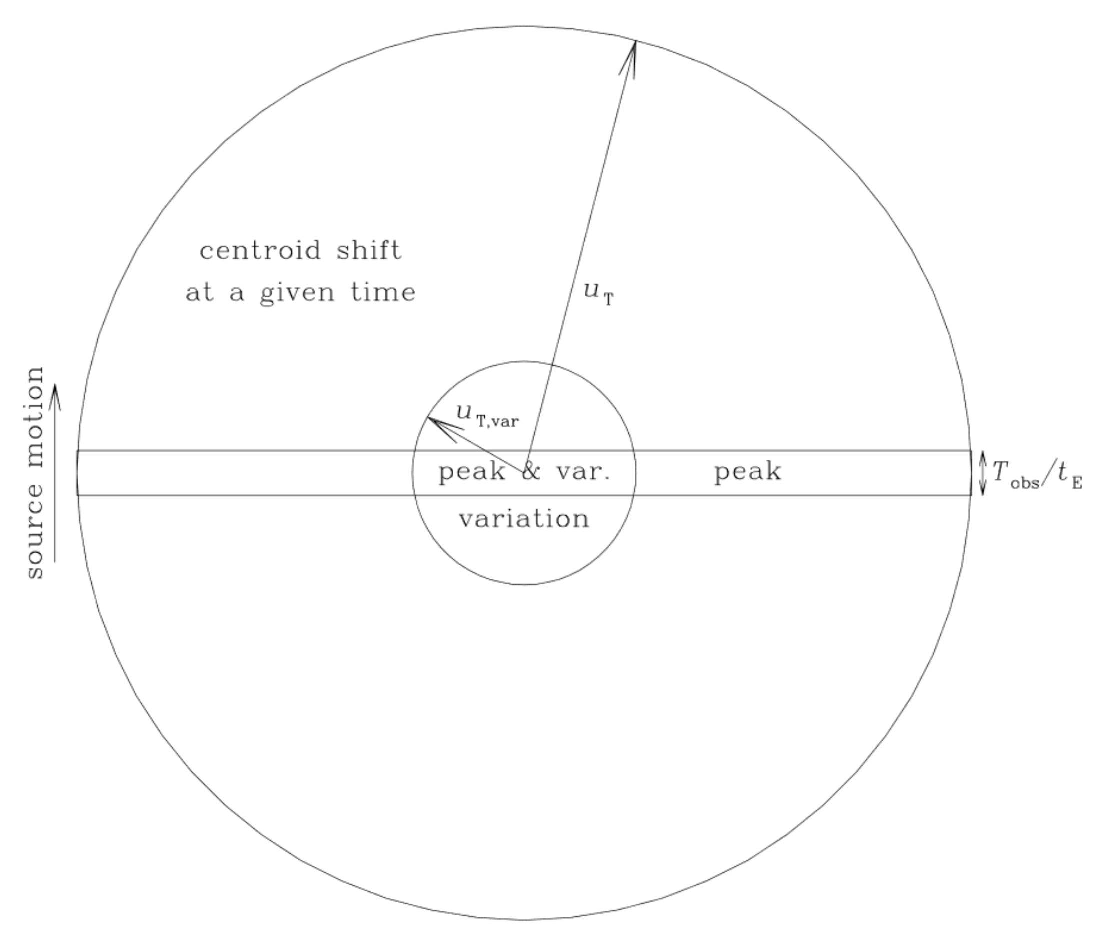

Planetary statistics

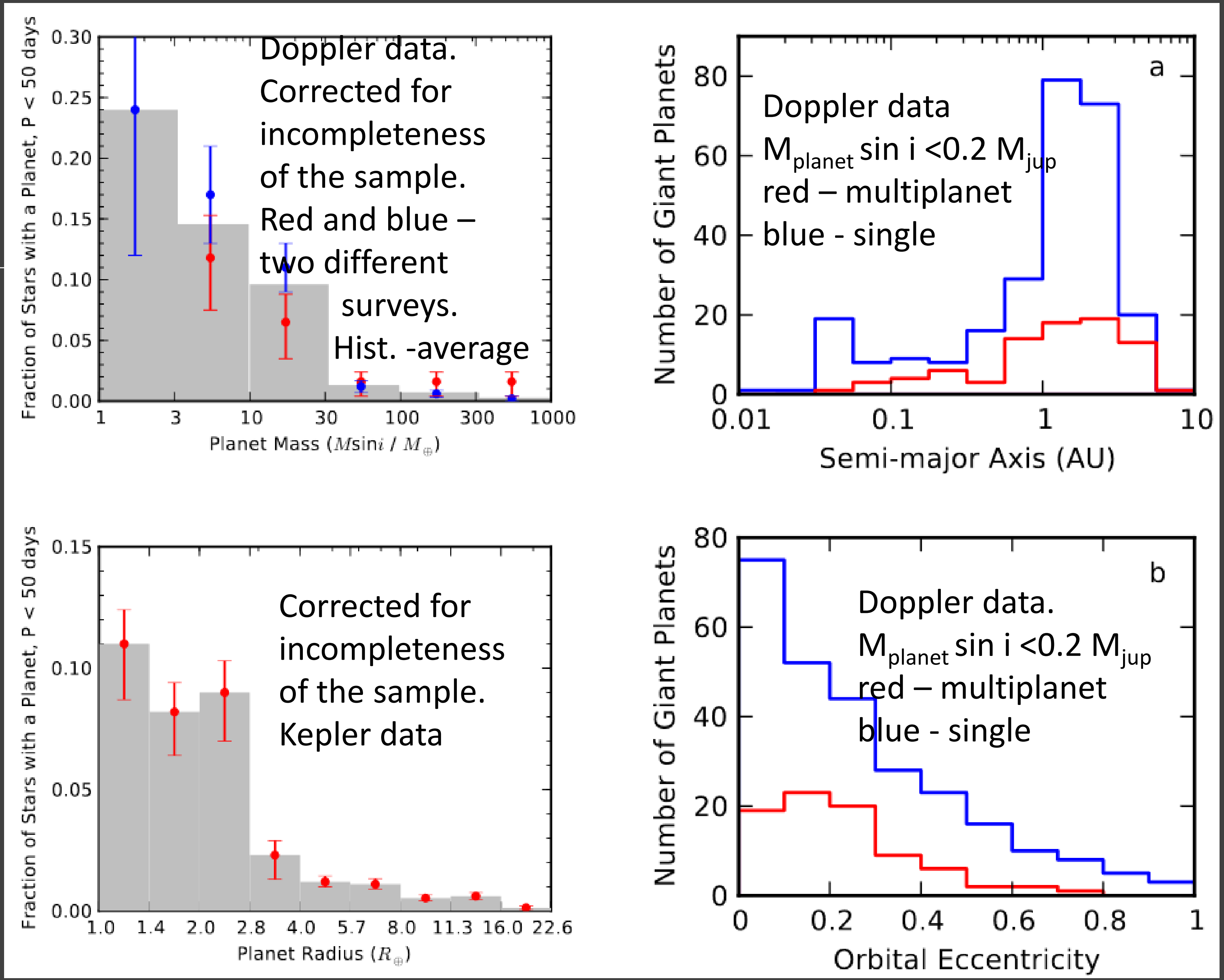

Literature

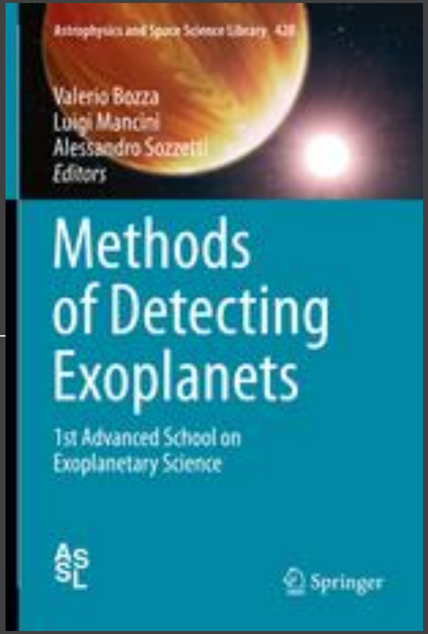

arxiv:1505.06869 Exoplanet Detection Techniques
arxiv:1504.04017 The Next Great Exoplanet Hunt
arxiv:1410.4199 The Occurrence and Architecture of Exoplanetary Systems

arXiv:1708.00896 Timing by Stellar Pulsations as an Exoplanet Discovery Method
arxiv:1706.09849 Transit Timing and Duration Variations for the Discovery and Characterization of Exoplanets
arxiv:1705.05791 Exoplanet Biosignatures: A Review of Remotely Detectable Signs of Life
arxiv:1704.07832 Mapping Exoplanets
arxiv:1701.05205 Characterizing Exoplanets for Habitability
arxiv:1411.1173 Astrometric exoplanet detection with Gaia
arxiv:1001.2010 Transits and Occultations
arxiv:0904.0965 Astrometric detection of earthlike planets
arXiv:0904.1100 Exoplanet search with astrometry
arxiv:0902.1761 Detection of extrasolar planets by gravitational microlensing
ApJ (2000) Dominik, Sahu Astrometric microlensing
arXiv:1810.02691 Microlensing searches for exoplanets